Model Description for the Sacramento River Winter-run Chinook Salmon Life Cycle Model: an implementation for the Sites Reservoir Project

Noble Hendrix[1]
Ann-Marie K. Osterback[2,3]
Vamsi Sridharan[2,3]
Doug Jackson[1]
Sara John[2,3]
Miles Daniels[2,3]
Eric Danner[2,3]
Eva Jennings[4]
Anne Criss[2,3]
Correigh M. Greene[5]
Hiroo Imaki[5]
Steven T. Lindley[2,3]

[1]QEDA Consulting, LLC
4007 Densmore Ave N
Seattle, WA 98103

[2]Institute of Marine Sciences
University of California, Santa Cruz
1156 High St
Santa Cruz, CA 95064

[3]National Marine Fisheries Service
Southwest Fisheries Science Center
Fisheries Ecology Division
110 McAllister Way
Santa Cruz, CA 95060

[2]Cheva Consulting
4106 Aikins Ave SW
Seattle, WA 98116

[5]National Marine Fisheries Service
Northwest Fisheries Science Center
2725 Montlake Blvd. East
Seattle, WA 98112-2097

March 15, 2023

I. Background and Model Structure

Given the goals of improving the reliability of water supply and improving the ecosystem health in California's Central Valley, NMFS-SWFSC is developing simulation models to evaluate the potential effects of water project operations and habitat restoration on the dynamics of Chinook salmon populations in the Central Valley. These life cycle models (LCMs) couple water planning models (CALSIM II), physical models (HEC-RAS, DSM2, DSM2-PTM, USBR river temperature model, etc.) and Chinook salmon life cycle models to predict how various salmon populations will respond to suites of management actions, including changes to flow and export regimes, modification of water extraction facilities, and large-scale habitat restoration. In this document, we describe a winter-run Chinook salmon life cycle model (WRLCM). In the following sections, we provide the general model structure, the transition equations that define the movement and survival throughout the life cycle, the life cycle model inputs that are calculated by external models for capacity and smolt survival, and the steps to calibrate the WRLCM.

Winter-run Life Cycle Model (WRLCM)

The WRLCM is structured spatially to include several habitats for each of the life history stages of spawning, rearing, smoltification (physiological and behavioral process of preparing for seaward migration as a smolt), outmigration, and ocean residency. We use discrete geographic regions of Upper River, Lower River, Floodplain, Delta, Bay, and Ocean (Figure 1). The temporal structure of winter-run Chinook is somewhat unique, with spawning occurring in the late spring and summer, the eggs incubating over the summer, emerging in the fall, rearing through the winter and outmigrating in the following spring (Figure 2). We capture these life-history stages within the WRLCM by using developmental stages of eggs, fry, smolts, ocean sub-adults, and mature adults (spawners). The goal of the WRLCM is consistent with that of Hendrix et al. (2014); that is, to quantitatively evaluate how Federal Central Valley Project (CVP) and California State Water Project (SWP) management actions affect Central Valley Chinook salmon populations.

In 2015, the WRLCM was reviewed by the Center for Independent Experts (CIE). In response to recommendations from the CIE, the following modifications were implemented in the WRLCM: 1) divided the River habitat to encompass above Red Bluff Diversion Dam (Upper River) and below Red Bluff Diversion Dam (Lower River); 2) incorporated hatchery fish into the WRLCM; 3) used 95% of observed density as an upper bound for calculation of habitat capacity; 4) re-parameterized the Beverton-Holt function; 5) used appropriate spawner sex-ratios for model calibration to account for bias in Keswick trap capture; 6) modified the WRLCM to a state-space form to incorporate measurement error and process noise; and 7) designed metrics and simulation studies to evaluate model performance. In addition, Hendrix et al. (2014) indicated that future work would use DSM2's enhanced particle tracking model to track salmon survival, which has now been implemented.

Additional comments received in the CIE review that have not been incorporated yet include: 1) expanding spatial structure for spring and fall-run; 2) tracking additional categories of juveniles (e.g., yearling) for applying an LCM to spring-run Chinook; 3) implementing shared capacity for fall and spring-run Chinook; 5) tracking monthly cohorts through the model; and 6) evaluating multiple model structural forms. We are actively working on improving the WRLCM and developing the spring-run LCM (SRLCM) and fall-run LCM (FRLCM). Many of the CIE recommendations will be implemented with subsequent versions of these models.

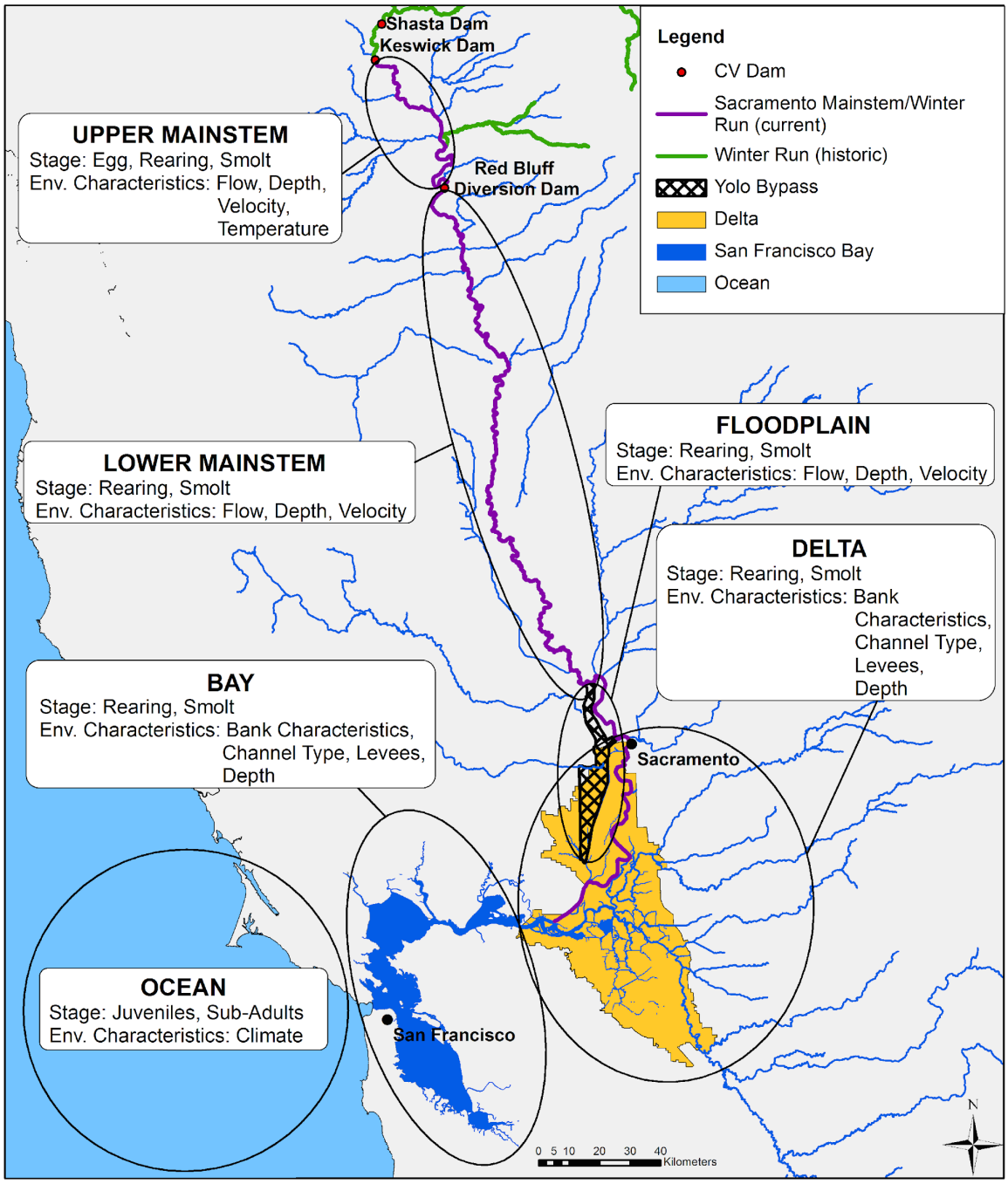

Figure 1. Geographic distribution of Chinook life stages and examples of environmental characteristics that influence survival.

The quantity and quality of rearing and migratory habitat are viewed as key drivers of reproduction, survival, and migration of freshwater life stages. Various life stages have velocity, depth, and temperature preferences and tolerances, and these factors are influenced by water project operations and climate.

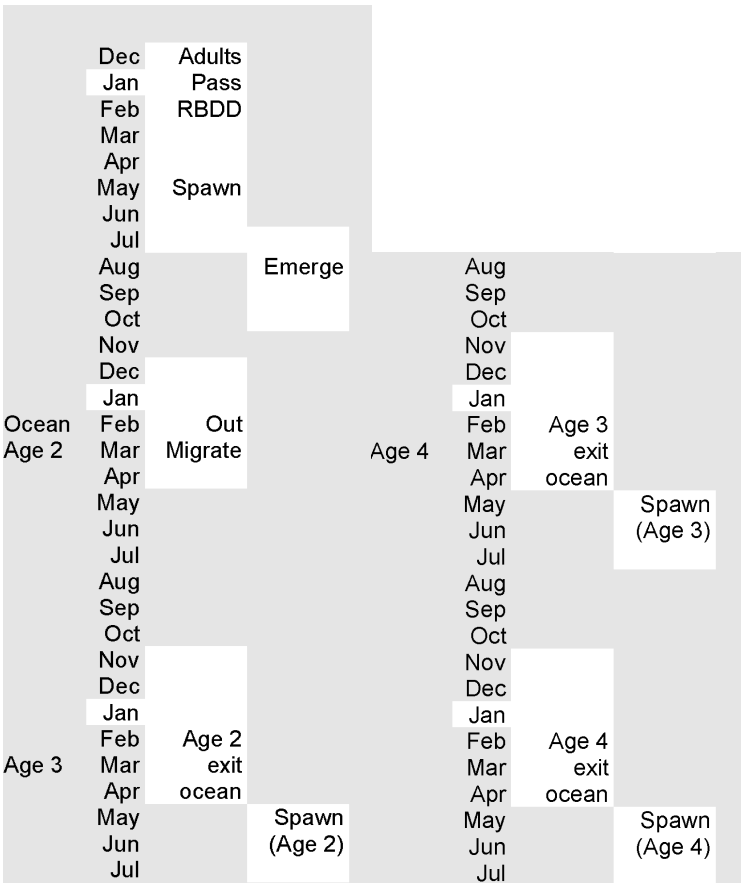

Figure 2. Temporal structure of the winter-run Chinook salmon. Each cohort begins in March of the brood year. Figure from Grover et al. (2004).

Hydrology (the amount and timing of flows) is modeled with the California Simulation Model II (CALSIM II). Hydraulics (depth and velocity) and water quality is modeled with the Delta Simulation Model II (DSM2) and its water quality sub-model QUAL, the Hydrologic Engineering Centers River Analysis System (HEC-RAS), the U.S. Bureau of Reclamation's (USBR) Sacramento River Water Quality Model (SRWQM), and other temperature models. The enhanced particle tracking model (ePTM) makes use of many of these DSM2 related products to calculate survival of outmigrating smolts originating from Lower River, Delta, and Floodplain habitats. Many of the stage transition equations describing the salmon life cycle are directly or indirectly functions of water quality, depth, or velocity, thereby linking management actions to the salmon life cycle. The combination of models and the linkages among them form a framework for analyzing alternative management scenarios (Figure 3).

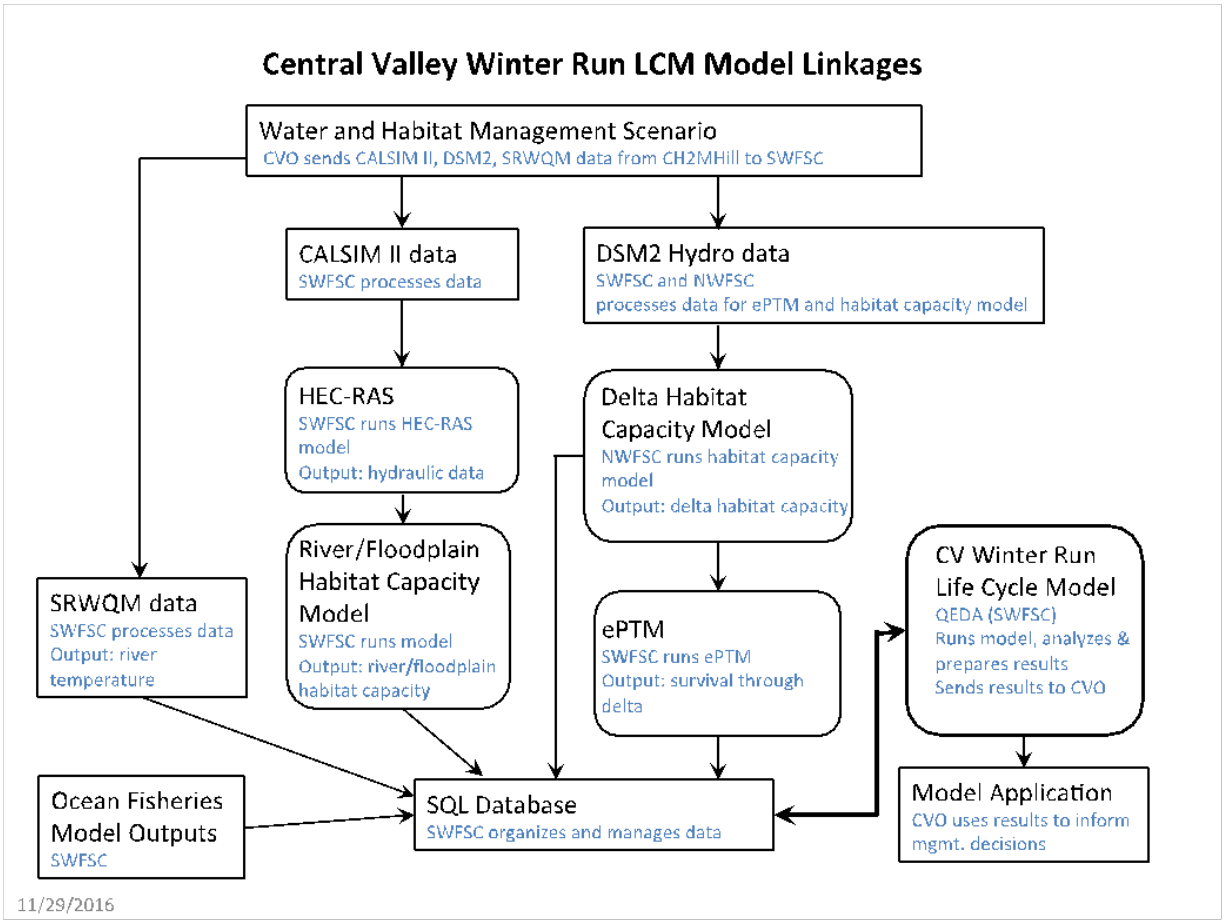

Figure 3. Submodels that support and provide parameter inputs that feed into the life cycle model.

The life cycle model is a stage-structured, stochastic life cycle model. Stages are defined by development and geography (Figure 1), and each stage transition is assigned a unique number (Figure 4).

II. Model Transition Equations

This section is divided into two parts. In the first part, we explain each of the transitions for the natural origin winter-run Chinook, which are described by the life cycle diagram (Figure 4). In the second part, we explain the transitions for hatchery origin fish. The transitions are described for an annual cohort; however, in most cases we have not included a subscript for the cohort brood year to simplify the equations. For those transitions in which there are multiple cohorts, such as the production of eggs in transition 22, a subscript to distinguish cohort is included in the equation.

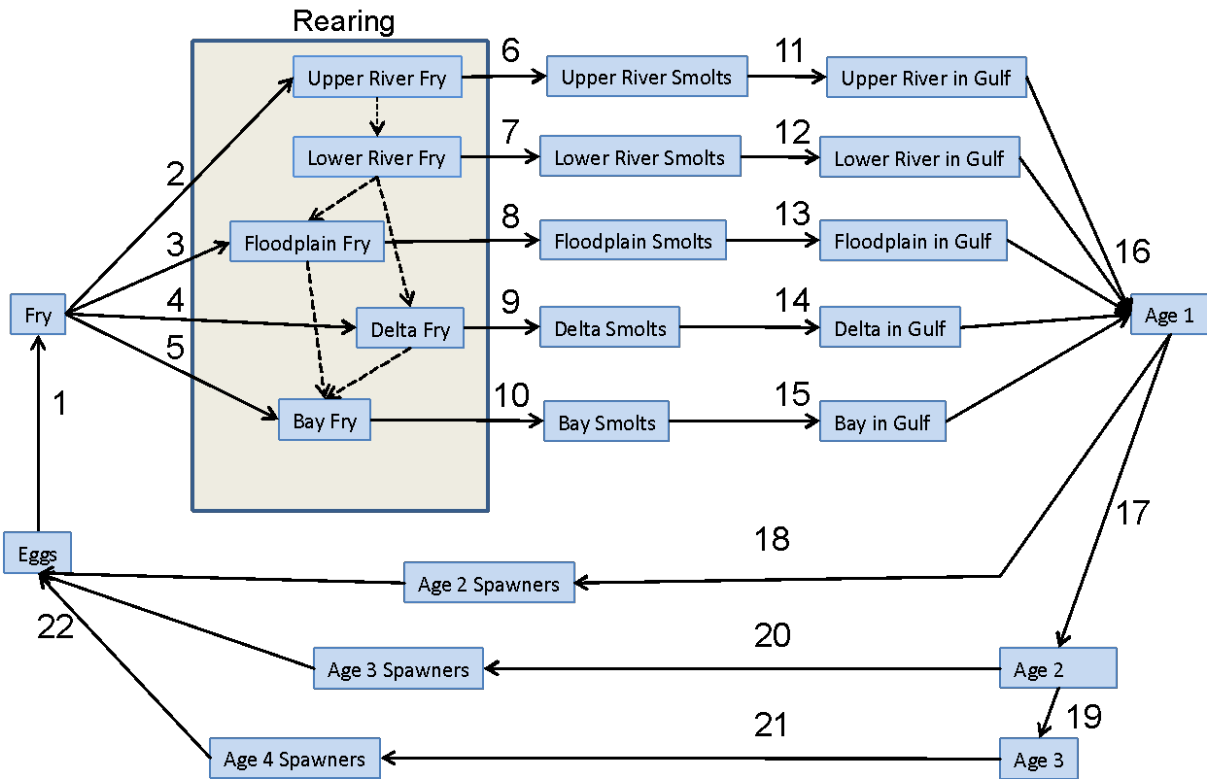

Figure 4. Central Valley Chinook transition stages. Each number represents a transition equation through which we can compute the survival probability of Chinook salmon moving from one life stage in a particular geographic area to another life stage in another geographic area.

Natural Origin Chinook

Transition 1

Definition: Survival from Egg to Fry

$Fry_{m+2} = Eggs_m * S_{eggs,\,m}$

$$logit(S_{eggs,m}) = \begin{cases} B0_1, & TEMP \le t.crit \\ B0_1 + B1_1(TEMP_m - t.crit), & TEMP > t.crit \end{cases}$$

where $S_{eggs,m}$ is the survival rate of fry as a function of the coefficients $B0_1$, $B1_1$ and *t.crit* (model parameter representing the critical temperature at which egg survival begins to be decline), logit(x) = log(x/[1-x]) is a function that ensures that the survival rate is within the interval [0,1], for months *m* = (2, …, 6) corresponding to April to August (Figure 5).

Factors affecting baseline survival $B0_1$

$B0_1 = B0a + B1a * X1$

Where B0a is the intercept and B1a is the slope of the regression relating the covariate X1 to the background survival rate. This formulation provides the ability to incorporate the influence of Thiamine deficiency, for example, which may affect the survival of eggs. In addition, this term could also be used to reflect density dependent mortality of eggs, which was identified as a possible factor

in Martin et al. (2017). The covariate $TEMP_m$ is defined as the equally weighted average of the month of spawning *m* and the following 2 months.

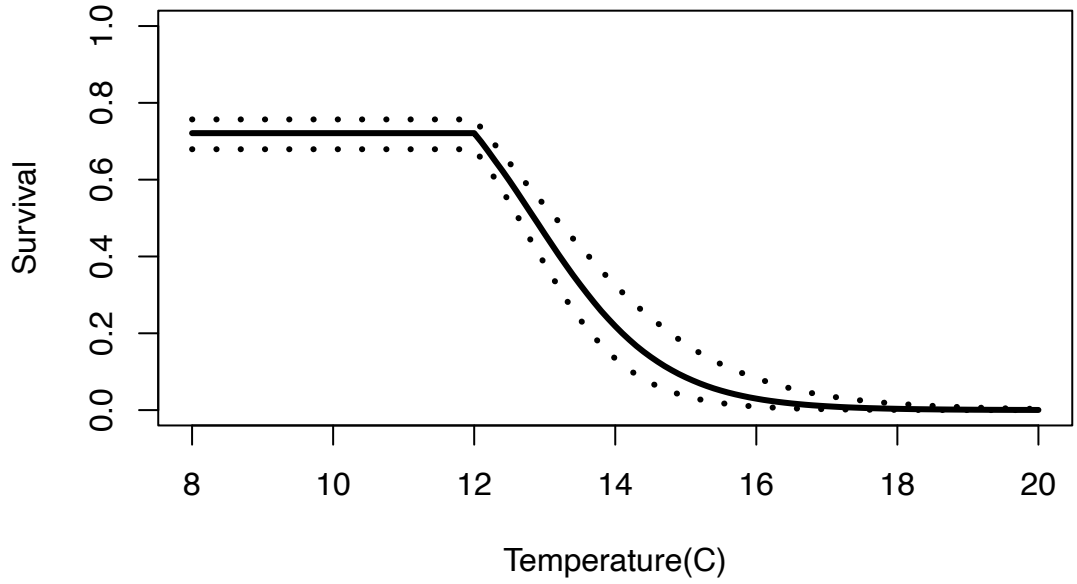

Figure 5. The relationship of egg to fry survival as a function of temperature below Keswick Dam. The solid line represents the median survival rate and the dotted lines represent the 95% CI from 1000 combinations of parameter estimates.

Transitions 2 - 5

Definition: Dispersal from fry in the natal reaches as tidal fry to the h habitats = Lower River (LR), Floodplain (FP), Delta (DE), and Bay (BA) in months *m* = (5, …, 10) corresponding to July to December. Fry that remain (in contrast to those that are tidal fry) rear in the Upper River (UR).

Tidal Fry and Upper River Rearing Fry (Transition 2)

$$TidalFry_{m,} = P_{TF,} * Fry_m$$

$$RearFry_{UR,m} = (1 - P_{TF}) * Fry_m$$

where P_{TF} is the proportion of fry moving out of the Upper River as tidal fry, and $RearFry_{UR,m}$ are the number remaining in the Upper River habitat (UR) as rearing fry.

Floodplain Tidal Fry (Transition 3)

Whenever there are flows into the Yolo Bypass, a proportion of the Tidal Fry move into the floodplain habitat:

$$TidalFry_{FP,m} = S_{TF,FP} * TidalFry_m * P_{FP,m}$$

where $P_{FP,\,m}$ is the proportion of fry that move into the Floodplain habitat, and $S_{TF,FP}$ is the monthly survival of tidal fry in the floodplain.

For the 2035 climate scenario evaluation, the $P_{FP,m}$ is modeled as a function of the expected flow onto the Floodplain habitat due to proposed modifications of the Fremont Weir.

$$P_{FP,m} = \begin{cases} min.p, & y.flow_m < 100 \\ min.p + \dfrac{(y.flow_m - 100) * (0.5 - min.p)}{5900}, & 100 \leq y.flow_m \leq 6000 \\ inv.logit\left(\dfrac{p.rate * (y.flow_m - 6000)}{1000}\right), & y.flow_m > 6000 \end{cases}$$

where $P_{FP,m}$ is the proportion of fry moving into the Floodplain as a function of the coefficients *min.p* (0.05) and *p.rate* (1.1), and the covariate $y.flow_m$. The function inv.logit(x) = $e^x/(1+ e^x)$ ensures that the proportion of fry moving into the Floodplain is within the interval [0,1]. The covariate $y.flow_m$ represents the monthly average flow rate (cfs) at the entrance to Yolo Bypass (CALSIM node D160). The relationship between $P_{FP,m}$ and flow is depicted in Figure 6.

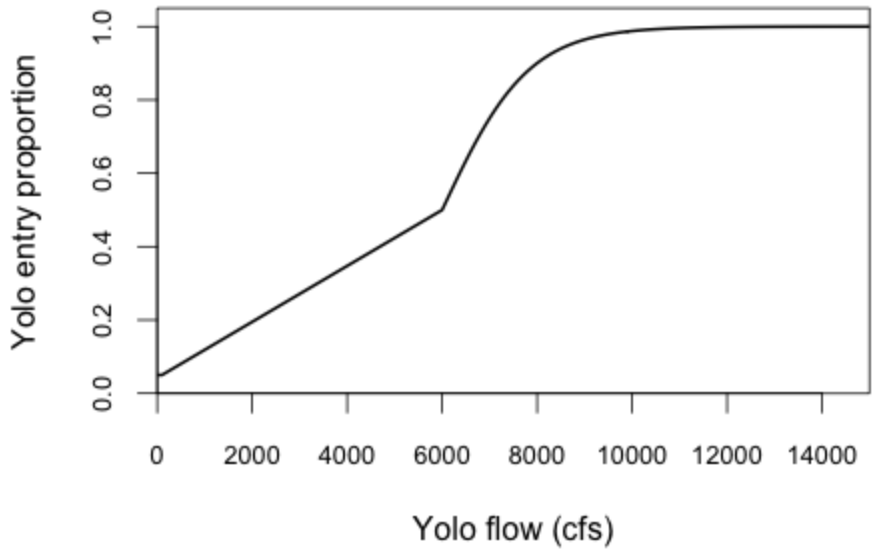

Figure 6. The relationship of Floodplain entry (Yolo bypass) entry proportion (P_{FP}) as a function of Yolo flow.

Delta and Bay Tidal Fry (Transition 4 and 5)

$TidalFry_{DE,m} = TidalFry_m * (1- P_{FP,m}) * (1 - P_{TF,\ BA,m}) * S_{TF,DE,m}$

$TidalFry_{BA,m} = TidalFry_m * (1- P_{FP,\ m}) * P_{TF,\ BA,m} * S_{TF,DE,m} * S_{TF,DE\text{-}BA}$

where $S_{TF,DE,m}$ is the survival to the Delta by Tidal Fry.

$\text{logit}(S_{TF,DE,m}) = B0_4 + B1_4 * DCC_m$

where $B0_4$ and $B1_4$ are model parameters, and DCC_m is the proportion of the transition month that the DCC gate is open.

$P_{TF,Bay,m}$ is the proportion of fish moving to the Bay from the Delta

$$\text{logit}(P_{TF,Bay,m}) = B0_5 + B1_5 * Q_{RioVista,m}$$

where $B0_5$ and $B1_5$ are model parameters, and $Q_{RioVista,m}$ is the flow anomaly (subtract mean and divide by standard deviation). The mean and standard deviation were calculated from 1970-2014 data at Rio Vista (mean = 11,360, standard deviation = 12166.73).

Rearing

Definition: Fry rear among Upper River, Lower River, Floodplain, Delta, and Bay habitats according to a density dependent movement function in months *m* = (5, …, 10) corresponding to July to December.

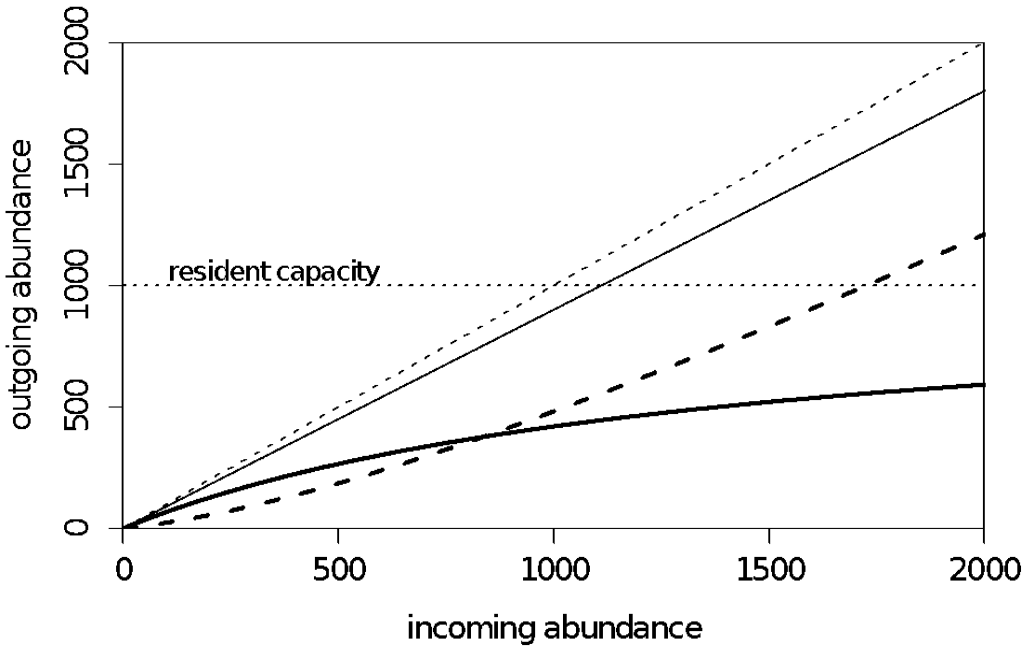

Figure 7. Example of the Beverton-Holt movement function in which the outgoing abundance (thin solid black line) is split between migrants (thick dashed line) and residents (solid dark line), that are affected by the resident capacity (thin dotted line). The 1:1 line (thin dashed line) is also plotted for reference. Parameter values used in the plotted relationship are survival, *S* = 0.90; migration, *m* = 0.2; and capacity, *K*= 1000.

The number fry that remain as residents in the month is calculated from the following equation (Figure 7):

$$Residents_{h,m} = S_{FRY,h,m} * (1 - mig_{h,m}) * N_{h,m} / (1 + S_{FRY,h,m} * [1 - mig_{h,m}] * N_{h,m}/K_{h,m})$$

$$Migrants_{h,m} = S_{FRY,h,m} * N_{h,m} - Residents_{h,m}$$

where $S_{FRY,h,m}$ is the survival rate in the absence of density dependence, $N_{h,m}$ is the pre-transition abundance composed of *Migrants* from upstream habitats in *m-1* and *Residents* from the current

habitat (Figure 7) in m-1, $K_{h,m}$ is the capacity for habitat type h and $mig_{h,m}$ is the migration rate in the absence of density dependence in month m.

The migration rate in the Upper River, $mig_{UR,m}$, is unique and is estimated by using the temporal patterns in fry abundance estimated at Red Bluff Diversion Dam (Poytress et al. 2014).

The migration rate in the Lower River, $mig_{LR,m}$, is modeled as a function of a flow threshold at Wilkins Slough

$$\text{logit}(mig_{LR,m}) = B0_M + B1_M * I(Q_{Wilkins,\,m} > 400\ m^3s^{-1})$$

whereas in all other habitats and months the migration rate $mig_{h,m}$ is a constant value (e.g., movement from the floodplain to the delta, the delta to the bay, and the bay to the gulf).

Survival of fry

Survival of resident and migrant fry $S_{FRY,h,m}$ are modeled as a function of a covariate $X_{h,m}$ that can vary for each habitat and month. The monthly survival rate of fry in habitat *h* and month *m* is modeled as

$$\text{logit}(S_{FRY,h,y,m}) = B0_F + B1_{F,h} * X_{h,y,m}$$

Smolting

Transitions 6 - 10

Definition: Smolting of *Residents* in the Upper River, Lower River, Floodplain, Delta, and Bay rearing habitats in months m = (11, … ,17) corresponding to January to July in the calendar year after spawning.

$$Smolts_{h,m} = P_{SM,m} * Residents_{h,m-1}$$

where $P_{SM,m}$ is the probability of smolting in month m which is assumed to be the same across habitats, by the *Residents* from the previous month (m-1) in that habitat.

The probability of smolting is modeled as a proportion ordered logistic regression model of the form:

$$\text{logit}(P_{SM,\,m}) = Z_k$$

where $-\infty < Z_1 < Z_2 ... < Z_k < \infty$ are the monthly rates of smoltification based on photoperiod (k = 1, …, 7 encompassing January to July).

The model performs the following steps during the months in which smoltification occurs:

1. Smoltification of Resident fry
2. Accumulation of the Migrant fry from the upstream habitats and Resident fry from the current habitat remaining from the previous month that did not smolt (Figure 8 shows connectivity among habitats)
3. Survival and movement of the fry calculated in step 2

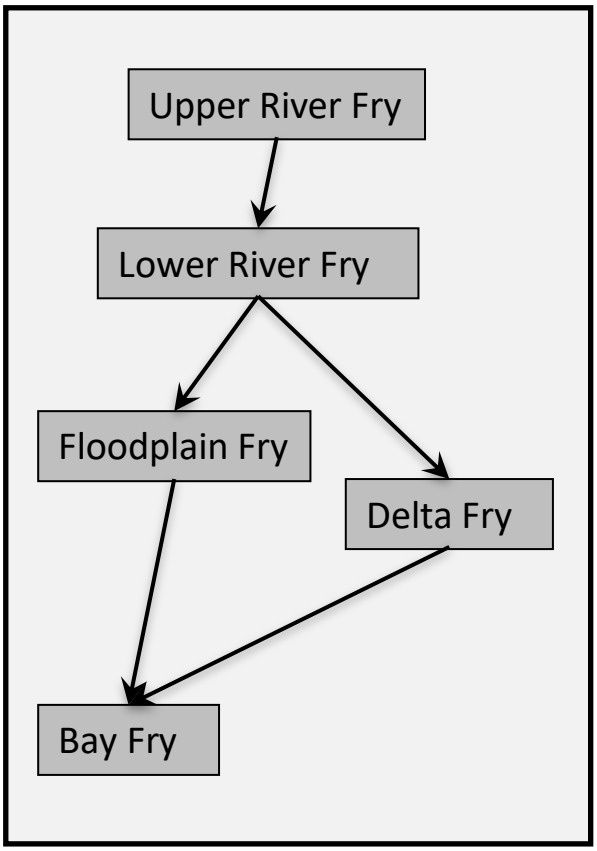

Figure 8. Connectivity among habitats for winter-run Chinook fry. Connections between the Lower River and Floodplain occur due to flooding of the Yolo bypass and are thus ephemeral.

Transitions 11 – 14

These transitions use a Smolt Survival Model (SSM) to calculate the smolt survival through the delta portion of their outmigration. Different models may be used to calculate this survival including Newman (2003) based on an analysis of coded wire tag recoveries, estimates of acoustically tagged survival rates analyzed by Perry et al. (2018) and given the name STARS, and an enhanced particle tracking model (ePTM version 2) that simulates smolt movement at fine temporal (15 min) and spatial (DSM2 8.2 grid structure) resolution. We have described the transition equations generically to be able to use the survival estimates in month *m* and habitat *h* from any of the above survival models using the acronym $SSM_{h,m}$ in the descriptions below.

Transitions 11 & 12

Definition: Smolts that reared in the Upper River and Lower River habitats migrate to the Golden Gate and thus end the freshwater phase of their life cycle in months *m* = (12, … ,18) corresponding to February to August.

Upper River smolt outmigration (Transition 11)

$Gate_{UR,m} = S_{11,UR,m-1} * Smolts_{UR,m-1}$

Lower River smolt outmigration (Transition 12)

$Gate_{LR,m} = S_{12,LR,m-1} * Smolts_{LR,m-1}$

where survival $S_{T,h,m}$ is the smolt survival rate from transition *T* (11, ..., 15) in habitat *h* (*UR, LR, FP, DE, BA*) in month *m.* The rates $S_{11.UR,m}$ and $S_{12,LR,m}$ are composed of three components: A) survival rate from the Upper or Lower River to the Sacramento River near Sacramento (Figure 9); B) survival through the Delta to Chipps Island; and C) survival from Chipps Island to Golden Gate.

$S_{11.UR,m} = {}^{A}S_{11,UR,m} * {}^{B}S_{12,LR,m} * {}^{C}S_{11}$
$S_{12,LR,m} = {}^{A}S_{12,LR,m} * {}^{B}S_{12,LR,m} * {}^{C}S_{11}$

The first smolt survival component is modeled as a function of flow at Bend Bridge

$\text{logit}({}^{A}S_{11,UR,m}) = B0_{11,UR} + B1_{11} * q.bb\_mod_m$
$\text{logit}({}^{A}S_{12,LR,m}) = B0_{12,LR} + B1_{11} * q.bb\_mod_m$

where $B0_{11,UR}$, $B0_{12,LR}$ and $B1_{11}$ are model parameters, and $q.bb\_mod_m$ is modified monthly flow at Bend Bridge which is the closest station to the Red Bluff Diversion Dam standardized relative to historic Bend Bridge flows from 1970-2014 (mean = 14593.96, standard deviation = 10984.20). To estimate riverine smolt survival rate for the implementation for the Sites Reservoir Project, flow at Bend Bridge ($q.bb_m$) was modified to account for the two Sites diversions located between Bend Bridge and Sacramento (River Mile [RM] 58): the Red Bluff Intake (RM 243) and the Hamilton City Intake (RM 205). To account for potential diversion effects on smolt survival, we used the following formula to modify Bend Bridge flow:

$q.bb\_mod_m = q.bb_m - q.bb\_RBI_m - (((205-58)/(243-58)) * q.bb\_HCI_m)$

where $q.bb_m$ is monthly flow at Bend Bridge, $q.bb\_RBI_m$ represents flow at the Red Bluff Intake Diversion, and $q.bb\_HCI_m$ represents flow at the Hamilton City Intake Diversion. The latter term accounts for the Hamilton City Intake being 79% (i.e., 147/(243-58)) of the distance to Sacramento from Red Bluff. In the baseline scenario $q.bb\_mod_m = q.bb_m$; that is, there is no alteration to flow at Bend Bridge.

${}^{B}S_{12.LR,m} = SSM_{LR,m}$

where $SSM_{LR,m}$ is a survival rate for smolts originating from the Sacramento River through the Delta to Chipps Island as calculated by the Smolt Survival Model. The value ${}^{C}S_{11}$ is a model parameter representing survival from Chipps Island to Golden Gate, and it was applied to smolts originating from all habitats.

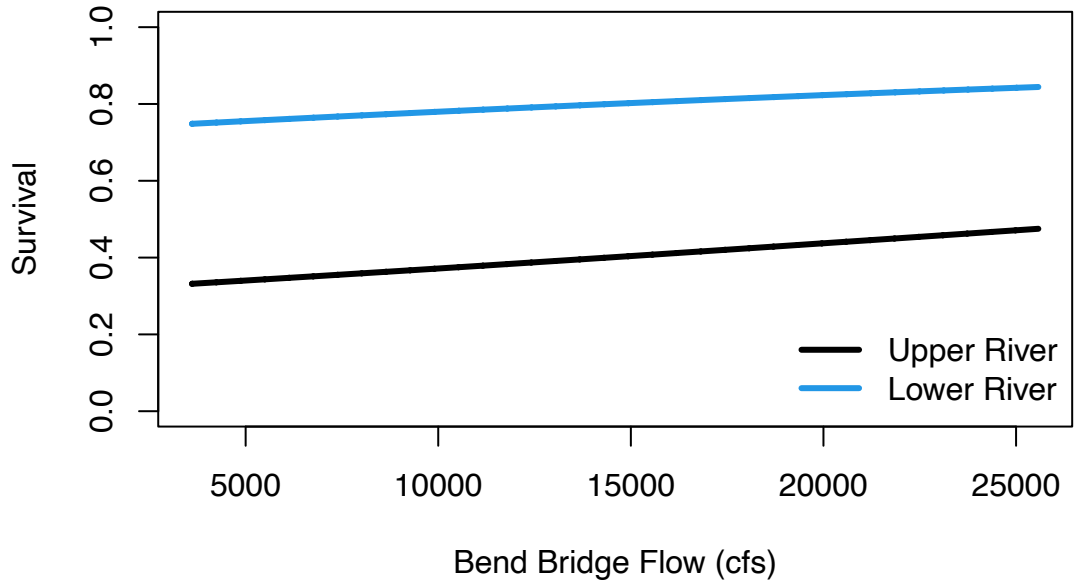

Figure 9. The relationship of smolt survival in the mainstem Sacramento for smolts originating from the Upper River or Lower River as a function of flow at Bend Bridge.

Transition 13

Definition: Smolts that reared in the Floodplain migrate to the Golden Gate arriving in months *m* = (12, … ,18) corresponding to February to August.

$Gate_{FP,m} = S_{13,FP,m-1}\, Smolts_{FP,m-1}$

The rate $S_{13,FP,m}$ is composed of three components: A) survival rate through the Floodplain to the Delta; B) survival through the Delta to Chipps Island; and C) survival from Chipps Island to Golden Gate.

$S_{13,FP,m} = {}^{A}S_{13,FP,m} * {}^{B}S_{13,FP,m} * {}^{C}S_{11}$

where ${}^{A}S_{12,FP,m}$ is survival in the Floodplain until the Smolt Survival Model estimate is applied for survival through the Delta.

${}^{B}S_{13.FP,m} = SSM_{FP,m}$

Transition 14

Definition: Smolts that reared in the Delta migrate to the Golden Gate arriving in months *m* = (12, … ,18) corresponding to February to August.

$Gate_{DE,m} = S_{14,DE,m-1} * Smolts_{DE,m-1}$

The rate $S_{14,DE,m}$ is composed of two components: survival through the Delta to Chipps Island (${}^{A}S_{14,DE,m}$) and survival from Chipps Island to Golden Gate (${}^{C}S_{11}$).

$S_{14,DE,m} = {}^{A}S_{14,DE,m} * {}^{C}S_{11}$

where ${}^{A}S_{14,DE,m} = SSM_{DE,m}$

Transition 15

Definition: Smolts that reared in the Bay migrate to the Golden Gate with an associated migration survival in months *m* = (12, … ,18) corresponding to February to August.

$Gate_{BA,m} = S_{15,BA} * Smolts_{BA,m-1}$

where $S_{15,BA}$ is the survival from the Bay habitat to the Golden Gate.

Transition 16

Definition: Smolts that reach the Golden Gate transition to the Gulf of the Farallones and the numbers in each month accumulate as a combination of the smolts in the Gulf the previous month and smolts that passed the Golden Gate in months *m* = (12, … ,20) corresponding to February to September.

$Gulf_{h,,m} = Gate_{h,m-1} * S_{ENTRY,\ m-1} + Gulf_{h,m-1} * S_{GULF,\ m-1}$

Where the survival rate $S_{ENTRY,\ m}$ is the survival rate during the month of ocean entry in the Gulf of the Farallones and the survival rate $S_{GULF,m}$ is the subsequent survival rate in month *m* after ocean entry.

The period of ocean entry can be a critical period of transition for salmonids and lack of available resources can have strong detrimental effects on the year class (Lindley et al. 2009). We therefore model the survival at ocean entry by using an indicator of ocean productivity as

$$\text{logit}(S_{ENTRY,m}) = B0_{ENTRY} + B1_{ENTRY} * OPI_{,m}$$

where $B0_{ENTRY}$ is a parameter describing the average survival rate , $OPI_{,m}$ is the ocean productivity index, and $B1_{ENTRY}$ is the coefficient describing the strength of the ocean productivity effect on ocean entry survival.

Finally, the transition to the ocean from all habitats includes a random effect term ε_y that is specific to each year *y* and is distributed as a normal random variable, that is $\varepsilon_y \sim N(0, \sigma_\varepsilon^2)$. The formulation used here is a biased-corrected form so the expected value of the random effects equals 0.

The total number of Age 1 fish entering the Gulf of the Farallones from all habitats arriving in a given month can be calculated by summing across each of the individual rearing areas. Furthermore, earlier arriving fish are retained in the Age 1 stage and an ocean survival rate is applied to those fish that were already in the Age 1 stage in the previous month. Fish arrive into the Age 1 stage in months *m* = (12, …, 20) corresponding to February through October.

$$Age1_{m} = Gulf_{UR,m} + Gulf_{LR,m} + Gulf_{FP,m} + Gulf_{DE,m} + Gulf_{BA,m} + Age1_{m-1} * S_{17}^{1/4}$$

Transition 17

Definition: Survival in the ocean from Age 1 to Age 2 (for Chinook that remain in the ocean)

$$Age2 = Age1_{m=21} * (1 - M_2) * S_{17}$$

where S_{17} is a model parameter representing the survival rate of Age 1 fish in the ocean to Age 2 and M_2 is a model parameter representing the maturation rate that leads to 2-year old spawners. The model transitions from a monthly time step (used for months 1 through 20) to an annual time step (used for Age 2, Age 3 and Age 4 fish) in this transition, thus the S_{17} survival represents a 4-month survival rate from 21 months to 24 months (November to February).

Transition 18

Definition: Maturation and migration for Age 2 males and females that will spawn as 2-year olds

$$Sp_{2,F} = Age1_{m=21} * S_{17} * M_2 * Fem_{Age2} * S_{sp2}$$
$$Sp_{2,M} = Age1_{m=21} * S_{17} * M_2 * (1 - Fem_{Age2}) * S_{sp2}$$

where S_{17} and M_2 are model parameters for maturation and survival as described in Transition 17. Fem_{Age2} is a model parameter representing the proportion of Age 2 spawners that are female, and S_{sp2} is a model parameter representing the natural survival rate of Age 2 spawners from the ocean to the spawning grounds.

Transition 19

Definition: Survival in the ocean from Age 2 to Age 3 (for Chinook that remain in the ocean)

$$Age3 = Age2 * (1 - I_3) * S_{19} * (1 - M_3)$$

where I_3 is the fishery impact rate for Age 3 fish, S_{19} is a model parameter representing natural survival rate for fish between Age 2 and Age 3, and M_3 is a model parameter representing maturation rate of Age 3 fish.

Transition 20

Definition: Maturation and migration for Age 3 males and females that will spawn as 3-year olds

$$Sp_{3,F} = Age2 * (1 - I_3) * S_{19} * M_3 * Fem_{Age3} * S_{sp3}$$
$$Sp_{3,M} = Age2 * (1 - I_3) * S_{19} * M_3 * (1 - Fem_{Age3}) * S_{sp3}$$

where I_3 is the Age 3 fishery impact rate, and M_3 and S_{19} are the Age 3 maturation and survival rates as described in Transition 19. Fem_{Age3} is a model parameter representing the proportion of Age 3 and 4 spawners that are female, and S_{sp3} is a model parameter representing the natural survival rate of Age 3 spawners from the ocean to the spawning grounds.

Transition 21
Definition: Maturation and migration for Age 3 males and females that will spawn as 4-year olds

$Sp_{4,F} = Age3 * (1- I_4) * S_{21} * Fem_{Age3} * S_{sp4}$
$Sp_{4,M} = Age3 * (1- I_4) * S_{21} * (1 - Fem_{Age3}) * S_{sp4}$

where I_4 is the Age 4 fishery impact rate, S_{21} is a model parameter representing survival rate from Age 3 to Age 4, Fem_{Age3} is a model parameter representing the proportion of Age 3 and 4 spawners that are female, and S_{sp4} is a model parameter representing the natural survival rate of Age 4 spawners from the ocean to the spawning grounds.

Transition 22
Definition: Number of eggs produced by spawners of Ages 2 – 4 in months m = (2, …, 6) corresponding to April to August.

$$Eggs_m = \frac{\sum_{j=2}^{4}(TSp_{j,F} - hat.f_j)P_{SP,m}V_{eggs,j}}{1 + \frac{\sum_{j=2}^{4}(TSp_{j,F} - hat.f_j)\,P_{SP,m}V_{eggs,j}}{K_{Sp,m}}}$$

where TSp_j are the total number of female spawners of age j = 2, 3, 4 (composed of both natural and hatchery origin), $V_{eggs,j}$ is the number of eggs per spawner of age j = 2, 3, 4, $K_{Sp,m}$ is the capacity of eggs in the spawning grounds per month, and $P_{SP,m}$ is the proportion of spawning that occurs in month m and is a function of April average temperature at Keswick Dam. Because the April temperature can vary among years, the monthly distribution varies as well to reflect observed patterns in spawn timing among the years from 1999 to 2012. Please see Appendix A for description of the analysis of historical patterns in spawn timing.

$TSp_{2,F} = Sp_{2,F}$

$TSp_{3,F} = Sp_{3,F} - hat.f$

$TSp_{4,F} = Sp_{4,F}$

$hat.f_j = 0.15 * Sp_3$ (min = 10; max = 60)

where $hat.f$ is the number of age-3 spawning females removed for use as hatchery broodstock, and $Sp_{j,Hatchery}$ for j = (2,3,4) is the spawners of age j hatchery origin, which are described below in the *Hatchery Origin Chinook* section.

Hatchery Origin Chinook

Transition 1H
Definition: Survival of hatchery fish from eggs to Age 2

$Age2_{Hatchery} = hat.f * 3000 * H_{S1}$

$H_{S1} = 2.3 * Age2_{Natural} / Fry_{Natural}$

where H_{S1} is the hatchery-origin survival rate from pre-smolt at release to Age 2 in the ocean, $Age2_{Natural}$ is the number of natural-origin Chinook that survived to Age 2 and remained in the ocean, and $Fry_{Natural}$ is the number of natural origin emerging Fry (see Transition 1 for Natural Origin Chinook). The multiplier of 3000 hatchery smolts per spawner was obtained from Winship et al. (2014). The multiplier of 2.3 was used to equate hatchery origin survival to the end of age 2 to natural origin survival to the end of age 2 as described in Winship et al. (2014).

Transition 2H

Definition: Maturation and spawning for hatchery origin Age 2

$Sp_{2,F,Hatchery} = Age2_{Hatchery} * M_2 * Fem_{Age2} * S_{sp2}$
$Sp_{2,M,Hatchery} = Age2_{Hatchery} * M_2 * (1 - Fem_{Age2}) * S_{sp2}$

where the coefficients are described under Transition 18.

Transition 3H

Definition: Survival of hatchery origin fish in the ocean from Age 2 to Age 3 (for Chinook that remain in the ocean)

$Age3_{Hatchery} = Age2_{Hatchery} * (1 - I_3) * S_{19} * (1 - M_3)$

where the coefficients are described under Transition 19.

Transition 4H

Definition: Maturation and spawning for hatchery origin Age 3

$Sp_{3,F,Hatchery} = Age2_{Hatchery} * (1 - I_3) * S_{19} * M_3 * Fem_{Age3} * S_{sp3}$
$Sp_{3,M,Hatchery} = Age2_{Hatchery} * (1 - I_3) * S_{19} * M_3 * (1 - Fem_{Age3}) * S_{sp3}$

where the coefficients are described under Transition 20.

Transition 5H

Definition: Survival and maturation rate for hatchery origin Age 4

$Sp_{4,F,Hatchery} = Age3_{Hatchery} * (1 - I_4) * S_{21} * Fem_{Age3} * S_{sp4}$
$Sp_{4,M,Hatchery} = Age_{Hatchery}\ 3\ (1 - I_4) * S_{21} * (1 - Fem_{Age3}) * S_{sp4}$

where the coefficients are described under Transition 21.

Fishery Dynamics

To simulate the winter-run population dynamics under alternative hydrologic scenarios, we include fishery dynamics that are consistent with a NMFS fishery control rule (NMFS 2012) (Figure 10). For each year of the simulation, the impact rate for age 3 (I_3) was calculated from the control rule by obtaining the 3-year trailing geometric average of spawner abundance. The age-4 impact rate (I_4) in that year was calculated as double the instantaneous age-3 impact rate (Winship et al. 2014).

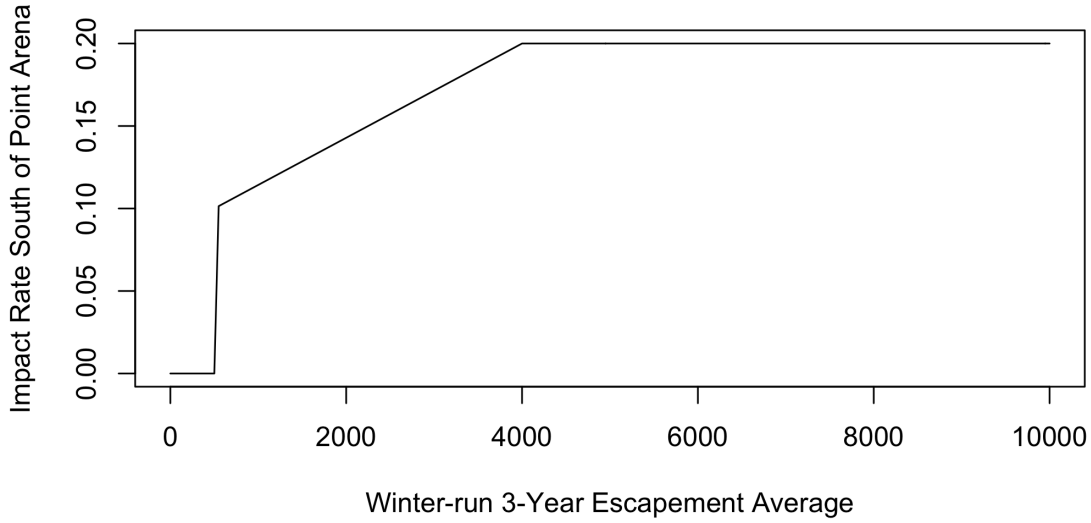

Figure 10. Fishery control rule determining the level of Age 3 impact rate as a function of trailing 3-year geometric mean in winter-run escapement.

III. Inputs to the Winter-run life-cycle model

Water Temperature

The life cycle model (LCM) incorporates monthly average temperature below Keswick Dam into the definition of egg to fry survival. The water temperature can be obtained from water quality gages on the Sacramento River (for model calibration) or from a forecasted water temperature model, such as the the Sacramento River Water Quality Model (SRWQM).

Fisheries

Estimates of impact rates on vulnerable age classes of Chinook salmon are computed as part of the Pacific Fisheries Management Council (PFMC) annual forecast of harvest rates and review of previous years' observed catch rates. For runs that are not actively targeted, such as winter-run and spring-run Chinook, analyses of coded wire tag (CWT) groups are used to infer impact rates for these races (e.g., O'Farrell et al. 2012).

Habitat Capacity

Juvenile salmonids rear in the mainstem Sacramento River, delta, floodplain, and bay habitats (Figure 1). The model incorporates the dynamics of rearing by using density-dependent movement out of habitats as a function of capacity for juvenile Chinook. The capacities of each of the habitats are calculated in each month using a series of habitat-specific models that relate habitat quality to a spatial capacity estimate for rearing juvenile Chinook salmon. Habitat quality is defined uniquely for each habitat type (mainstem, delta, etc.) with the goal of reflecting the unique habitat attributes in that specific habitat type. For example, the mainstem habitat quality is a function of velocity and depth (Beechie et al. 2005). Areas with vegetated cover along banks are preferred in other systems by Chinook salmon (Beamer et al. 2005, Semmens 2008), and areas associated with cover in the delta were assumed to be higher quality habitats because they provide protection from predators (Semmens 2008) and offer subsidies of terrestrial insect prey. In the bay, salinity is a factor that predicts suitable habitat, as fish monitoring data in both Skagit River and San Francisco Bay have shown high likelihood of fry presence in water with salinity less than 10 ppt. Higher quality habitats are capable of supporting higher densities of rearing Chinook salmon, with the range of densities being determined from studies in the Central Valley and in river systems in the Pacific Northwest where appropriate. Note, the current version of the model uses densities from the Skagit River, Washington, which are shown in Figure 11.

Defining habitat capacity. For each habitat type (mainstem, delta, and bay), capacity was calculated each month as:

$$K_i = \sum_{j=1}^{n} A_j d_j$$

where K_i is the capacity for a given habitat type i, n is the total number of categories describing habitat variation, A_j is the total habitat area for a particular category, and d_j is the maximum density attributable to a habitat of a specific category. Three variables were determined for each habitat, the ranges of each were divided into high and low quality, and all combinations were examined, resulting in a total of eight categories (2 x 2 x 2) of habitat quality for each habitat type (Table 1). The exception was mainstem habitats (Upper River, Lower River, and Yolo Bypass), which were subdivided into 4 (2x2) bins of habitat quality. Ranges of high and low habitat quality were based on published studies of habitat use by Chinook salmon fry across their range and examination of data collected by USFWS within the Sacramento-San Joaquin Delta and San Francisco Bay.

Defining maximum densities. Determining maximum densities for each combination of habitat variables is complicated by the fact that most river systems in the Central Valley are now hatchery-dominated with fish primed for outmigration. In addition, the Central Valley river system is at historically low natural abundance levels compared to expected or potential density levels. Because of this deficiency in the Central Valley system, salmon fry density data from the Skagit River system were used, which in contrast has very low hatchery inputs, has been monitored in mainstem, delta, and bay habitats, and exhibits evidence of reaching maximum density in years of high abundance (Greene et al. 2005; Beamer et al. 2005). These data from the Skagit River were compared with Central Valley density estimates calculated by USFWS. For each of these data sets, the upper 95

percentile levels of density defined a range of maximum density levels, assuming that the highest five percentile of density levels were sampling outliers. The comparison indicated that Skagit River values represented conservative estimates of maximum density (Figure 11).

Table 1. Habitat variables influencing capacity for each habitat type.

Habitat type	Variable	Habitat quality	Variable range
Mainstem & Bypass	Velocity	High	<= 0.15 m/s
		Low	> 0.15 m/s
	Depth	High	> 0.2 m, <= 1 m
		Low	<= 0.2 m, > 1 m
Delta	Channel type	High	Blind channels
		Low	Mainstem, distributaries, open water
	Depth	High	> 0.2 m, <= 1.5 m
		Low	<= 0.2 m, > 1.5 m
	Cover	High	Vegetated
		Low	Not vegetated
Bay	Shoreline type	High	Beaches, marshes, vegetated banks, tidal flats
		Low	Riprap, structures, rocky shores, exposed habitats
	Depth	High	> 0.2 m, <= 1.5 m
		Low	<= 0.2 m, > 1.5 m
	Salinity	High	< 10 ppt

Habitat type	Variable	Habitat quality	Variable range
		Low	>= 10 ppt

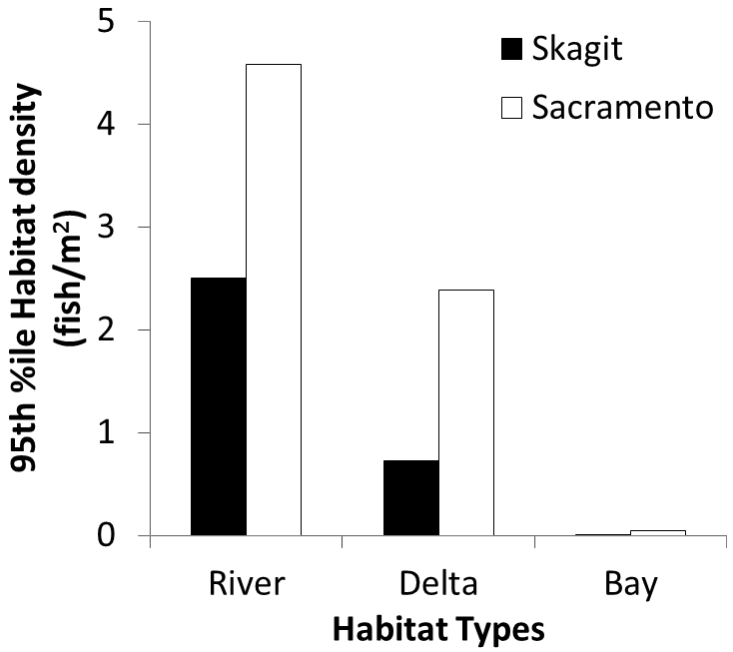

Figure 11. 95th percentile values of densities in river, delta, and bay habitats in the Skagit and Sacramento Rivers. Skagit data are based on electroshocking in mainstems and beach seining in delta and bay habitats (Beamer et al. 2005), while Sacramento data are based on beach seining across all habitat types (USFWS 2007).

Determining habitat areas. Two approaches were used to map the spatial extents of different combinations of habitat variables. To estimate river and Yolo Bypass capacities based on channel velocity and depth, a suite of HEC-RAS models at varying discharge values (2,000-200,000 ft^3/sec) were simulated on the Sacramento River and Yolo Bypass. The HEC-RAS geometry was based on a series of cross-sections that define locations surveyed in the mid-1990s at longitudinal intervals of approximately 500m. From the HEC-RAS output, the cross-sectional width of a given river reach was broken up into 45 lateral sections (i.e., cells), with the main channel composed of 25 cells and the banks composed of 20 cells (10 left and 10 right bank; example shown in Figure 12). Main channel and bank stations are defined in the original HEC-RAS model and denoted in Figure 12 with red cross-section stations. To estimate depth and velocity in each cell, we used the flow distribution methods outlined by HEC, which can be found at: https://www.hec.usace.army.mil/confluence/rasdocs/ras1dtechref/latest/overview-of-optional-capabilities/flow-distribution-calculations

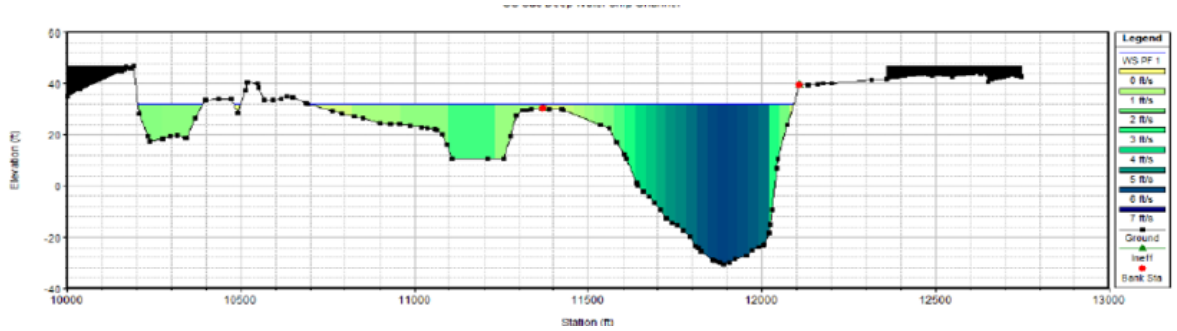

Figure 12: Example of method used to split up a HEC-RAS cross-sectional output into 45 lateral sections. Note that main channel locations are within the red cross-sections stations and bank locations are outside of the red cross-sections stations

At each lateral cell, the HEC-RAS simulated channel depth and velocity were grouped into one of the four habitat capacity categories described above. Each cell in the cross-section has a depth and velocity, and altering the flow changes the depth and velocity of a particular cell. The area of each cell that corresponded to a specific combination of velocity and depth category was tabulated for each mean monthly flow (extracted from CalSim results) associated with a cross-section. The appropriate density of Chinook salmon for each of the four categories was applied to each lateral cell by taking the product of area for a given preference and the 95th percentile density estimate for that preference. To arrive at a monthly capacity estimate for the Sacramento River and Yolo Bypass habitats, we summed the capacity estimates for each lateral and longitudinal cell in each habitat. Figure 13 shows how habitat capacity changes as a function of flow for the Sacramento River and Yolo Bypass.

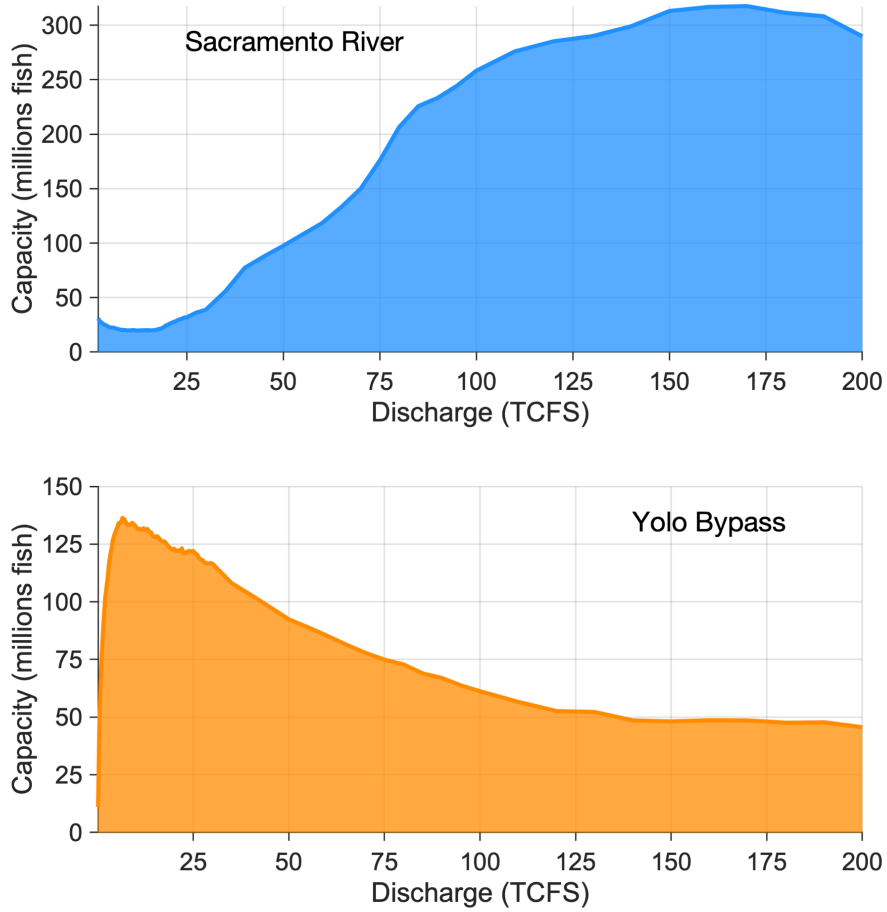

Figure 13: Habitat capacity to flow (thousand cfs) relationship for the Sacramento River and Yolo Bypass under the 95th percentile density estimate.

For the delta and bay, geographic data products were used to map habitat variables, including cover, shoreline type, salinity, and depth. Vector GIS files were converted to raster, and all habitat variables were mapped onto a common $10m^2$ grid. To obtain the spatial extent of channels and wetlands, National Wetland Inventory (NWI) data (USFWS 2006) were used in the delta, and Bay Area Aquatic Resource Inventory (BAARI) v 2.1 data (SFEI ASC 2017) were used in the bay. A geographic buffer was applied where required to ensure that the full extent of the channels were included, and a levee file (DWR 2018) was utilized to ensure that no inaccessible areas were included. For each cell, the habitat variables listed in Table 1 above were determined to be of high or low quality. Cover data were obtained from the Coastal Change Analysis Program (C-CAP) (NOAA OCM 2017). Areas that had vegetation (forested areas, scrub/shrub area, etc.) were considered high quality cover, and cells within 30 meters were marked as high-quality cover. Shoreline data were obtained from BAARI v 2.1 (SFEI ASC 2017) and the Environmental Sensitivity Index (NOAA OR&R 2017). Cells within marshes, tidal flats, and vegetated areas, and cells within 30 meters were marked as high quality, whereas areas near rip-rap, rocky areas, and exposed areas were marked as low quality.

For salinity, monthly X2 values, representing the distance from the Golden Gate Bridge to the 2 ppt isohaline position (Jassby et al. 1995), were obtained from CalSim simulations. X10 values were calculated as 75% of X2 values (Monismith et al. 2002, Jassby et al. 1995). Distance to the Golden Gate was mapped, and cells upstream of the X10 value were marked as high quality.

Water depth was calculated from bathymetric data (Wang et al. 2018) and water level from DSM2 simulations. Each cell was assigned to its corresponding DSM2 channel, and for each DSM2 channel, monthly median water level was calculated. This value was subtracted from the bathymetric measurement in order to obtain monthly water depth for each cell.

Blind tidal channels within wetland areas were not able to be mapped directly with the available data. Therefore, we estimated these areas using allometric relationships between tidal wetland areas and blind tidal channel areas. We tested allometric equations developed in the Skagit River by Beamer et al. (2005) and Hood (2007) to determine which equations were best suited to apply to the Central Valley and chose an allometric equation that returned conservative estimation results:

$$A_{btc} = 0.0024 * {A_w}^{1.56}$$

where A_{btc} is blind tidal channel area in hectares and A_w is wetland area in hectares. We also applied the minimum area requirement (0.94 ha) to form blind tidal channels in a wetland from Hood (2007). To ensure that habitat area was not double counted in wetland areas through the previously described mapping methods and the blind tidal channel calculation, the habitat area of each cell in tidal wetlands was reduced by the proportion of the area of the wetland that is blind tidal channel. Finally, the habitat areas from all cells, along with the habitat area from blind tidal channels, was summed in order to get the total monthly habitat areas for each of the eight habitat quality categories.

Enhanced Particle Tracking Model

The survival rate of juvenile Chinook salmon within and migrating through the Delta is modeled using the Enhanced Particle Tracking Model (ePTM) version 2.0 (Hereafter, ePTM v2). This rate is defined as the survival at Chipps Island of simulated juvenile salmon released at any location within the Delta. The ePTM v2 survival computation includes movement, orientation, holding and routing behaviors and predation mortality (Sridharan et al., in prep.). The ePTM v2 is based on the Delta Simulation Model II Particle Tracking Model (DSM2 PTM) developed by the Department of Water Resources (DWR), California. Model code and documentation for the ePTM v2 is hosted at https://github.com/cvclcm/ePTM_v2.

DSM2

The DSM2 PTM transports particles on a one-dimensional network representation of the Delta, driven by the flows computed by HYDRO, the hydrodynamic module of DSM2 written in FORTRAN (Anderson and Mierzwa, 2002). The DSM2 HYDRO module computes the flow and stage at different locations in the Delta by solving the cross-sectionally averaged one-dimensional shallow water wave equations on a network of links, continuously stirred tank reactors (CSTR) and nodes which respectively represent channels, flooded and leveed islands, floodplains and forebays, and channel junctions (Figure 14). River inflows and in-delta consumptive use flows are estimated from CALSIM, a water budget model for California. Gate operations are provided by DWR. Details of the numerical solution method can be found in DeLong et al. (1997) and a peer review of the model can be found in Sridharan et al. (2018). DSM2 HYDRO is typically run with a time step of 15 minutes to one hour.

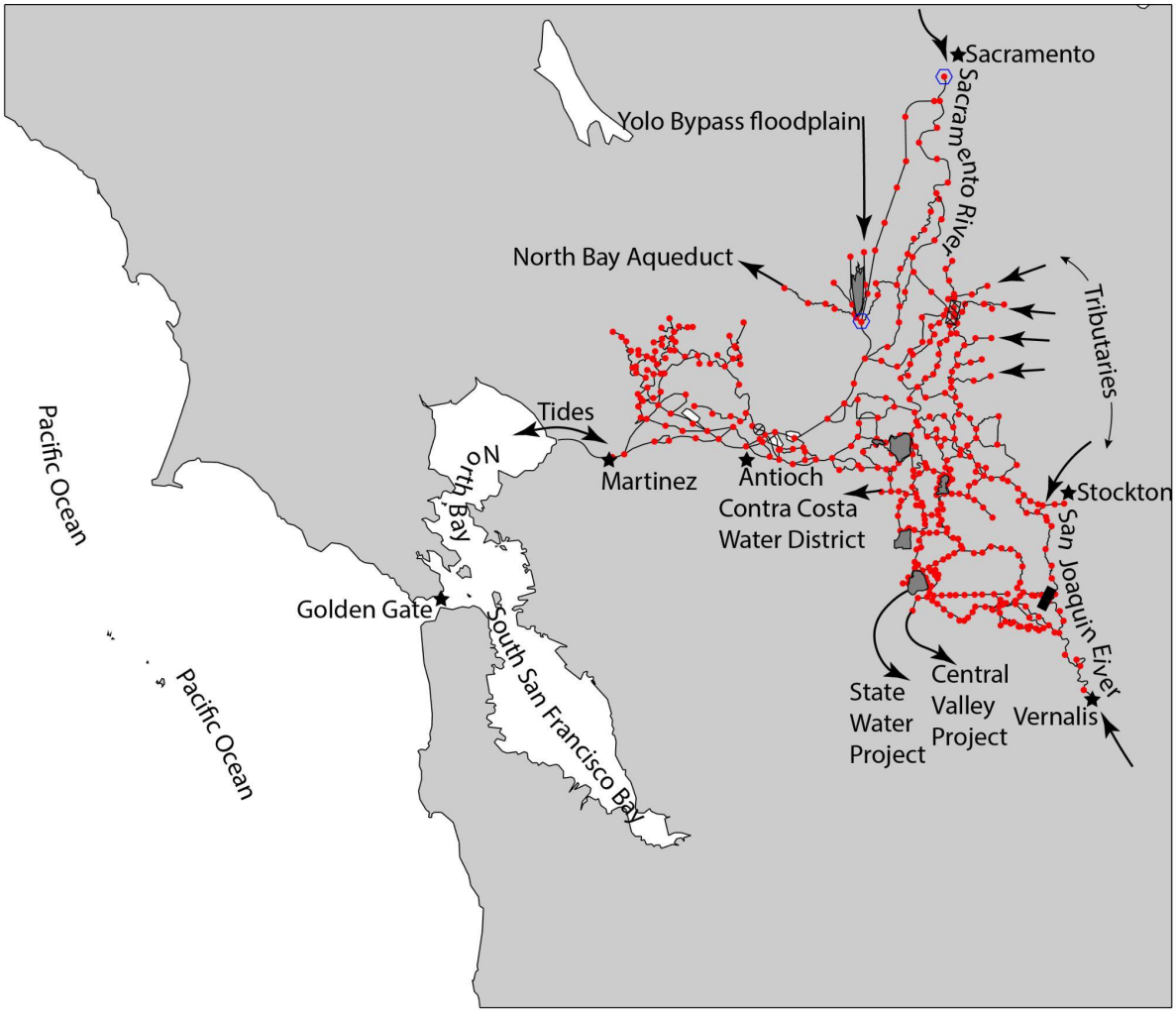

Figure 14. The Sacramento-San Joaquin Delta and the DSM2 grid. Arrows represent inflows and outflows. Grey lines, dark grey shaded regions and red dots respectively represent DSM2 channels, reservoirs and nodes. The Hatched box, crossed out circle and solid box respectively represent the Delta Cross Channel, the salinity control gate in Montezuma Slough and the temporary salmon passage barrier in Mossdale. The blue boxes represent nodes in which fry rearing in the Sacramento River and the Yolo Bypass floodplain are seeded as simulated smolts into the ePTM v2. Simulated smolt seeded in all other nodes represent fry rearing within the Delta.

The DSM2 PTM module, written in JAVA, is a pseudo three-dimensional model with a turbulent law of the wall logarithmic vertical velocity (Prandlt 1935) and a fourth order polynomial transverse velocity profile (Wilbur 2000) imposed onto the solved mean flows through a cross-section. The links are represented as rectangular prismoids whose cross-sections preserve the hydraulic radii and water column depth in the channels they represent. It uses constant cross-sectional eddy diffusivities in a zeroth-order turbulence closure to move particles laterally and vertically. Particles are advected in the streamwise direction with the hydrodynamic velocity at their locations and moved randomly in the lateral and vertical direction with the diffusivities at their locations using Forward Euler numerical integration. DSM2 PTM is capable of modeling about 5,000 particles (Kimmerer and Nobriga, 2008). It does not have any temporal interpolation of hydrodynamic quantities between DSM2 HYDRO time steps, and randomizes particles arriving at nodes and assigns them to new links based on the flow splits at the nodes. Their new cross-sectional positions are also

randomized. ePTM v2 builds on the basic framework of the DSM2 PTM by adopting conceptual and performance updates described in Sridharan et al. (2017) and adds behavior to simulated particles.

ePTM v2

The ePTM v2 adds juvenile salmon swimming behavior and predation mortality to the DSM2 PTM (Sridharan et al. in prep.). Apart from these additions, the ePTM v2 linearly interpolates all hydraulic and hydrodynamic quantities between DSM2 HYDRO time steps to account for simulated salmon movement within an ePTM v2 time substep. Broadly, the scope of the ePTM v2 can be summarized into its representation of the hydrodynamics, the fish behavior, and the mortality of simulated salmon.

Hydrodynamics

Simulated smolt trajectories are given by (Visser 1997)

$$\frac{dx}{dt} = u + u_S;\ \frac{dy}{dt} = R_y\sqrt{\frac{2}{r}\frac{\varepsilon_H}{\Delta t}} + \frac{d\varepsilon_H}{dy};\frac{dz}{dt} = R_z\sqrt{\frac{2}{r}\frac{\varepsilon_V}{\Delta t}} + \frac{d\varepsilon_V}{dz}$$

where u is the hydrodynamic velocity at the particle position, u_s is the swimming velocity, ε_H and ε_V are the lateral and vertical eddy diffusivities, Δt is the ePTM v2 timestep, R_Y and R_Z are uniform random variables between -1 and 1, r is the variance of a standard normal distribution and is equal to 1. In order to realistically represent fish movements, channel curvature has been included in ePTM v2.

The curvature of a channel is determined by fitting both a Theil-Sen robust linear regressor (Gilbert 1987), as well as a Chernov-Lesort robust circular regressor (Chernov, 2010). If the Pearson correlation coefficient value of the linear fit exceeds that of the circular fit, or if the estimated radius of curvature exceeds 10 Km, the channel is assumed as straight. The bend angle is computed as the ratio of the total distance along the river and the radius of curvature. Meanders occurring on a scale smaller than the channel length can be incorporated by refining the DSM2 model grid as needed.

For straight channels, we have (DWR, 1998):

$$u = Uf_Vf_H$$

$$f_V = 1 + \left(\frac{0.1}{\kappa}\right)\left[1 + ln\left(\frac{z}{H}\right)\right];\frac{z}{H} \geq 0.01 \text{ and } f_V = 0;\frac{z}{H} < 0.01$$

$$f_H = A + B\left(\frac{2y}{W}\right)^2 + C\left(\frac{2y}{W}\right)^4$$

where f_V and f_H are the water velocity profiles in the lateral and vertical dimensions, W and H are respectively the width and depth of the channel, U is the mean streamwise velocity, A, B and C are constants that can vary with the river, κ=0.41 is von Karman's constant, and the diffusion coefficients in the lateral and vertical dimension are

$$\varepsilon_H = C_THu^*;\ u^* = 0.1U$$

$$\varepsilon_V = \kappa \frac{z}{H}\left(1 - \frac{z}{H}\right)$$

$$\boldsymbol{\frac{d\varepsilon_V}{dz} = \frac{\kappa}{H}\left(1 - 2\frac{z}{H}\right)}$$

where C_T=0.6 is a constant and u^* is the friction velocity.

For curved channels, the experimental results of Gandhi et al. (2016) of turbulent open rectangular channel flow in around bends of varying curvature from a straight channel to up to 90° are used. For angles beyond 90°, we assume that the flow adjustment will not be significantly different (Blanckaert and De Vriend, 2004), and so we use the distribution at 90° itself. We use the best-fit regression of Gandhi et al. (2016) to their data to generate the flow profiles. Using the force balance between the turbulent eddy diffusivity and the shear stress by assuming a linear decay of the shear stress from its peak value at the channel banks to zero at the lateral position of peak flow defined from the left bank, y_{Max} (and similarly for the right bank),

$$\varepsilon_H \frac{du}{dy} = u^{*2}\left(1 - 2\frac{y}{y_{Max}}\right)$$

where $\frac{du}{dy}$ is obtained from the data, and smoothing the resulting profile of ε_H to remove spurious discontinuities, we get profiles of the flow and mixing terms. A mixed layer is implemented near the channel banks that is 20% of the width of the channel (Ross and Sharples 2004).

Time substeps are chosen to be 20 seconds. A simulated salmon leaves a given channel through its upstream or downstream end when its streamwise displacement during a time step exceeds the distance between its current position and the end of the channel. The channel bottom, banks and free surface are treated as fully reflecting boundaries.

Simulated salmon that enter reservoirs or flooded islands are held there over a random period between 0 and 24 hours and subsequently randomly released depending on the flow into a connecting channel.

Behavior

ePTM v2 is a spatially explicit model, in that behaviors of fish are allowed to vary spatially through the Delta domain. Such spatial variability is supported by numerous reports from the literature, and observations within the Delta that migrating smolts vary their behavior as they move closer to the ocean (McCleave 1978; Solomon 1978; Healey 1980; Moser et al. 1991; Lacroix and McCurdy 1996; McCormick et al. 1998; Moore et al. 1998; Miller and Sadro 2003; Lacroix et al. 2005; Hedger et al. 2008; Kelly and Klimley 2012; Chapman et al. 2013; DWR 2015; DWR 2016). The ePTM v2 incorporates five behaviors based on literature reviews and observations in the data (Sridharan et al. In prep) that include:

(i) active swimming,

(ii) orientation towards or away from the ocean,

(iii) Holding against the flow,

(iv) routing at channel junctions, and

(v) mortality due to predation.

All these behaviors are allowed to vary at the scale of the regions defined in Figure 15.

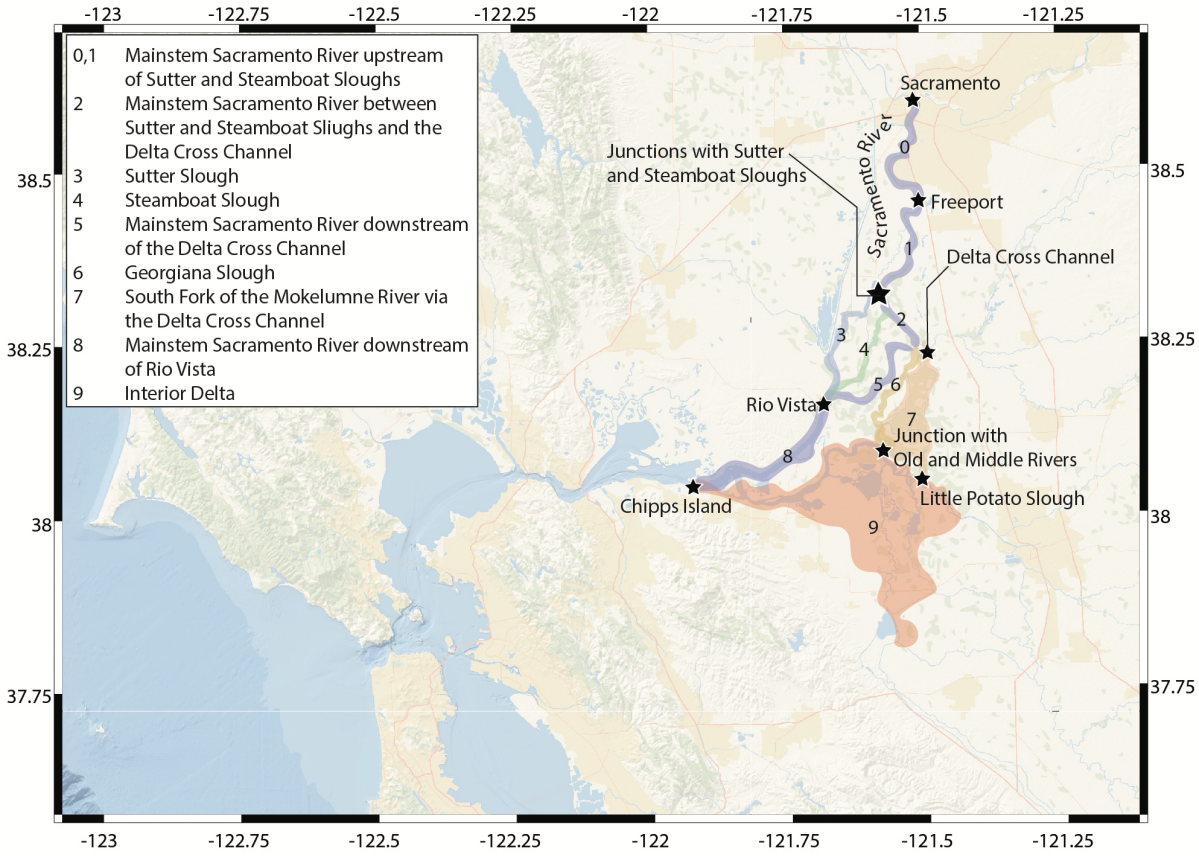

Figure 15. Calibration regions for ePTM v2 behaviors. Colors uniquely identify the different calibration regions. All blue colored regions indicate the mainstem Sacramento River.

Active swimming

A biological swimming velocity is added to the water velocity at the location of the simulated salmon at each time step. Simulated salmon can swim in the along stream direction with swimming speeds that are drawn from a lognormal distribution $lnN(\mu, \sigma)$ in which

$$\mu = 2ln(U_S) - \frac{1}{2}ln(\sigma_s^2 + U_S^2) \text{ and } \sigma = \sqrt{ln(\sigma_s^2 + U_S^2) - 2ln(U_S)}.$$

Here, the mean and standard deviation of observed swimming speeds are respectively U_S and σ_s. To ensure that randomly drawn swimming speeds remain within the range of biologically plausible speeds, the log-normal distribution is truncated at the 95th percentile and rescaled appropriately.

Orientation

In the *ePTM v2*, a probabilistic swimming direction rule determines each simulated salmon's swimming direction at each timestep. The swimming direction is influenced by the migrant's previous swimming direction, as well as the flow it experiences as follows. If a Bernoulli draw to determine persistence results in a zero, the fish's swimming direction is determined by a stochastic decision based on the flow it experiences, $\frac{|u|}{|U|}$, during the current timestep as

$$p_{SWF} = 0.5 + (p_{Rheo} - 0.5)\left[\frac{1}{1 + e^{-\left(c + b\ln\frac{|u|}{|U|}\right)}}\right]$$

Here, U is the mean flow observed in the Delta from 1962 to 2014, and is used to simply normalize the values of u. There is no assumption that the fish somehow knows what U is. p_{SWF} is the probability of orienting with the flow, and p_{Rheo}, c and b are calibration constants.

For positive values of c and small values of b, fish response to flow signals is sluggish in that only at very strong water speeds will fish make decisions that are not random. For negative values of c and large values of b, fish responses to small changes in the flow will be very sharp, i.e., decisions will be nonrandom even for weak flows. The p_{Rheo} parameter determines if the fish is likely to orient with or against the flow. If $p_{Rheo} \approx 0$, then as flows become stronger, fish will have a tendency to orient against the flow. If $p_{Rheo} \approx 0.5$, orientation decisions will be random. If 1, then as flows become stronger, fish will have a tendency to orient with the flow.

Holding Position Relative to Flow

The simulated salmon also holds position via Selective Tidal-Stream Transport (STST) (Gibson 2003), a hypothesis for optimal energy expenditure while achieving average travel speeds greater than the average flow velocity in tidal regions. During the ebb phase of the tide, the simulated salmon allow themselves to be advected. On a flood tide, when the upstream flow exceeds some threshold, they hold position with a certain probability (Liao, 2007). The ePTM v2 also parameterizes diel swimming behavior (Chapman et al. 2013) by assigning a probability of swimming during the light hours.

Routing at Channel Junctions

Anadromous salmonids often make decisions on which route to adopt (Gleichauf et al. 2014; Perry et al. 2014; Hance et al. 2021). Sridharan et al. (2017) demonstrated the importance of correctly representing the movement of simulated fish through channel junctions. In the ePTM v2, we allow fish to move into downstream channels at junctions depending on their lateral position relative to the critical streakline (Perry et al. 2014), also known as the bifurcating streamline.

When a simulated migrant reaches the end of a channel within a sub-timestep, the routing process is invoked, and it is moved into a downstream channel or open water body. Subsequently, the remaining trajectory computation is completed for that sub-timestep in the new channel beginning from a random cross-sectional position in the new channel. If the fish enters an open water body, it waits for a random length of time between zero seconds and one day and then leaves the open water body

randomly into a connecting downstream channel. This mechanism ensures that fish move through the system in a manner consistent with the critical streakline hypothesis, while allowing for random lateral and vertical movements to occur within the time taken to move through the junction.

When a simulated fish reaches a channel junction, it is assigned to one channel or the other based on its lateral location relative to the location of the critical streakline (see Perry et a. 2018 or Sridharan et al. 2017 for an explanation of how the location of the critical streakline is calculated). Thus, the routing module does not contain any fitted free parameters. When there are junctions with more than three channels, a tree-search algorithm is implemented in which the junction is dynamically deconstructed into a sequence of bifurcations with two downstream channels from the point of view of the channel from which the fish enters the junction. Recently, nonphysical barriers and fish guidance mechanisms such as bubble curtains and strobe lights have been investigated to steer fish into favorable migration routes in the Delta (Perry et al. 2014; DWR 2015; DWR 2016). Such mechanisms can be represented in the model as a "particle filter," which restricts a fraction of fish from entering a specific waterbody. Any number of filters can be applied at any junction in the system domain with specified efficiencies. Such filters will simply divert the fraction of fish into the next nearest downstream channel that does not have a filter.

Predation Mortality

The ePTM v2 adds predator-induced mortality according to the XT model (Anderson et al. 2005). The probability of a simulated salmon surviving passage through a region, S, is as follows:

$$S = e^{-\left(\frac{1}{\lambda}\sqrt{x^2+\omega^2 t^2}\right)}$$

where x is the distance traveled and t is the travel time. The mean free path, λ, is

$$\lambda = \frac{1}{\rho \pi r^2}$$

where ρ is the density of predators and r is the encounter distance. The term ω is the random component of prey speed. The implementation of the XT model in the ePTM v2 involves recording the x and t for each channel that a simulated salmon traverses in a given 15-minute time step. A survival probability for each of these sub time steps is then calculated using the λ values for the individual channels. The overall probability that the simulated salmon survives the 15-minute time step is the product of the survival probabilities of the sub time steps, i.e.:

$$S = \prod_{i=1}^{n} e^{-\left(\frac{1}{\lambda_i}\sqrt{x_i^2+\omega_i^2 t_i^2}\right)}$$

where n is the number of channels that the simulated salmon traversed during the time step, x_i is the distance traveled in channel i, t_i is the time spent in channel i, and λ_i and ω_i are the channel-specific mortality parameters. In the ePTM v2, only the parameters λ_i and ω_i are specified explicitly (Table 2).

Model Calibration and Validation

The parameters of the ePTM v2 were estimated from tagging studies of late Fall-run Chinook salmon (2006-2010) released in the Sacramento River and passing through the Delta (Perry et al. 2010). This tagging study included a total of 1,591 tagged late-Fall juveniles that were released in the Sacramento River in eight release groups over the five year period. These fish were tagged with VEMCO V5 acoustic tags and were tracked through the system at hydroacoustic receiver arrays (Figure 15). By tracking fish through these receiver arrays, their passage through the Delta could be naturally quantified along the nine regions connected by key river junctions (Figure 15). A Cormack-Jolly-Seber (CJS) mark-recapture model was fit within a hierarchical Bayesian framework to concurrently estimate detection, routing and survival probabilities through the different regions (Perry et al. 2010; Perry et al. 2018). In addition to the region-scale survival estimates, the data was also processed (Russ Perry, personal communication) to include fist detection times for each fish whenever it was detected at a receiver array.

To estimate all 99 ePTM v2 parameters (11 parameters in each of the nine calibration regions) from the calibration data described above, the following steps were applied. First, for each parameter, bounds were identified on the permissible range of parameter values to constrain the parameter search space. These bounds were set based on a thorough review of the literature including laboratory experiments and field data, and reasonable biological expectations when insights could not be gained from the literature. Then, a four-stage calibration process was incorporated. In this process, first, it was determined that the movement (swimming, orientation and holding) parameters could be fit independently of the survival parameters (Sridharan et al. In prep.). Second, a coarse grid search on a large number of movement parameter values was performed to narrow in on the best local optima defined within a multiobjective optimization framework. Third, the parameter space was zoomed into in the neighborhoods of the best local optima to perform a fine grid search using the multiobjective optimization framework to identify the global optimum movement parameter values. Fourth, the movement parameters were held at their optimum values and performed a grid search over the survival parameters to find the optimum values of these parameters. These values are listed in Table 2. In lieu of an uncertainty analysis, a sensitivity analysis was performed on the parameters (Sridharan et al. In prep.). The calibrated model was also validated with out-of-sample data using Juvenile Salmon Acoustic Telemetry System (JSATS) tagged Chinook smolts (see Sridharan et al. In prep.). Both the calibration and validation results are archived in the ePTM v2 GitHub repository.

Table 2. ePTM v2 model parameters

Behavior	Description	Parameter	Search bounds	Optimal value	Evidence
Swimming	Mean swimming speed	U_S	[0,0.5m/s]	region 1: 0.50 m/s region 2: 0.37 m/s region 3: 0.32 m/s region 4: 0.43 m/s region 5: 0.50 m/s region 6: 0.15 m/s region 7: 0.35 m/s	Swimming speeds observed by Dougan 1993; Anglea et al. 2004; Brown et al. 2006;

Behavior	Description	Parameter	Search bounds	Optimal value	Evidence
				region 8: 0.39 m/s region 9: 0.33 m/s	Walker et al. 2016; Lehman et al. 2017
	Standard deviation of swimming speed	σ_S	[0,0.5m/s]	region 1: 0.16 m/s region 2: 0.47 m/s region 3: 0.45 m/s region 4: 0.43 m/s region 5: 0.01 m/s region 6: 0.32 m/s region 7: 0.01 m/s region 8: 0.43 m/s region 9: 0.44 m/s	Swimming speeds observed by Dougan 1993; Anglea et al. 2004; Brown et al. 2006; Walker et al. 2016; Lehman et al. 2017
Orientation	Probability of memory persistence	$p_{Persistence}$	[0,1]	region 1: 0.81 region 2: 0.97 region 3: 0.86 region 4: 0.78 region 5: 0.61 region 6: 0.87 region 7: 0.37 region 8: 0.32 region 9: 0.71	Normal probability range
	Probability of rheotaxis	p_{Rheo}	[0,1]	region 1: 0.38 region 2: 0.15 region 3: 0.05 region 4: 0.17 region 5: 0.03 region 6: 0.40 region 7: 0.11 region 8: 0.90 region 9: 0.41	Normal probability range
	Half-saturation point of logistic function	c	[-10,10]	region 1: 7.55 region 2: 5.91 region 3: 2.09 region 4: 8.19 region 5: -0.19 region 6: 0.91 region 7: 2.68 region 8: -2.53 region 9: -0.55	Encompassing various shapes of logistic curve for 95% of flows observed in the Delta
	Slope of logistic function	b	[0,10]	region 1: 5.89 region 2: 5.34 region 3: 0.88 region 4: 6.40	Encompassing various shapes of logistic curve for 95%

Behavior	Description	Parameter	Search bounds	Optimal value	Evidence
				region 5: 5.77 region 6: 6.02 region 7: 4.47 region 8: 7.16 region 9: 8.56	of flows observed in the Delta
Holding	Landward holding threshold water velocity	u_H	[0,1.5m/s]	region 1: 0.70 m/s region 2: 1.44 m/s region 3: 1.17 m/s region 4: 1.26 m/s region 5: 0.70 m/s region 6: 0.67 m/s region 7: 1.48 m/s region 8: 1.13 m/s region 9: 1.14 m/s	0 to peak tidal water velocity computed by DSM2 between 1962 and 2014
	Holding probability	p_H	[0,1]	region 1: 0.80 region 2: 0.58 region 3: 0.65 region 4: 0.33 region 5: 0.60 region 6: 0.66 region 7: 0.96 region 8: 0.73 region 9: 0.32	Normal probability range
	Daytime swimming probability	p_{DS}	[0,1]	region 1: 0.63 region 2: 0.11 region 3: 0.62 region 4: 0.01 region 5: 0.70 region 6: 0.00 region 7: 0.16 region 8: 0.62 region 9: 0.68	Probabilities reported in Chapman et al. (2013)
Mortality	Mean free path length	λ	[10,1000Km]	region 1: 753 Km region 2: 629 Km region 3: 1000 Km region 4: 876 Km region 5: 1000 Km region 6: 794 Km region 7: 711 Km region 8: 918 Km region 9: 753 Km	Synthetic survival model predictions encompassing range of survivals predicted in Perry et al. (2018)
	Random prey speed	ω	[0,2m/s]	region 1: 0.58 m/s region 2: 0.92 m/s region 3: 1.42 m/s	Synthetic survival model predictions

Behavior	Description	Parameter	Search bounds	Optimal value	Evidence
				region 4: 0.08 m/s region 5: 0.08 m/s region 6: 0.75 m/s region 7: 0.50 m/s region 8: 0.00 m/s region 9: 0.00 m/s	encompassing range of survivals predicted in Perry et al. (2018)

Spatial Patterns in Calibrated Model Parameters

A detailed analysis of the spatial patterns in the calibrated behaviors will be presented in Sridharan et al. (In prep.); here we merely present a synopsis.

For the active swimming component of the model, in the North Delta regions upstream of Rio Vista (regions 1 to 5) and the confluence of Georgiana Slough with the San Joaquin River (region 6), simulated salmon actively swim against strong non-reversing riverine flows. In the more tidally reversing Central (region 7), Western (region 8) and South Delta (region 9), fish execute either movements that are directed weakly with or against the flow. Together, these parameters result in actions by the fish that increase migration rate and dispersion with increasing proximity to the ocean, as is observed in the acoustic telemetry datasets.

The orientation and holding parameters allow simulated fish to hold position against the flow, and even swim against the flow during the landward flood phase of the tide. In the regions where the oceanward flow does not reverse, the net effect is to orient fish against the flow much more often than with the flow. In the parts of the system where the flow reverses tidally, fish orientations are more likely to switch between with and against the flow. During strong landward flow reversals, fish approximately maintain position relative to the flow. The probability of swimming during the day is consistent with the values obtained in this region from acoustic telemetry experiments reported in Chapman et al. (2013).

The mean-free path length and random prey speed result in an overall increasing likelihood of survival through the downstream regions of the system. In the Delta, predator densities are generally higher in the fresh Sacramento and San Joaquin River waters than in the Western, more salty parts of the system (Michel 2020). The spatial distribution of the mortality parameters thus mirror a lower likelihood of predation in the Western Delta than in the Eastern Delta.

ePTM v2 Application

For a given climate change, water operations or restoration scenario, ePTM v2 is used in conjunction with the habitat capacity model, and the USGS juvenile Chinook beach seine abundance model (Perry et al. 2016) to predict mean and variance in monthly survivals for fish rearing in the Sacramento River, the Yolo Bypass floodplain, and in the interior Delta. In a multi-year scenario, 50 simulated salmon are released uniformly over the first month of each simulation at each DSM2 node East of Chipps Island and the survivals estimated from each of these releases is bootstrapped into 1,000 survival samples. Each ePTM v2 simulation for fish released in a given month is run for three

months to allow fish to reach their ultimate fate, and survival is reported based on fish that arrive at Chipps Island. River- and floodplain-rearing smolt survivals are reported as the survivals estimated by releasing fish at the relevant nodes (Figure 14), while Delta-rearing smolt survivals are reported by reweighting the survivals in the target month estimated from in-Delta node releases using the carrying capacity associated with each Delta node three months prior to the release month. The carrying capacities are estimated three months prior to the release month to reflect the fact that rearing juveniles would have selected a habitat patch to rear based on the conditions at the time that they arrived there. This reweighting assumes an ideal free distribution of fish in the Delta. The reweighting is done as follows:

First, the density of smolt abundance per unit area in four different regions representing the Delta [regions 2 through 5 in Figure 16 adapted from an United States Fish and Wildlife Service memo (Barnard 2019)] are estimated using the USGS abundance model for each month in each year between 2000 and 2020.

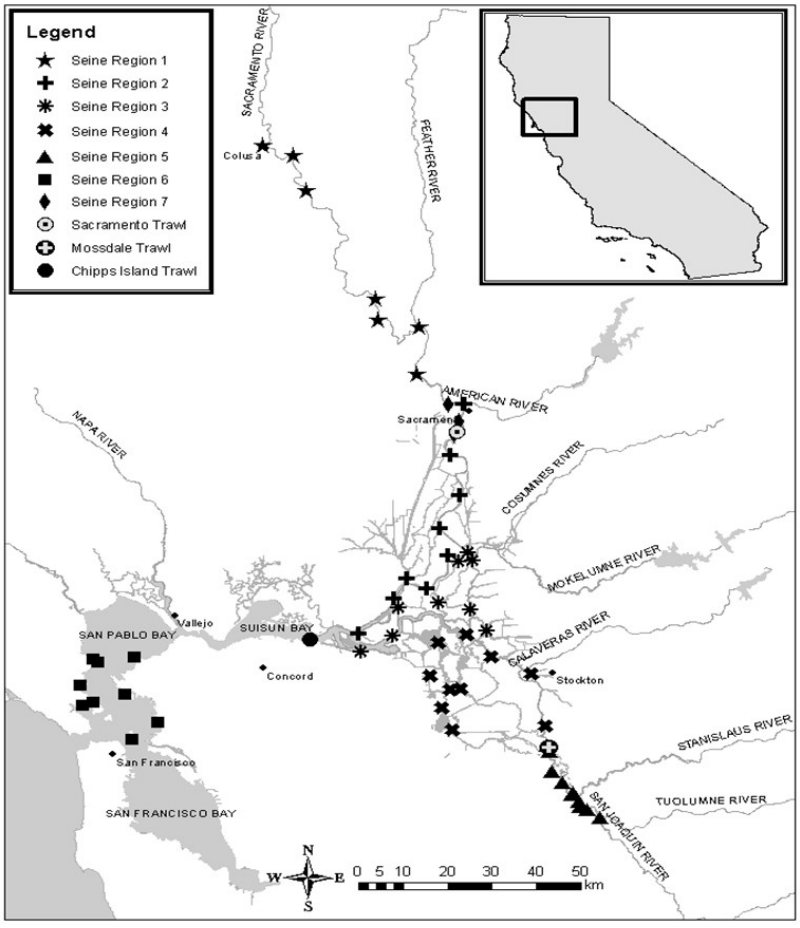

Figure 16. Beach-seine based abundance density model regions. Regions 2, 3, 4 and 5 are used in the habitat capacity-based reweighting scheme. From Barnard 2019.

Then, for each month in each year in the scenario that is being evaluated, the density in each region is estimated by using a K-nearest neighbors model which sets the abundance in a given month as

$$d_{m,r} = \frac{\sum_{j=1}^{K} d_{j,Historical,i}}{K}$$

where $d_{m,i}$ is the density in region r in month m of the scenario, $d_{j,Historical,i}$ is the density in that region in the jth month of K months within the historical period that are within the cluster of months closest to the mth month hydrologically. The hydrological similarity index used to cluster historical months is given by the Euclidean distance between the hydrologic conditions representative of a given region, which are

Region 1 based on Sacramento River flow: $\sqrt{\left(Q_{Sac,m} - Q_{Sac,j}\right)^2}$

Region 2 based on Sacramento River flow and Delta Cross Channel operation:
$\sqrt{\left(Q_{Sac,m} - Q_{Sac,j}\right)^2 + \left(Q_{DCC,m} - Q_{DCC,j}\right)^2}$

Region 3 based on Sacramento River flow and Delta Cross Channel operation:
$\sqrt{\left(Q_{Sac,m} - Q_{Sac,j}\right)^2 + \left(Q_{DCC,m} - Q_{DCC,j}\right)^2}$

Region 4 based on San Joaquin River flow: $\sqrt{\left(Q_{SJR,m} - Q_{SJR,j}\right)^2}$

and, w_j is the inverse Euclidean distance between the hydrologic conditions representative of a given region within the cluster of points closest to the month m. The number of clusters is dynamically determined by minimizing the sum of squared errors obtained by successively leaving one month out of the historical dataset. These errors are the sum of the Euclidean separation between a training point and the sum of other points in a cluster weighted by the inverse Euclidean separation between those points and the training point.

Second, the area within each of the eight habitat classes, c, associated with a node, i, with l connecting channels is given by

$$a_{i,c} = \frac{1}{2}\sum_{j=1}^{l} a_{i,c}$$

The density associated with each habitat class is given by d_c.

Third, the weight associated with each region in the Delta is estimated as

$$w_r = \frac{\sum_{c=1}^{8} d_c\left(\sum_{i=1}^{n} a_{i,c}\right)}{\sum_{r=1}^{4} w_r}$$

This formula ensures that regions with predominantly poor habitats are weighted lower as locations where fish would likely rear. As the USGS density model collapses beach seine data into the four regions depicted in Figure 16 and finer resolution is not possible, the assumption here is that the carrying capacity associated with each node within a given region is identical.

Fourth, the carrying capacity (K) of each region is then given by

$$K_{m,r} = w_r d_{m,r}$$

Finally, the reweighted survival from a given DSM2 node i in month m is given as

$$S_{m,i,Reweighted} = \frac{K_{m-3,r}}{\sum_{r=1}^{4} K_{m-3,r}} S_{m,i}$$

Caveats

Currently, the ePTM v2 can represent either the current geomorphology and hydrology of the Delta (Current), a historic representation of the Delta before Liberty Island flooded (Historic), or any other configuration representing restoration actions or other water operations. We note that in order to investigate these alternate configurations, some effort would be required to set up the overarching CALSIM simulations and the Delta hydrodynamics DSM2 model. The development of these models for specific scenarios is currently beyond the scope of the LCM team. The ePTM v2 results are based on a simplified one-dimensional network representation of the Delta, and hence do not account for complex geo-morphological and hydrodynamic transport and mixing phenomena such as tide induced chaotic dispersion, wind generated transport and gravitational circulation. The ePTM v2 results do not include the effects of environmental stressors such as water quality, temperature, nutrients, channel scale, temporal variability in predation dynamics, and foraging behavior or energy management dynamics. There is a significant data gap in addressing more complex spatio-temporal patterns in biological behavior and habitat interactions, as well as a need for easy model deployment and speed, so the ePTM v2 parameterizes only simple hypotheses about these effects.

Cloud-based Implementation of ePTM v2 for Tractable Scenario Evaluation

In a typical application of the WRLCM for evaluation of a proposed project or water management scenario, the ePTM v2 is used to generate monthly survival estimates across multiple decades. The resampling procedure described above requires survival estimates for smolts originating throughout the Delta for every year and month, which implies that a large number of ePTM v2 simulations are required for a single scenario evaluation.

For example, a typical scenario evaluation could span 90 years and eight months per year, for a total of 720 year-month combinations. The exact number of ePTM v2 insertion nodes depends on the DSM2 grid, which may vary by scenario, but there are approximately 370 relevant insertion nodes east of Chipps Island. Therefore, the example scenario evaluation would require approximately 266,400 simulations (90 years x 8 months x 370 simulations/year-month). A single ePTM v2 simulation with 50 SJS requires on the order of one minute to complete. Performing all of the required simulations on a single machine would take approximately 1.65 X 10^7 seconds, or 190 days.

Given that the elapsed real time required to complete these ePTM v2 simulations on a single machine would be prohibitive, we have deployed the ePTM v2 on the Amazon Web Services (AWS) cloud computing platform to allow for massively parallel computation. Using AWS, we are able to distribute the ePTM v2 simulations across hundreds of instances (virtual machines), allowing completion of a scenario evaluation in less than a day of elapsed real time.

We employed three primary components of AWS to implement the cloud-based ePTM v2 workflow. Simulations are performed using Elastic Cloud Compute (EC2) instances. Communication between a local machine and the EC2 instances (e.g., for scheduling jobs and downloading metadata for the

completed jobs) is implemented via the Simple Queue Service (SQS). ePTM v2 outputs from the EC2 instances are stored using Simple Storage Service (S3) buckets.

Creating virtual machines on EC2 requires an Amazon Machine Image (AMI), which is essentially a template that can be used to spawn one or more EC2 instances. It can be thought of as an image of a single computer that can be copied any number of times to create multiple, identical, virtual computers running in the cloud. The AMI specifies the operating system, all of the installed software, and other software configuration details. The same AMI can be used to launch EC2 instances with a variety of hardware configurations, meaning that a more or less powerful hardware configuration can be selected as needed at runtime.

For the ePTM v2, we created a custom AMI based on Windows and the x86_64 platform with the ePTM v2 and all required supporting software installed. The AMI was configured to automatically log in and begin polling SQS for available jobs upon launch, and to automatically terminate after a set period of time with no new jobs. For typical applications, we use the c5.large EC2 instance type, which is a compute-optimized instance with 2 virtual CPUs (vCPUs) and 4 GiB of memory.

We used a series of Python scripts, running on both a local machine and the cloud instances, to implement the workflow. The workflow includes scheduling the jobs from the local machine, polling the job queues on the cloud instances, downloading the ePTM v2 outputs to the local machine, and post-processing the results. Interaction with AWS is accomplished using the Boto3 AWS Software Development Kit (SDK) for Python.

Each ePTM v2 simulation provides a survival estimate for SJS inserted into a particular DSM2 node for a given year and month. To obtain survival estimates representing the entire month, we insert 50 SJS with insertion dates and times distributed uniformly throughout the specified month. For each SJS, the ePTM v2 calculates a survival probability in each time step, so the cumulative survival probability from the insertion location to the Delta exit at Chipps Island is the product of the survival probabilities for the individual time steps. Survival probabilities for SJS that did not pass Chipps Island are assumed to be zero.

Summarizing, the standard workflow for running the ePTM v2 on AWS includes the following steps:

· use a Python script on a local machine to post jobs on SQS for all years, months, and insertion nodes required for the scenario evaluation

· launch up to hundreds of c5.large EC2 instances using a custom Windows-based AMI configured to automatically log in, poll the SQS job queue, claim a particular job, perform the ePTM v2 simulation, save the run metadata to the SQS queue, and save the raw ePTM v2 outputs to an S3 bucket

· after all scheduled simulations are complete, use a Python script to download the raw ePTM v2 outputs to a local machine for post-processing

· run a Python post-processing script to quality assure (QA) the ePTM v2 outputs and perform bootstrap resampling

IV. Model Calibration

The WRLCM framework is flexible in that it may be used to generate many different trajectories of abundance and spatial patterns of habitat use by varying the parameters of the model. The WRLCM should reflect historical trends and spatial patterns in abundance, however. As a result, we calibrated the WRLCM to multiple winter-run abundance indices by fixing some model parameters and estimating other parameters with a statistical fitting algorithm.

One goal of the WRLCM was to construct a model that was sensitive to alternative hydro management actions in the Central Valley; thus the model was structured such that it is sensitive to hydrologic drivers. An unintended consequence of this approach is that the statistical properties of the model are not optimal. In particular, some model parameters are not uniquely identifiable; that is, the same abundance can occur through several different parameter combinations. Because this property of the LCM makes statistical estimation difficult, the values of some parameters must be constrained using biological information, previous studies, or expert opinion, so that other parameters can be estimated. We provide the parameters that were constrained and provide justification for their values before moving to the statistical estimation of the remaining parameters.

Fixed Parameters and Their Justifications

Spawn Timing Parameters

Historically, the spawning of winter-run Chinook has not been uniform among the months April to August. Instead, higher proportions of winter-run spawned in June and July relative to April, May, and August. In addition, the proportions of winter-run that spawned in each month were not constant across years, but instead varied yearly. We analyzed the historical proportion of spawning among each month from 2003 – 2014 using carcass counts (assuming a 2 week period between spawning and senescence), and estimated the proportion of winter-run spawning in each month as a function of April temperatures at Keswick (Appendix A). We compared this model to one that used a static proportion among years, and found that the model based on April temperatures outperformed the static model. The general relationship identified through this multinomial regression model was that hotter April temperatures caused later initiation of spawning in winter-run Chinook. This may be explained mechanistically if the female spawners were laying their eggs to target an emergence time. Hotter temperatures in April indicated that a shorter incubation window was needed, whereas cooler temperatures indicated a longer incubation window. Please see Appendix A for additional information on this analysis.

These equations provided a method of shifting spawning distribution among months as a function of April temperatures (Table 3 and Appendix A). The April water temperatures were standardized in the analysis and thus need to be standardized for use in the simulation model (mean = 10.00 C, standard deviation = 0.70).

Table 3. Parameter values related to monthly spawn timing (SD = standard deviation).

Parameter	Mean	SD	Description
$B0_{Apr}$	-4.145	0.060	Intercept for proportion of spawners in April
$B1_{Apr}$	0.0538	0.062	Effect of temperature on proportion of spawners in April
$B0_{May}$	-1.796	0.020	Intercept for proportion of spawners in May
$B1_{May}$	-0.2031	0.020	Effect of temperature on proportion of spawners in May
$B0_{Jul}$	-0.332	0.012	Intercept for proportion of spawners in July
$B1_{Jul}$	0.3852	0.012	Effect of temperature on proportion of spawners in July
$B0_{Aug}$	-3.443	0.044	Intercept for proportion of spawners in August
$B1_{Aug}$	0.7921	0.045	Effect of temperature on proportion of spawners in August

Tidal Fry and Fry Related Parameters

Winter-run Chinook generally have not had a high tidal fry proportion (on the order of less than 5%). Furthermore, the location of tidal fry has varied among years, and they have been susceptible to movement downstream in the Sacramento River under high flow conditions (Pat Brandes, USFWS *personal communication*). The WRLCM parameters for the tidal fry and fry stages reflected these assumptions (Table 4).

Table 4. Fixed parameter values related to the tidal fry and fry stage.

Parameter	Value	Description
$t.crit$	12.0	Temperature at which thermal morality initiates in the egg to emerging fry survival in Transition 1. Value of 12.0 obtained from Martin et al. (2017).
$B1_A$	0.0	Effect of covariate on background survival in egg to emerging fry survival in Transition 1. A value of 0 indicates no annual variability in background survival.
$P_{TF,\,m}$	0.047	Proportion tidal fry
$S_{TF,FP}$	0.731	Survival tidal fry in floodplain
$P_{FP,m}$	0.88	Proportion entering Floodplain if flooding (Pope et al. 2018)
$B0_4$	0.5	Average survival tidal fry to delta intercept
$B1_4$	-1.0	Effect of DCC gate (value is in logit space)*
$B0_5$	0.5	Average proportion of tidal fry to bay intercept
$B1_5$	2.0	Effect of Rio Vista flow (value is in logit space)*

Parameter	Value	Description
$B0_M$	0.003	Proportion of fry moving from the Lower River to the Delta in the absence of density dependence when Wilkins Slough Flows are < 400 cms.
$B1_M$	0.377	Proportion of fry moving from the Lower River to the Delta in the absence of density dependence when Wilkins Slough Flows are $\geq$ 400 cms.

Smoltification Timing Parameters

The timing of smoltification of winter-run Chinook salmon historically begins in January with a majority of winter-run sized smolts outmigrating by March (delRosario et al. 2013). In the WRLCM, all fry are assumed to have smolted by April and migrated in May (Table 5). The timing of smoltification in the WRLCM has been parameterized to coincide with winter-run sized Chinook salmon in Chipps Island trawl data (delRosario et al. 2013) and by using Chipps Island abundance indices as described below in the *Parameter Estimation* section.

Table 5. Smoltification timing parameters for winter-run Chinook.

Parameter	Value	Description
Z_1	0.269	January smolt probability
Z_2	0.5	February smolt probability
Z_3	0.953	March smolt probability
Z_4	0.999	April smolt probability
Z_5	1	May smolt probability
Z_6	1	June smolt probability
Z_7	1	July smolt probability

Maturation Rate Probabilities

The age-specific maturation probabilities for winter-run Chinook salmon were fixed to values based on analysis of coded wire tagged hatchery fish (Grover et al. 2004). The probability of maturation of age 2 fish was 0.10 (M_2), the conditional probability of maturation at age 3 was 0.90 (M_3), and the conditional probability of maturation at age 4 was 1.0.

Age-specific sex ratios were applied to obtain age and sex specific escapement values. Males dominate age-2 escapement, thus the female sex ratio for age-2 fish (Fem_{Age2}) was set at 0.01. Estimates of the proportion of age-3 female spawners (Fem_{Age3}) may vary among years, and we accounted for this historical annual variability by using an annual sex spawner ratio value calculated from Keswick trap counts 2001 – 2014 (mean = 0.595, sd = 0.077). These values were also used in the annual calculation of natural origin escapement from carcass surveys over the period 2001 –

2014 (Doug Killam, CDFW Redding, CA, *personal communication*). In the absence of an estimate of the age-3 sex ratio, a value of 0.5 was assumed for 1970 – 2000.

Egg production per age-2 female ($V_{eggs,2}$) was 3000 for age 2 females (3200 reported in Newman and Lindley, 2006) and production per age-3 and age-4 female ($V_{eggs,3}$ and $V_{eggs,4}$) was 5000 (Winship et al. 2014).

Smolt Survival

The ePTM v2 calculates month and year-specific smolt survival probabilities; however, some survival probabilities were needed to move the smolts from their areas of rearing to the location in which the ePTM v2 survival rates were applied. Smolt survival from the Lower River to the Delta ($B0_{11,LR}$) was fixed at 0.8 (estimates of survival ranged from 0.73 - 0.875 Colusa to Sacramento in the 2012-2015 WR acoustic tag data, Arnold Ammann, SWFSC NMFS Santa Cruz *personal communication*). Smolt survival from the Upper River to the Delta ($B0_{10,UR}$) was fixed at 0.4 (estimates of survival averaged 0.456 from release to Sacramento in the 2012-2015 WR acoustic tag data, Arnold Ammann, SWFSC NMFS Santa Cruz *personal communication*). Smolt survival from the Yolo bypass to insertion into the DSM2 grid for incorporation into the ePTM v2 (${}^{A}S_{13,FP}$) was assumed to be 1.0 per month.

Survival of smolts from Chipps Island to the Golden Gate bridge (${}^{c}S_{11}$) was incorporated into the survival during early ocean survival (described below) and therefore assumed to be 1.0. Survival of smolts that reared in the Bay to the Golden Gate bridge ($S_{15,BA}$) was assumed to be 0.8.

Ocean Survival

Survival of smolts that reared in the Upper River, Lower River, Delta, Yolo, and Bay habitats (S_{G1}) have the same gulf survival, which was estimated through statistical fitting (see below in the *Parameter Estimation* section).

Survival during the first four months in the ocean (S_{17}) was assumed to have a rate of 0.79, which equates to an annual survival of 0.5, whereas annual survival in the ocean for age-3 and age-4 (S_{19} and S_{21}) was assumed to be 0.8. These annual natural survival rates are consistent with winter-run reconstruction conducted annually as part of the fishery management of Sacramento River salmon (Grover et al. 2004, O'Farrell et al. 2012).

Statistical Estimation

One of our objectives is to ensure that the WRLCM can reflect the historical patterns in winter-run Chinook population dynamics in the Sacramento River. In order to meet this objective, we calibrated the LCM to observe winter-run indices of abundance throughout the life cycle (Table 6). Not all indices of abundance were available for the entire period of model calibration of 1970-2014. This data limitation is not a problem for fitting the WRLCM, however. The WRLCM can be fitted to the specific indices of abundance for the period over which they were available by pairing observed indices of abundance with WRLCM predictions over the appropriate period. Then, the sampling

distribution provided a likelihood function by which the model predictions were statistically evaluated given the observed data (Hilborn and Mangel 1997).

This type of model, in which multiple data sources are used to inform multiple life-history stages, is called an integrated population model and has notable advantages over piecewise model composition (Newman et al. 2014). In particular, the model parameter estimates can utilize all of the available data simultaneously, which can improve the parameter estimates by allowing the model to "fill in the gaps" over portions of the life cycle that are unobserved (Newman et al. 2014).

Table 6. Indices of abundance used to calibrate the winter-run life cycle model.

Data	Date	Standard Deviation	Sampling Distribution	Data time step
Natural	1970-2002	0.25	lognormal	Annual
Escapement				
Escapement by sex and jack/jill vs adult	2003-2016	0.25	lognormal	Annual
RBDD monthly juvenile counts	1996-1999, 2002-2016	0.8	lognormal	Monthly
Chipps Island monthly juvenile abundance	2008 - 2011	0.9	lognormal	Monthly

Modification of the WRLCM for Estimating Parameters

Annual impact rates of age-3 (I_3) and age-4 (I_4) were obtained from estimated harvest rates over the 1970- 2014 period (O'Farrell and Satterthwaite 2015). Survival of age-2 (S_{sp2}), age-3 (S_{sp3}), and age-4 (S_{sp4}) through the freshwater prior to spawning is assumed to be 0.9 to incorporate in-river harvest, which historically included levels of approximately 7 percent (Grover et al. 2004) and pre-spawn mortality.

To reflect the historical dynamics of access to the Floodplain habitat (Yolo bypass), the following transition equation was used to describe the proportion of Tidal Fry that enter the floodplain habitat ($P_{FP,m}$)

$$P_{FP,m} = B1_{FP} * \mathrm{I}(Q_{Verona,m} > 991.1 \text{ m}^3\text{s}^{-1})$$

where $Q_{Verona,m}$ was the Sacramento River flow at Verona in month m, $\mathrm{I}(\,)$ is an indicator function that equates to 1 when the condition in the parenthesis is met, and $B1_{FP}$ is the proportion of fry that enter the Yolo under flooding conditions, which was 0.8.

Bayesian Estimation

Given the fixed parameter values described above, the remaining parameters were estimated in a Bayesian statistical fitting framework. An initial evaluation of model complexity (not shown) indicated that approximately 10 parameters were identifiable in the mechanistic portion of the model, depending upon which parameters were chosen. We estimated 8 parameters in addition to 45 annual random effects (i.e, the ε_y) in the model calibration.

These parameters were estimated by sampling from the posterior distribution (the combination of the likelihood specified by the sampling distribution and the prior distribution for model parameters) of observing the winter-run abundance indices (Hilborn and Mangel 1997, Gelman et al. 2013). That is, parameter combinations can be used to make predictions on the escapement in each year, the number of juveniles passing RBDD in each month, and monthly abundance estimates at Chipps Island (Table 6). Some parameter combinations provide predictions that are closer to the observed abundance indices than others. The parameter combinations that provide the closest fit to the observed indices are retained in the Markov Chain Monte Carlo (MCMC) sampling algorithm, leading to a set of samples from the posterior distribution of the model parameters. The MCMC algorithm also provides estimates of the state variables, which include the abundance at each sampling location at the appropriate time scale (Table 6) for comparison of the model predictions to the observed abundance data.

Model parameters were estimated by implementing the Bayesian statistical fitting in the programming language NIMBLE (de Valpine et al. 2017, deValpine et al. 2022a). In order to implement the MCMC algorithm, the WRLCM had to be written into the NIMBLE language as NIMBLE uses a specific syntax that it subsequently converts to C++ code so that the MCMC algorithm can be implemented in a fast computational environment. All life stages of the WRLCM were coded into the NIMBLE version of the WRLCM with the exception of tidal fry. Tidal fry compose a small portion of the overall dynamics of winter-run (~5.0%) and field data have not been collected for this life stage. As a result, the NIMBLE model has no observations on which to evaluate this life stage, and therefore tidal fry were not included in the NIMBLE code; however, their dynamics were included in the evaluation of the projects using the fixed parameter values described above. More details on the NIMBLE programming language can be found at de Valpine et al. (2022b).

Fits to Abundance Indices

Fits to the abundance indices generally followed patterns in the observed data. Annual patterns in natural origin escapement were well estimated by the model (Figure 17), as were monthly patterns in juvenile abundance estimates at RBDD (Figure 18).

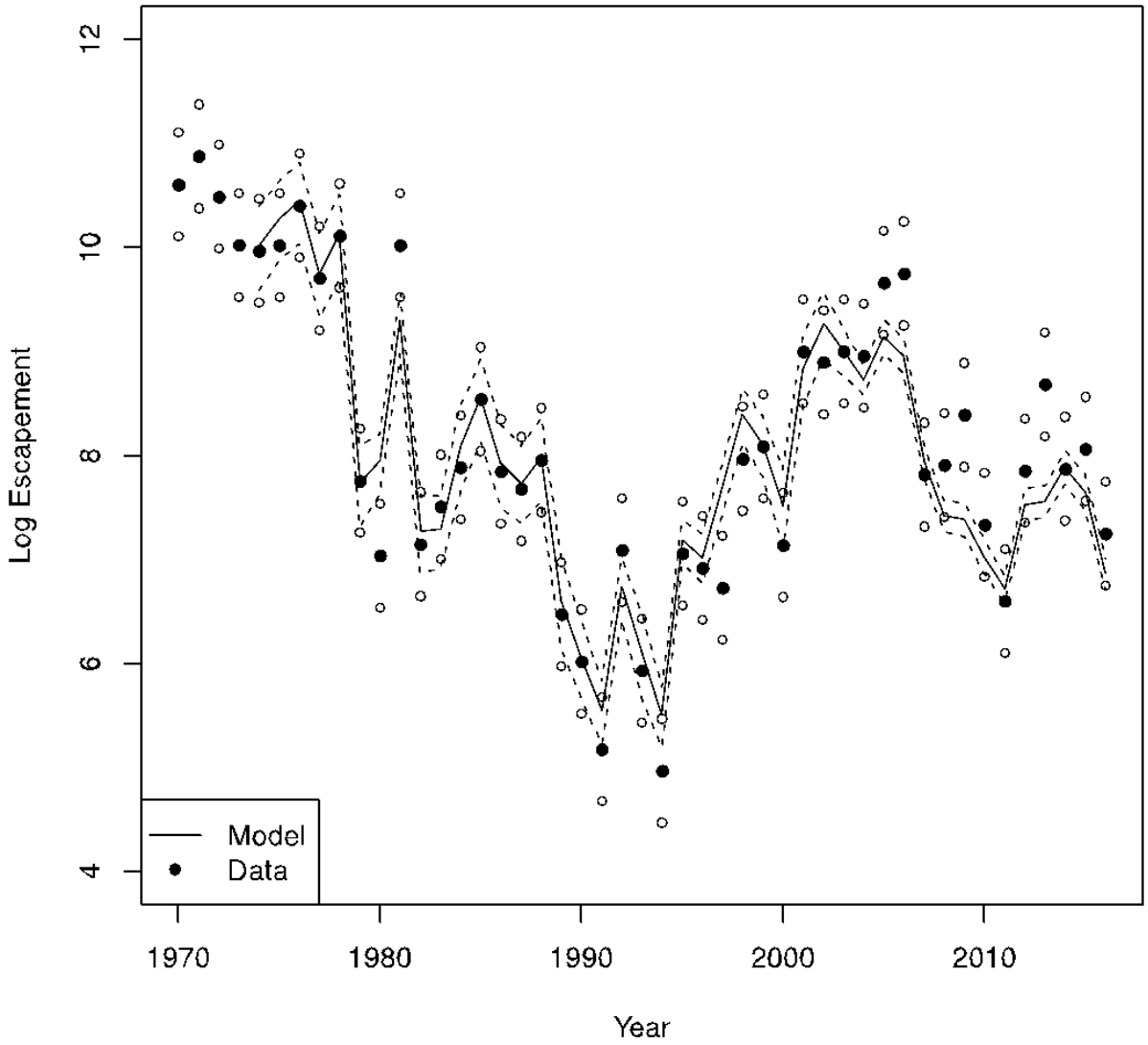

Figure 17. Model fit (line) with 95% credible intervals on model predictions (dashed line) to log natural origin escapement data (solid circles) with 95% interval on measurement error (open circles).

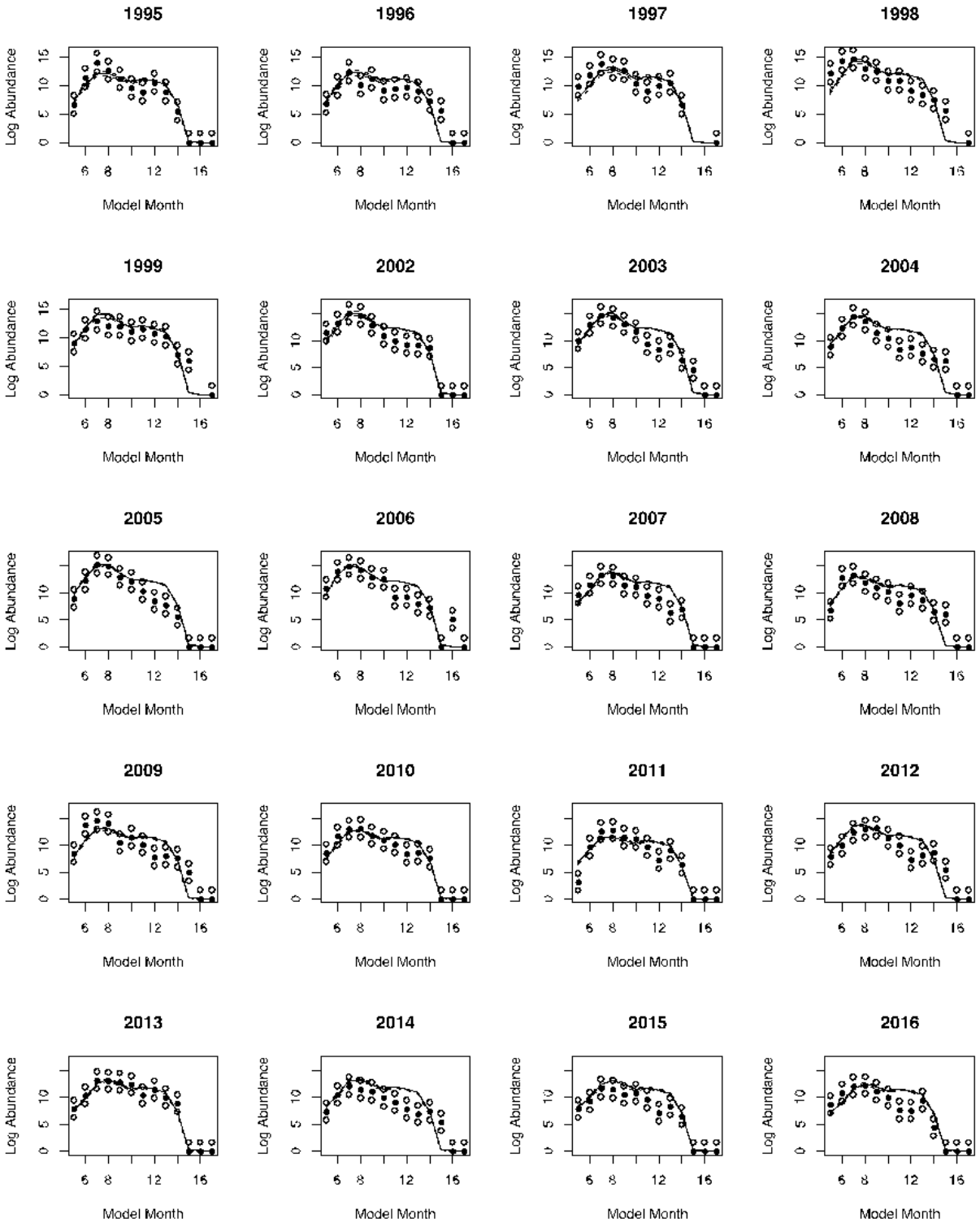

Figure 18. Model fit (line) with 95% credible intervals on model predictions (dashed line) to log juvenile abundance at Red Bluff Diversion Dam (solid circles) with 95% interval on measurement error (open circles).

Finally, the WRLCM was able to capture the monthly patterns in Chipps Island abundance trends from 2008 – 2011, reflecting the outmigration patterns of winter-run from each of the rearing habitats (Figure 19).

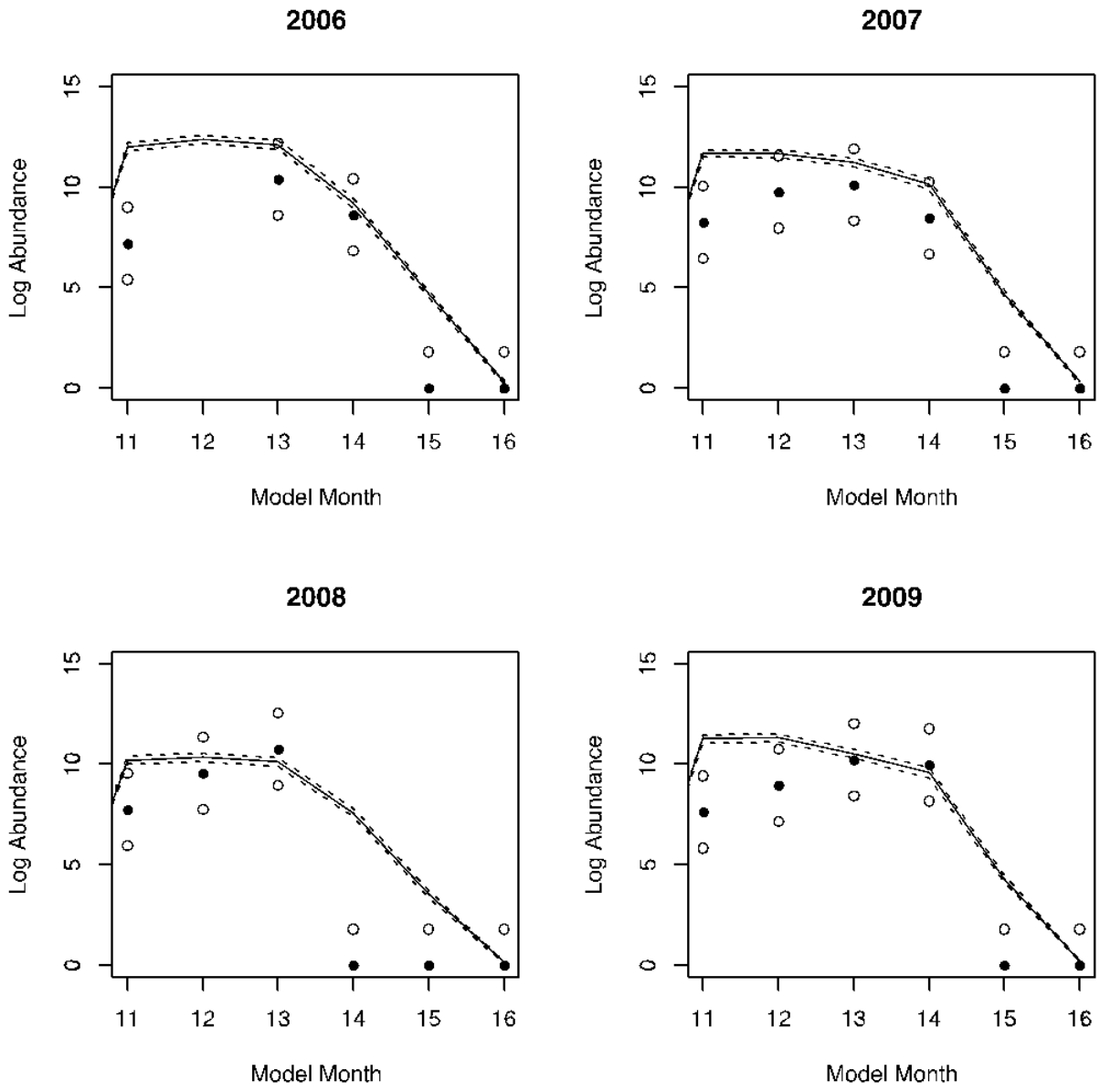

Figure 19. Model fit (line) with 95% credible intervals on model predictions (dashed line) to log juvenile abundance at Chipps Island (solid circles) with 95% interval on measurement error (open circles).

The estimated parameter values from the MCMC algorithm are provided in Table 7. The table provides the parameter estimate, the standard deviation of the estimate (SD), a transformed value of the parameter estimate, and a note defining the parameter. We attempted to estimate all parameters of the survival of egg to fry as a function of temperature (Transition 1); however, there was strong correlation among the three parameters that caused problems with parameter identifiability. We assumed that the critical temperature at which thermal mortality starts to affect egg to fry survival was 12.0 C, which is the value determined from an analysis of egg to fry survival by Martin et al. (2017). The survival of egg to fry below this critical temperature was a value (logit($B0_1$)) for the 3-month period, whereas above this threshold the survival was reduced for every degree above the critical temperature.

mig_m is a constant value (e.g., movement from the floodplain to the delta, the delta to the bay, and the bay to the gulf).

The other parameter value that was set was the variance on the random effect in process noise (σ_{ε}^2), and it was set to have a value of 1. This variance allowed the model to estimate the annual random effect parameters (ε_y) to have values of approximately $\pm$ 2. These parameter values corresponded to a range in annual variability in survival of (0.17, 7.4) due to the lognormal structure of the random effects.

Table 7. WRLCM parameter estimates from the model calibration to winter-run indices of abundance (Table 6).

Parameter	mean	sd	2.50%	97.50%	Rhat	Description
$B0_A$	0.95	0.096	0.764	1.139	1.00	Survival below critical temperature value (logit space)
$B1_1$	-1.11	0.144	-1.412	-0.847	1.09	Rate of reduction in egg to fry survival (logit space)
S_{FRY}	0.872	0.062	0.758	0.997	1.00	Winter run fry survival (logit space)
mig_m	0.224	0.126	0.017	0.486	1.00	Proportion migrating per month from floodplain, delta, and bay in absence of density dependence
$mig_{UR,m}$	0.128	0.012	0.105	0.153	1.00	Proportion of fry in upper river migrating to lower river per month in absence of density dependence
S_{G0}	-3.165	0.297	-3.723	-2.557	1.02	Average survival during gulf entry (logit space)
S_{G1}	-0.338	0.233	-0.786	0.144	1.04	Effect of upwelling index on survival during gulf entry (logit space)
σ_{ε}	1.645	0.194	1.255	1.974	1.01	Standard deviation of random effects during gulf entry

Using 1500 samples from the posterior, we calculated the correlation among estimated model parameters (Table 8). In general, the absolute value in correlations among parameters was less than 0.6. Parameters with absolute correlations greater than 0.5 included the standard deviation in the random effects (σ_{ε}) and the average ocean entry survival (S_{G0}), which were negatively related, and the effect of thermal mortality ($B1_1$) and the ocean entry average ocean entry survival (S_{G0}), which was also negatively related. These negative correlations reflect the lack of observations on winter-run between Chipps Island (in a few years) and spawner escapement. As a result, the observed patterns in abundance can be explained by having high thermal mortality and low gulf entry survival (and vice versa). Likewise, the abundance data can be explained by allowing the annual variability in gulf survival to be more variable if the thermal mortality rate is low and less variable if the thermal mortality rate is high. These correlations reflect unknown relationships due to limited data; that is, we do not have data sets that can determine the specific rates and thus multiple combinations of these parameters can produce the same patterns in abundance. This is an important aspect to the model fitting in that the correlations in posterior draws can be passed to the evaluation of the project effects.

Table 8. Correlation matrix for estimated parameters in the WRLCM calibration.

	mig_m	$mig_{UR,m}$	S_{G0}	S_{G1}	$B0_A$	S_{FRY}	$B1_1$	σ_ε
mig_m	1	0.152	-0.08	-0.009	0.083	0.279	0.023	-0.09
$mig_{UR,m}$	0.152	1	-0.102	-0.062	-0.228	0.442	-0.01	-0.014
S_{G0}	-0.08	-0.102	1	0.172	-0.081	-0.232	-0.564	0.353
S_{G1}	-0.009	-0.062	0.172	1	0.024	-0.091	-0.259	0.262
$B0_A$	0.083	-0.228	-0.081	0.024	1	-0.25	-0.035	-0.063
S_{FRY}	0.279	0.442	-0.232	-0.091	-0.25	1	-0.071	-0.031
$B1_1$	0.023	-0.01	-0.564	-0.259	-0.035	-0.071	1	-0.564
σ_ε	-0.09	-0.014	0.353	0.262	-0.063	-0.031	-0.564	1

Incorporating Uncertainty in the Analysis of Hydrologic Alternatives

Our goal is to be able to account for multiple sources of uncertainty in the analysis of the proposed alternatives relative to the existing condition (or baseline). We incorporated three forms of uncertainty in the DCP analysis: 1) parameter uncertainty, 2) natural variability in cohort productivity, and 3) model uncertainty in the smolt survival function (ePTMv2). We then used Monte Carlo simulation to incorporate all three sources of uncertainty in the WRLCM outputs.

To incorporate parameter uncertainty, we used 1000 posterior samples from the parameters estimated via MCMC. With two exceptions, we used the draws that were defined by the posterior credible intervals described in Table 7. The two parameters that used different values were the standard deviation in the random effects (σ_ε) and the ocean entry survival (S_{G0}). The ocean entry survival was fixed at a value of 0.12 for gulf entry survival (corresponding to an inverse logit transformed value of -2), because the estimated value of 0.043 (corresponding to an inverse logit transformed value of -3.1) was leading to extremely low population sizes given the survival rates in the other parts of the life cycle. We also fixed the standard deviation in the random effects (σ_ε) to its mean value (1.645).

To incorporate natural variability in cohort productivity, we incorporated a unique random effect for each cohort in the 81-year time series. We repeated this 81-year series over 1000 iterations to simulate a set of 1000 x 81 random effects that corresponded to 1000 iterations and 81 years of the time series. The random effects were bias corrected random variables (to ensure that when they were exponentiated they retained a mean of 1) from a normal distribution with mean = 0 and standard deviation = 1.645.

Finally, to incorporate uncertainty in the smolt survival model (ePTMv2), we used 1000 bootstrapped samples of survival rates estimated for each model month 11 to 17 (January to July) and the Lower River, Floodplain, and Delta rearing habitats. These 1000 samples by month and habitat were calculated for each alternative and the baseline existing condition. Within each scenario, we ordered the survival estimates within each month and rearing habitat such that the first value was the lowest survival rate for that month and habitat and the last value was the highest survival rate for that month and habitat. We then used the ordered smolt survival rates in the effects analysis, which ensured that the lowest monthly survival for a given habitat under the existing condition was being paired with the lowest monthly survival for the same habitat under the

alternative. This ordering also ensured that this comparison was made for the second lowest survival and through to the highest survival.

V. References

Anderson, J. J., Gurarie, E., and Zabel, R. W. 2005. Mean free-path length theory of predator–prey interactions: Application to juvenile salmon migration. *Ecological Modelling*, *186*(2), 196-211. DOI: https://doi.org/10.1016/j.ecolmodel.2005.01.014.

Anderson, J., and Mierzwa, M. 2002. An introduction to the Delta Simulation Model II (DSM2) for simulation of hydrodynamics and water quality of the Sacramento-San Joaquin Delta, Delta Modeling Section, Office of State Water Project Planning, California Department of Water Resources, Sacram., Ca.

Anglea, S. M., Geist, D. R., Brown, R. S., Deters, K. A., and McDonald, R. D. 2004. Effects of acoustic transmitters on swimming performance and predator avoidance of juvenile Chinook salmon. *North American Journal of Fisheries Management*, *24*(1), 162-170. DOI: https://doi.org/10.1577/M03-065.

Barnard, D. 2019. Metadata for the Lodi Fish and Wildlife Office's Delta Juvenile Fish Monitoring Program. US Fish and Wildlife Service Memorandum.

Beamer, E., A. McBride, C. Greene, R. Henderson, G. Hood, K. Wolf, K. Larsen, C. Rice, and K. L. Fresh. 2005. Delta and nearshore restoration for the recovery of wild Skagit River Chinook salmon: Linking estuary restoration to wild Chinook salmon populations. Appendix D of the Skagit Chinook Recovery Plan, Skagit River System Cooperative, LaConner, WA. Available at: www.skagitcoop.org.

Beechie, T. J., Martin Liermann, E. M. Beamer, and R. Henderson. "A classification of habitat types in a large river and their use by juvenile salmonids." Transactions of the American Fisheries Society 134, no. 3 (2005): 717-729.

Blanckaert, K., and De Vriend, H. J. 2004. Secondary flow in sharp open-channel bends. *Journal of Fluid Mechanics*, *498*, 353-380. DOI: 10.1017/S0022112003006979.

Brown, R. S., Geist, D. R., Deters, K. A., and Grassell, A. 2006. Effects of surgically implanted acoustic transmitters> 2% of body mass on the swimming performance, survival and growth of juvenile sockeye and Chinook salmon. *Journal of Fish Biology*, *69*(6), 1626-1638. DOI: https://doi.org/10.1111/j.1095-8649.2006.01227.x.

California Department of Water Resources. 1998. *Methodology for flow and salinity estimates in the Sacramento-San Joaquin Delta and Suisun Marsh*. Nineteenth Annual Progress Report to the State Water Resources Control Board. 170p. Sacramento, CA. Accessed December 24, 2021. Available at: https://data.cnra.ca.gov/dataset/methodology-for-flow-and-salinity-estimates-in-the-sacramento-san-joaquin-delta-and-suisun-marsh/resource/44093c61-51fe-411f-8425-efc167d1ec6f.

California Department of Water Resources. 2015. *2012 Georgiana Slough non-physical barrier performance evaluation final project report*. Final Project Report. 298p. Bay-Delta Office. Sacramento, California.

California Department of Water Resources. 2016. *2014 Georgiana Slough floating fish guidance structure performance evaluation project report*. Final Project Report. 486p. Bay-Delta Office. Sacramento, California.

California Department of Water Resources (DWR). 2018. Delta levee anatomy basemap, derived from 2007-08 LIDAR. GIS Data. https://www.arcgis.com/home/item.html?id=ab87d67b27e842ee80ffc2b4d80ec7df#overview

Chapman, E. D., Hearn, A. R., Michel, C. J., Ammann, A. J., Lindley, S. T., Thomas, M. J., Singer, G. P., Peterson, M. L., MacFarlane, R. B. and Klimley, A. P. 2013. Diel movements of out-migrating Chinook salmon (Oncorhynchus tshawytscha) and steelhead trout (Oncorhynchus mykiss) smolts in the Sacramento/San Joaquin watershed. *Environmental Biology of Fishes*, *96*(2), 273-286. DOI: https://doi.org/10.1007/s10641-012-0001-x.

Chernov, N. 2010. *Circular and linear regression: Fitting circles and lines by least squares*. 286p. CRC Press.

DeLong, L. L., Lewis, L., Thompson, D. B., and Lee, J. K. (1997). "The computer program FourPt (version 95.01): A model for simulating one-dimensional, unsteady, open-channel flow." Water-Resources Investigation Rep., 97-4016, USGS, Reston, VA.

del Rosario, R. B., Y. J.Redler., K. Newman, P. L. Brandes, T. Sommer, K. Reece, and R. Vincik. 2013. Migration patterns of juvenile winter-run-sized Chinook salmon (Oncorhynchus tshawytscha) through the Sacramento–San Joaquin Delta. San Francisco Estuary and Watershed Science 11(1).

de Valpine P, Paciorek C, Turek D, Michaud N, Anderson-Bergman C, Obermeyer F, Wehrhahn Cortes C, Rodrìguez A, Temple Lang D, Paganin S. 2022a. *NIMBLE: MCMC, Particle Filtering, and Programmable Hierarchical Modeling*. doi: 10.5281/zenodo.1211190, R package version 0.12.2, https://cran.r-project.org/package=nimble.

de Valpine P, Paciorek C, Turek D, Michaud N, Anderson-Bergman C, Obermeyer F, Wehrhahn Cortes C, Rodrìguez A, Temple Lang D, Paganin S. 2022b. *NIMBLE User Manual*. doi: 10.5281/zenodo.1211190, R package manual version 0.12.2, https://r-nimble.org.

de Valpine P, Turek D, Paciorek C, Anderson-Bergman C, Temple Lang D, Bodik R (2017). "Programming with models: writing statistical algorithms for general model structures with NIMBLE." *Journal of Computational and Graphical Statistics*, **26**, 403-413. doi: 10.1080/10618600.2016.1172487.

Dougan, M. C. 1993. Growth and development of chinook salmon, Oncorhynchus tshawytscha: effects of exercise training and seawater transfer. Doctoral Thesis. University of Canterbury. Christchurch, New Zealand. Accessed December 24, 2021. Available at: https://ir.canterbury.ac.nz/handle/10092/6068.

Gandhi, B. K., Verma, H. K., and Abraham, B. 2016. Mathematical modeling and simulation of flow velocity profile for rectangular open channels. *ISH Journal of Hydraulic Engineering*, *22*(2), 193-203. DOI: https://doi.org/10.1080/09715010.2015.1136244.

Gelman, A., Carlin, J.B., Stern, H.S., Dunson, D.B., Vehtari, A. and Rubin, D.B., 2013. Bayesian data analysis, third edition. CRC press. Boca Raton, FL.

Gibson, R.N., 2003. Go with the flow: tidal migration in marine animals, In Migration and Dispersal of Marin Organisms, 153-161, Springer, Netherlands.

Gilbert, Richard O. 1987. Sen's Nonparametric Estimator of Slope. Statistical Methods for Environmental Pollution Monitoring, John Wiley and Sons, pp. 217–219, ISBN: 978-0-471-28878-7.

Gleichauf, K. T., Wolfram, P. J., Monsen, N. E., Fringer, O. B., and Monismith, S. G. 2014. Dispersion mechanisms of a tidal river junction in the Sacramento–San Joaquin Delta, California. *San Francisco Estuary and Watershed Science*, *12*(LA-UR-14-29557). DOI: https://doi.org/10.15447/sfews.2014v12iss4art1.

Greene, C.M., D.W. Jensen, E. Beamer, G.R. Pess, and E.A. Steel. 2005. Effects of environmental conditions during stream, estuary, and ocean residency on Chinook salmon return rates in the Skagit River, WA. Transactions of the American Fisheries Society, 134:1562-1581.

Grover, A., A. Lowe, P. Ward, J. Smith, M. Mohr, D. Viele, and C. Tracy. 2004. Recommendations for developing fishery management plan conservation objectives for Sacramento River winter Chinook and Sacramento River spring Chinook. Interagency Workgroup Progress Report. February 2004.

Hance, D. J., Perry, R. W., Burau, J. R., Blake, A., Stumpner, P., Wang, X., and Pope, A. 2021. Combining models of the critical streakline and the cross-sectional distribution of juvenile salmon to predict fish routing at river junctions. *San Francisco Estuary and Watershed Science*, *18*(1). DOI: https://doi.org/10.15447/sfews.2020v18iss1art3.

Healey, M. C. 1980. Utilization of the Nanaimo River estuary by juvenile Chinook salmon, Oncorhynchus tshawytscha. *Fishery Bulletin*, *77*(3).

Hedger, R. D., Martin, F., Hatin, D., Caron, F., Whoriskey, F. G., and Dodson, J. J. 2008. Active migration of wild Atlantic salmon Salmo salar smolt through a coastal embayment. Marine Ecology Progress Series, 355, 235-246. DOI: https://doi.org/10.3354/meps07239.

Hendrix, N., Criss, A., Danner, E., Greene, C.M., Imaki, H., Pike, A., and Lindley, S.T. 2014. Life cycle modeling framework for Sacramento River Winter run Chinook salmon, NOAA Technical Memorandum 530, National Marine Fisheries Service, Southwest Fisheries Science Center, Santa Cruz, Ca.

Hilborn, R. and M. Mangel. 1997. The ecological detective: confronting models with data. Princeton University Press.

Hood, W.G. 2007. Scaling tidal channel geometry with marsh island area: a tool for habitat restoration, linked to channel formation process. Water Resources Research 43(3). DOI: https://doi.org/10.1029/2006WR005083.

Jassby, A. D., W.J. Kimmerer, S.G. Monismith, C. Armor, J.E. Cloern, T.M. Powell, J.R. Schubel, and T.J. Vendlinski. 1995. Isohaline position as a habitat indicator for estuarine populations. Ecological Applications 5: 272-289.

Kelly, J. T., and Klimley, A. P. 2012. Relating the swimming movements of green sturgeon to the movement of water currents. *Environmental Biology of Fishes*, *93*(2), 151-167. DOI: https://doi.org/10.1007/s10641-011-9898-8.

Kimmerer, W.J., and Nobriga, M.L. 2008. Investigating particle transport and fate in the Sacramento-San Joaquin Delta using a particle tracking model. San Francisco Estuary Watershed Sci., 6(1).

Lacroix, G. L., and McCurdy, P. 1996. Migratory behaviour of post-smolt Atlantic salmon during initial stages of seaward migration. *Journal of Fish Biology*, *49*(6), 1086-1101. DOI: https://doi.org/10.1111/j.1095-8649.1996.tb01780.x.

Lacroix, G. L., Knox, D., & Stokesbury, M. J. W. (2005). Survival and behaviour of post-smolt Atlantic salmon in coastal habitat with extreme tides. *Journal of Fish Biology*, *66*(2), 485-498.

Lehman, B., Huff, D. D., Hayes, S. A., and Lindley, S. T. 2017. Relationships between Chinook salmon swimming performance and water quality in the San Joaquin River, California. *Transactions of the American Fisheries Society*, *146*(2), 349-358. DOI: https://doi.org/10.1080/00028487.2016.1271827.

Liao, J. C. 2007. A review of fish swimming mechanics and behaviour in altered flows. *Philosophical Transactions of the Royal Society B: Biological Sciences*, *362*(1487), 1973-1993. DOI: https://doi.org/10.1098/rstb.2007.2082.

Lindley, S.T., Grimes, C., Mohr, M., Peterson, W., Stein, J., Anderson, J., Botsford, L., Bottom, D., Busack, C., Collier, T., Ferguson, J., Garza, J., Grover, A., Hankin, D., Kope, R., Lawson, P., Low, A., MacFarlane, R.B., Moore, K., Palmer-Zwahlen, M., Schwing, F., Smith, J., Tracy, C., Webb, R., Wells, B.K., and Williams, T. 2009. What caused the Sacramento River fall Chinook stock collapse? NOAA Tech. Memo. NOAA-TM-NMFS-SWFSC-447: 1–57.

Martin, B.T., Pike, A., John, S.N., Hamda, N., Roberts, J., Lindley, S.T., and Danner, E.M. 2017. Phenomenological vs. biophysical models of thermal stress in aquatic eggs. Ecol. Lett. **20**: 50–59. doi: 10.1111/ele.12705.

McCleave, J. D. 1978. Rhythmic aspects of estuarine migration of hatchery-reared Atlantic salmon (Salmo salar) smolts. *Journal of Fish Biology*, *12*(6), 559-570. DOI: https://doi.org/10.1111/j.1095-8649.1978.tb04202.x.

McCormick, S. D., Hansen, L. P., Quinn, T. P., and Saunders, R. L. 1998. Movement, migration, and smolting of Atlantic salmon (Salmo salar). *Canadian Journal of Fisheries and Aquatic Sciences*, *55*(S1), 77-92. DOI: https://doi.org/10.1139/d98-011.

Michel, C. J., Henderson, M. J., Loomis, C. M., Smith, J. M., Demetras, N. J., Iglesias, I. S., Lehman, B. M. and Huff, D. D. 2020. Fish predation on a landscape scale. *Ecosphere*, *11*(6), e03168. DOI: https://doi.org/10.1002/ecs2.3168.

Miller, B. A., and Sadro, S. 2003. Residence time and seasonal movements of juvenile Coho salmon in the ecotone and lower estuary of Winchester Creek, South Slough, Oregon. *Transactions of the American Fisheries Society*, *132*(3), 546-559. DOI: https://doi.org/10.1577/1548-8659(2003)132<0546:RTASMO>2.0.CO;2.

Monismith, S.G., W. Kimmerer, J.R. Burau, and M.T Stacey. 2002. Structure and flow-induced variability of the subtidal salinity field in northern San Francisco Bay. Journal of Physical Oceanography, 32: 3003-3019.

Moore, A., Ives, S., Mead, T. A., and Talks, L. 1998. *The migratory behaviour of wild Atlantic salmon (Salmo salar L.) smolts in the River Test and Southampton Water, southern England*. pp. 295-204. In Advances in Invertebrates and Fish Telemetry. Springer, Dordrecht, The Netherlands.

Moser, M. L., Olson, A. F., and Quinn, T. P. 1991. Riverine and estuarine migratory behavior of coho salmon (Oncorhynchus kisutch) smolts. *Canadian Journal of Fisheries and Aquatic Sciences*, *48*(9), 1670-1678. DOI: https://doi.org/10.1139/f91-198.

National Marine Fisheries Service (NMFS) 2012. Final Implementation of the 2010 Reasonable and Prudent Alternative Sacramento River winter-run Chinook Management Framework for the Pacific Coast Salmon Fishery Management Plan. National Marine Fisheries Service, Southwest Region.

National Oceanic and Atmospheric Administration Office for Coastal Management (NOAA OCM). 2017. 2016 Coastal Change Analysis Program (C-CAP) Regional Land Cover. GIS Data. Accessed June 2021. www.coast.noaa.gov/htdata/raster1/landcover/bulkdownload/30m_lc/

National Oceanic and Atmospheric Administration Office of Response and Restoration (NOAA OR&R). 2017. National Environmental Sensitivity Index Shoreline. GIS Data. Accessed June 2021. https://response.restoration.noaa.gov/esi_download

Newman, K.B. 2003. Modelling paired release-recovery data in the presence of survival and capture heterogeneity with application to marked juvenile salmon. Stat. Modelling **3**: 157–177. doi: 10.1191/1471082X03st055oa.

Newman, K., S.T. Buckland, B. Morgan, R. King, D.L. Borchers, D. Cole, P. Besbeas, O. Gimenez, and L. Thomas. 2014. Modelling population dynamics. Springer.

O'Farrell, M. and W. H. Satterthwaite. 2015. Inferred historical fishing mortality rates for an endangered population of Chinook salmon (Oncorhynchus tshawytscha). Fishery Bulletin, 113(3):341-352.

O'Farrell, M. R., M. S. Mohr, A. M. Grover, and W. H. Satterthwaite. 2012. Sacramento River winter Chinook cohort reconstruction: analysis of ocean fishery impacts. NOAA Technical Memorandum NOAA-TM-NMFS- SWFSC-491.

Perry, R.W., Kirsch, J.E., and Hendrix, A.N. 2016. Estimating Juvenile Chinook Salmon (Oncorhynchus tshawytscha) Abundance from Beach Seine Data Collected in the Sacramento– San Joaquin Delta and San Francisco Bay, California. USGS Open File Report 2016-1099.

Perry, R. W., Pope, A. C., Romine, J. G., Brandes, P. L., Burau, J. R., Blake, A. R., Ammann, A. J., and Michel, C. J. 2018. Flow-mediated effects on travel time, routing, and survival of juvenile Chinook salmon in a spatially complex, tidally forced river delta. *Canadian Journal of Fisheries and Aquatic Sciences*, *75*(11), 1886-1901. DOI: https://doi.org/10.1139/cjfas-2017-0310.

Perry, R. W., Romine, J. G., Adams, N. S., Blake, A. R., Burau, J. R., Johnston, S. V., and Liedtke, T. L. 2014. Using a non-physical behavioural barrier to alter migration routing of juvenile chinook salmon in the Sacramento–San Joaquin River delta*. River Research and Applications*, *30*(2), 192-203. DOI: https://doi.org/10.1002/rra.2628.

Perry, R. W., Skalski, J. R., Brandes, P. L., Sandstrom, P. T., Klimley, A. P., Ammann, A., and MacFarlane, B. 2010. Estimating survival and migration route probabilities of juvenile Chinook salmon in the Sacramento–San Joaquin River Delta. *North American Journal of Fisheries Management*, *30*(1), 142-156. DOI: https://doi.org/10.1577/M08-200.1.

Pope, A.C., Perry, R.W., Hance, D.J., and Hansel, H.C., 2018, Survival, travel time, and utilization of Yolo Bypass, California, by outmigrating acoustic-tagged late-fall Chinook salmon: U.S. Geological Survey Open-File Report 2018-1118, 33 p., https://doi.org/10.3133/ofr20181118.

Poytress, W. R., J. J. Gruber, F. D. Carrillo and S. D. Voss. 2014. Compendium Report of Red Bluff Diversion Dam Rotary Trap Juvenile Anadromous Fish Production Indices for Years 2002-2012. Report of U.S. Fish and Wildlife Service to California Department of Fish and Wildlife and US Bureau of Reclamation.

Prandtl, L. 1935. The mechanics of viscous fluids, In Aerodynamic Theory, Ed. Durand W.F., 3, 34-208. R Core Development Team (RCDT). 2016. R: A language and environment for statistical computing. R Foundation for Statistical Computing, Vienna, Austria. https://www.R-project.org/.

Ross, O. N., and Sharples, J. 2004. Recipe for 1-D Lagrangian particle tracking models in space-varying diffusivity. *Limnology and Oceanography: Methods*, *2*(9), 289-302. DOI: https://doi.org/10.4319/lom.2004.2.289.

San Francisco Estuary Institute and Aquatic Science Center (SFEI ASC). 2017. Bay Area Aquatic Resource Inventory (BAARI) Version 2.1. GIS Data. Accessed June 2021. http://www.sfei.org/data/baari-version-21-gis-data

Semmens, B. X. 2008. Acoustically derived fine-scale behaviors of juvenile Chinook salmon (Oncorhynchus tshawytscha) associated with intertidal benthic habitats in an estuary. Canadian Journal of Fisheries and Aquatic Sciences, 65: 2053-2062.

Solomon, D. J. (1978). Migration of smolts of Atlantic salmon (Salmo salar L.) and sea trout (Salmo trutta L.) in a chalkstream. *Environmental Biology of Fishes*, *3*(2), 223-229.

Sridharan, V. K., Monismith, S. G., Fong, D. A., and Hench, J. L. 2017. One-dimensional particle tracking with streamline preserving junctions for flows in channel networks. *Journal of Hydraulic Engineering*, *144*(2), 04017063. DOI: https://doi.org/10.1061/(ASCE)HY.1943-7900.0001399.

Sridharan, V.K., Jackson, D., Hein, A.M., Perry, R.W., Pope, A.C., Hendrix, N., Danner, E.M., and Lindley, S.T. In prep. Predicting the migration dynamics of juvenile salmonids through rivers and estuaries using a hydrodynamically driven enhanced particle tracking model.

Sridharan, V. K., Monismith, S. G., Fringer, O. B., and Fong, D. A. 2018. Evaluation of the Delta Simulation Model-2 in Computing Tidally Driven Flows in the Sacramento-San Joaquin Delta. San Francisco Estuary and Watershed Science, 16(2). DOI: https://doi.org/10.15447/sfews.2018v16iss2art6.

U.S. Fish and Wildlife Service. 2007. 2001-2005 annual progress report: "Abundance and survival of juvenile chinook salmon in the Sacramento-San Joaquin Estuary". Stockton, CA. https://www.fws.gov/lodi/juvenile_fish_monitoring_program/jfmp_reports.htm

U.S. Fish and Wildlife Service (USFWS). 2006. National Wetland Inventory. GIS Data. Accessed July 2012. http://www.fws.gov/wetlands/Data/Mapper.html

Visser, A. 1997. Using random walk models to simulate the vertical distribution of particles in a turbulent water column. Mar. Ecol. Prog. Ser., 158, 275-281.

Walker, R. W., Ashton, N. K., Brown, R. S., Liss, S. A., Colotelo, A. H., Beirão, B. V., Townsend, R. L., Deng, Z. D., and Eppard, M. B. 2016. Effects of a novel acoustic transmitter on swimming performance and predator avoidance of juvenile Chinook Salmon: determination of a size threshold. *Fisheries Research*, *176*, 48-54. DOI: https://doi.org/10.1016/j.fishres.2015.12.007.

Wang, R., E. Ateljevich, T.A. Fregoso, and B.E. Jaffe. 2018. A Revised Continuous Surface Elevation Model for Modeling (Chapter 5). In Methodology for Flow and Salinity Estimates in the Sacramento-San Joaquin Delta and Suisun Marsh, 38th Annual Progress Report to the State Water Resources Control Board. California Department of Water Resources, Bay-Delta Office, Delta Modeling Section.

Wilbur R. 2000. Validation of dispersion using the particle tracking model in the Sacramento-San Joaquin Delta. Master's Thesis, University of California, Davis, Ca.

Winship, A.J., M.R. O'Farrell and M.S. Mohr. 2014. Fishery and hatchery effects on an endangered salmon population with low productivity. Transactions of the American Fisheries Society, 143(4):957-971.

Appendix A. Analysis of winter-run monthly spawn timing

To estimate the proportion of winter-run spawning among the months of April to August, we conducted an analysis of the numbers of winter-run carcasses detected in each of the months April to August. We were interested in understanding whether the proportions spawning among months were static across all years, or alternatively, whether the proportions varied among years due to the environmental conditions in that year. That is, whether there were some environmental conditions that caused shifts to earlier spawning in some years.

Data

Winter-run carcass observations by date were shifted two weeks earlier to generate "observed" number of fish spawning by date. These spawning numbers by date were coalesced by month to form $N.spawn_{m,t}$ the observed (based on carcass counts) number of winter-run Chinook spawning in month m in year t.

To evaluate annual variability in the proportion spawning in a given month, we calculated a spawning proportion anomaly as the standardized proportion of fish spawning each month ($SPr_{m,t}$). For example, the values of the standardized April values were

$$SP_{Apr,t} = \frac{P.spawn_{Apr,t} - mean(P.spawn_{Apr})}{std\ dev(P.spawn_{Apr})}$$

where the proportion spawning in each month for a given year t (subscript suppressed) was calculated as

$P.spawn_m = \frac{N.spawn_m}{\sum_m \ N.spawn_m}$.

To understand how these annual anomalies varied as a function of water temperature, we calculated the Pearson's correlation coefficient between mean monthly temperature below Keswick Dam between January and June and the standardized proportions (Figure A1).

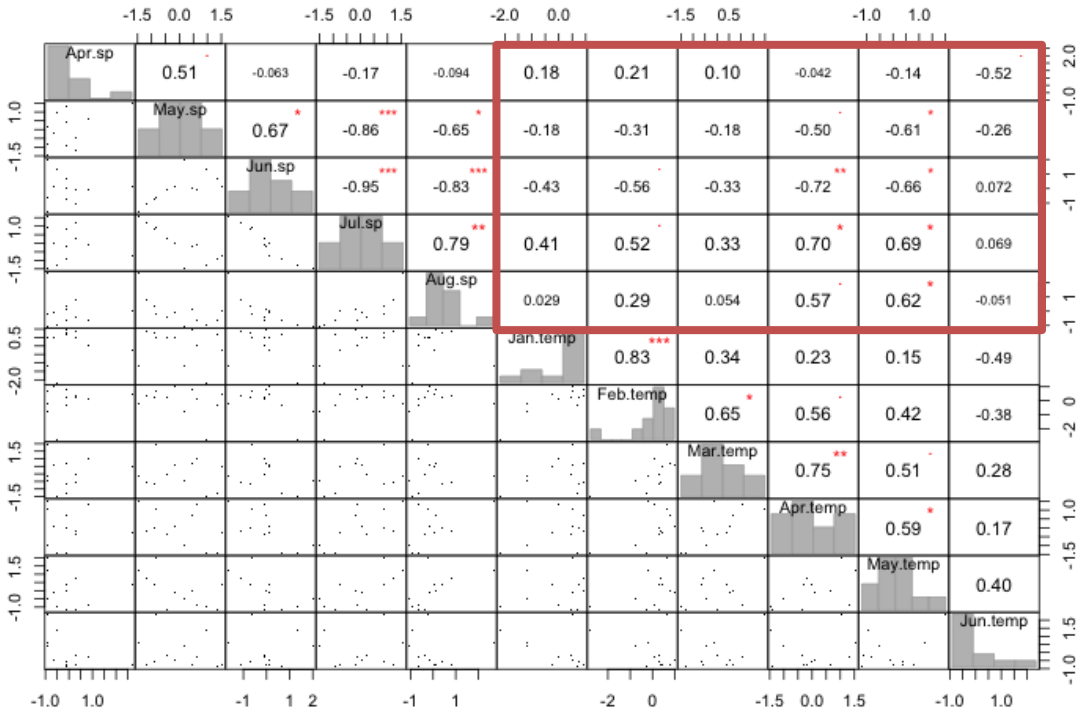

Figure A1. Pearson correlation coefficients (upper triangle), histograms (diagonal) and scatter plots (lower triangle) for all combinations of monthly spawning proportion anomalies and Keswick water temperatures. The red box indicates the month by temperature correlations, and red asterisks indicate significant correlation coefficients.

Statistical Analysis

We fit a multinomial logistic regression using the *multinom* function from the *nnet* package in R to the number of winter-run Chinook spawning in each month, $N.spawn_{m,t}$. We evaluated the ability of April Keswick temperatures to explain annual variability in the spawning timing. We focused on April temperatures because April is the first month of spawning, and April would allow this physical variable to be used as a predictor of spawn timing for future years. The monthly average April temperatures at Keswick were standardized (subtracted mean and divided by standard deviation) for use in the multinomial model.

We fit a base model without the April temperature effect and we fit the model with the April effect and used Akaike Information Criterion (AIC) to compare the models. The AIC value for the base multinomial model was 75822, whereas the value for the multinomial model including April temperature as a covariate was 74209. The difference in AIC was 1613, providing strong support for the model with the April temperature covariate.

The model coefficients for the multinomial model with April covariate indicated increasing spawning in July and August (positive coefficient values) when April temperatures increased (Table A1 and Figure A2). The model coefficients (Table A1) can thus be used for making predictions of spawning proportions using standardized April temperatures as displayed in Figure A2.

Table A1. Coefficient estimates of the multinomial model including April covariate. The effect of the April covariate is reflected in the B1 coefficient estimate.

	Estimate		Standard Error	
Month	B0	B1	B0	B1
Apr	-4.145	0.054	0.06	0.062
May	-1.796	-0.203	0.02	0.02
Jul	-0.332	0.385	0.012	0.012
Aug	-3.443	0.792	0.044	0.045

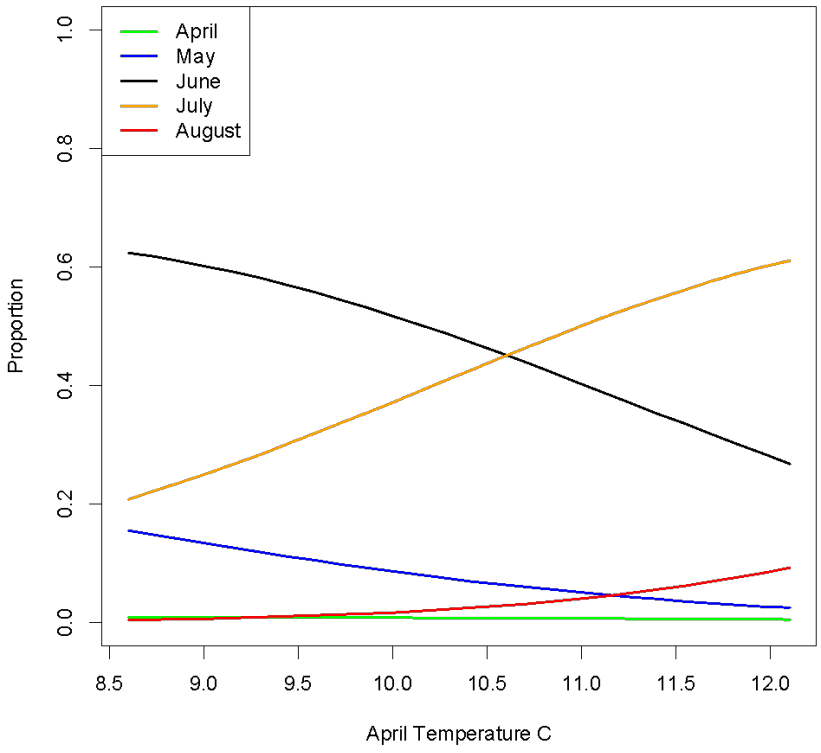

Figure A2. Predictions of the proportion of winter-run Chinook spawning from the multinomial regression model using April temperatures at Keswick Dam as a predictor variable.

Appendix B. Table of parameter values for WRLCM

Table B1. Parameter values, standard deviation (SD), transformed values, transition numbers in which parameters are found and brief description of parameters.

Name	Value	SD*	Transformed Value	Transition	Description
t.crit	12.0	0	12.0	1	Critical temperature (C) at which egg to fry survival is reduced
$B0_1$	0.95	0.096	0.72	1	Survival below critical temperature value (logit space)
$B1_1$	-1.11	0.144	NA	1	Rate of reduction in egg to fry survival (logit space)
$P_{TF,\,m}$	-3	0	0.047	2	Proportion tidal fry
$S_{TF,FP}$	1	0	0.731	3	Survival tidal fry in floodplain
min.p	0.05	0	0.05	3	Minimum proportion entering Yolo bypass under flow < 100 cfs under modified design
p.rate	1.1	0	NA	3	Rate of increase in proportion entering Yolo bypass for flows > 6000 cfs under modified design
$B0_4$	0	0	0.5	4	Average survival tidal fry to delta intercept
$B1_4$	-1	0	NA	4	Effect of DCC gate (value is in logit space)*
$B0_5$	0	0	0.5	5	Average proportion of tidal fry to bay intercept
$B1_5$	2	0	NA	5	Proportion tidal fry to bay - flow at Rio Vista effect
$S_{TF,DE\text{-}BA}$	-1	0	0.269	5	Survival of tidal fry from delta to bay
S_{FRY}	0.872	0.062	0.705	Rearing	Winter run fry survival
$mig_{UR,m}$	0.128	0.012	0.128	Rearing	Proportion of fry in upper river migrating from upper river to lower river per month
$B0_M$	-6.0	0	0.002	Rearing	Wilkins slough movement without trigger (value is in logit space)

Name	Value	SD*	Transformed Value	Transition	Description
$B1_M$	5.5	0	0.377	Rearing	Wilkins slough movement with flow trigger (value is in logit space), movement rate under flow trigger is 0.377
mig_m	0.224	0.126	0.224	Rearing	Probability of migration from habitats
$S_{FRY,BA}$	-7	0	0.001	Rearing	Survival of bay rearing fry pushed to gulf
Z_1	-1	0	0.269	11 to 15	January smolt probability
Z_2	0	0	0.5	11 to 15	February smolt probability
Z_3	3	0	0.953	11 to 15	March smolt probability
Z_4	8	0	1	11 to 15	April smolt probability
Z_5	10	0	1	11 to 15	May smolt probability
Z_6	10	0	1	11 to 15	June smolt probability
Z_7	10	0	1	11 to 15	July smolt probability
$B0_{11,LR}$	1.39	0	0.801	12	Smolt survival lower river to delta
$B0_{10,UR}$	-0.4	0	0.401	11	Survival of upper river fish to lower river
$B1_{10}$	0.3	0.053	NA	11,12	River smolt survival from flow effect
$C_{S_{11}}$	12	0	0.999	11 to 14	Survival smolt chipps to ocean – survival captured in gulf survival
$A_{S_{13,FP,m}}$	12	0	0.999	13	survival from Yolo until Delta, assume 0.999 since Yolo nodes being captured in ePTMv2
$S_{15,BA}$	0	0	0.5	15	Survival of smolts bay to ocean

Name	Value	SD*	Transformed Value	Transition	Description
S_{G0}	-2.0	0	0.12	16	Average survival of smolts entering the gulf
S_{G1}	-0.338	0.233	0.157	11, 12, 13	Gulf entry covariate effect (PCUI) for all rearing areas in logit space
σ_{ϵ}	1.6	0	1	16	Standard deviation of annual random effects in process noise
S_{17}	1.35	0	0.794	17, 18	Probability of survival age 1 to age 2 over 4 months
M_2	-2.2	0	0.1	17,18	Probability of maturation age 2
S_{sp2}	2.2	0	0.9	18	Survival ocean exit to spawning ground age 2
S_{19}	1.4	0	0.802	19	Probability of survival age 2 to age 3
M_3	2.2	0	0.9	19, 20	Conditional probability of maturation at age 3
S_{sp3}	2.2	0	0.9	20	Survival ocean exit to spawning ground age 3
S_{21}	1.4	0	0.802	21	Survival age 3 to age 4
S_{sp4}	2.2	0	0.9	21	Survival ocean exit to spawning ground age 4
$V_{eggs,2}$	3000	0	3000	22	Eggs per spawner age 2
$V_{eggs,3}$	5000	0	5000	22	Eggs per spawner age 3
$V_{eggs,4}$	5000	0	5000	22	Eggs per spawner age 4
$B0_{Apr}$	-4.145	0.060	NA	22	Intercept for proportion of spawners in April
$B1_{Apr}$	0.0538	0.062	NA	22	Effect of temperature on proportion of spawners in April
$B0_{May}$	-1.796	0.020	NA	22	Intercept for proportion of spawners in May

Name	Value	SD*	Transformed Value	Transition	Description
$B1_{May}$	-0.2031	0.020	NA	22	Effect of temperature on proportion of spawners in May
$B0_{Jul}$	-0.332	0.012	NA	22	Intercept for proportion of spawners in July
$B1_{Jul}$	0.3852	0.012	NA	22	Effect of temperature on proportion of spawners in July
$B0_{Aug}$	-3.443	0.044	NA	22	Intercept for proportion of spawners in August
$B1_{Aug}$	0.7921	0.045	NA	22	Effect of temperature on proportion of spawners in August
Fem_{Age2}	0.01	0	0.01	18	Proportion of age 2 spawners that are female
Fem_{Age3}	0.5	0	0.5	20	Proportion of age 3 and 4 that are female
$K_{Sp,m}$	9000	0	9000	22	Capacity of female age -3 spawners in the spawning reaches by month

*Estimated parameter values have associated standard deviations (SD)

WRLCM Report 2035, Sites Alt3A_Mod, Alt3B_Mod, and NAA DRAFT

QEDA Consulting, LLC

March 29, 2023

Note: For the WRLCM figures that are broken out by WYT, results for some lifestages (e.g., egg survival) will be summarized by the Water Year that matches the broodyear, whereas other lifestages (e.g., fry survival, smolt survival) will be summarized by the following year, when fry rearing and smolt outmigration occurs (water year = broodyear + 1).

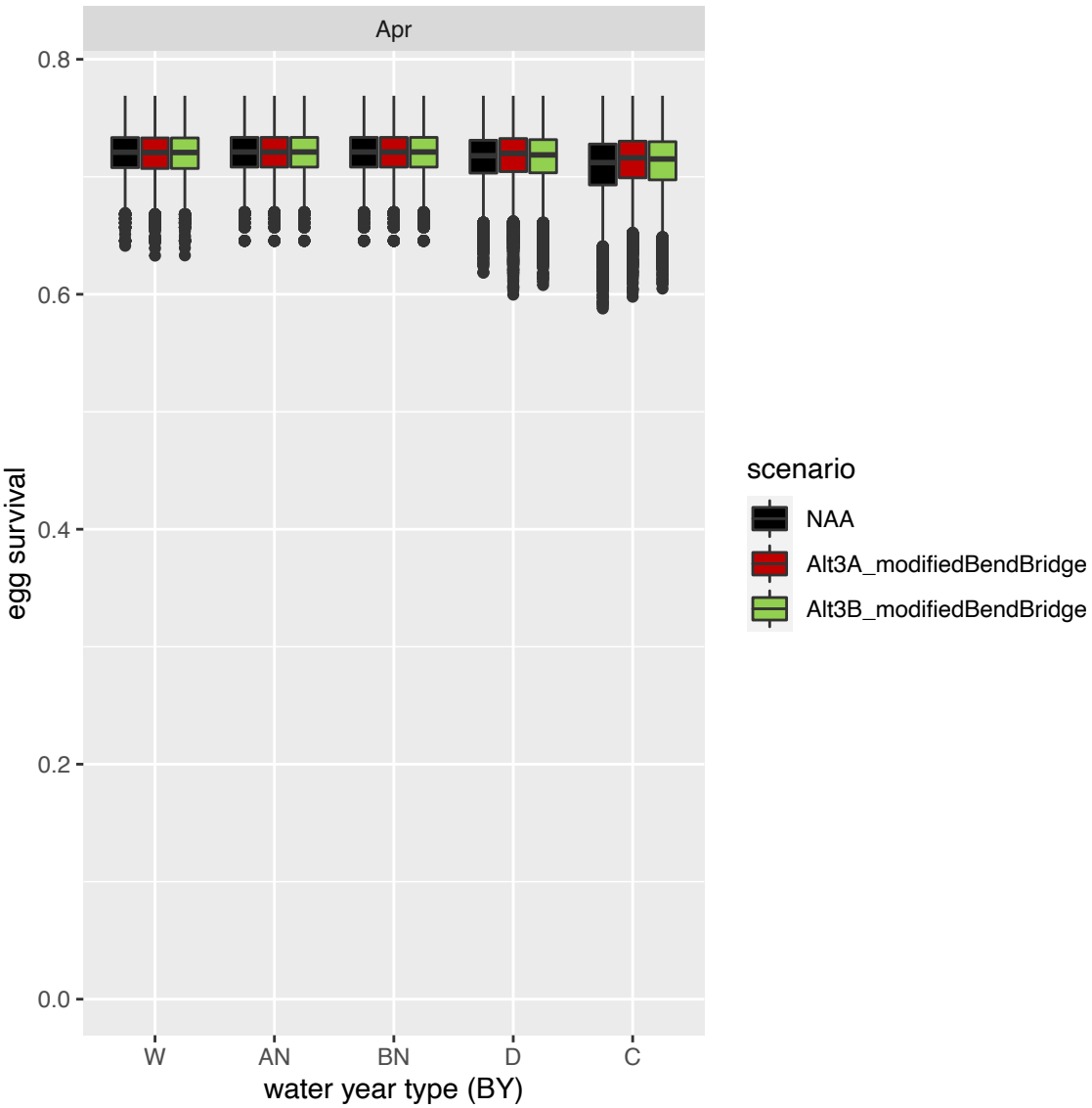

Figure 1: Apr egg survival by water year type.

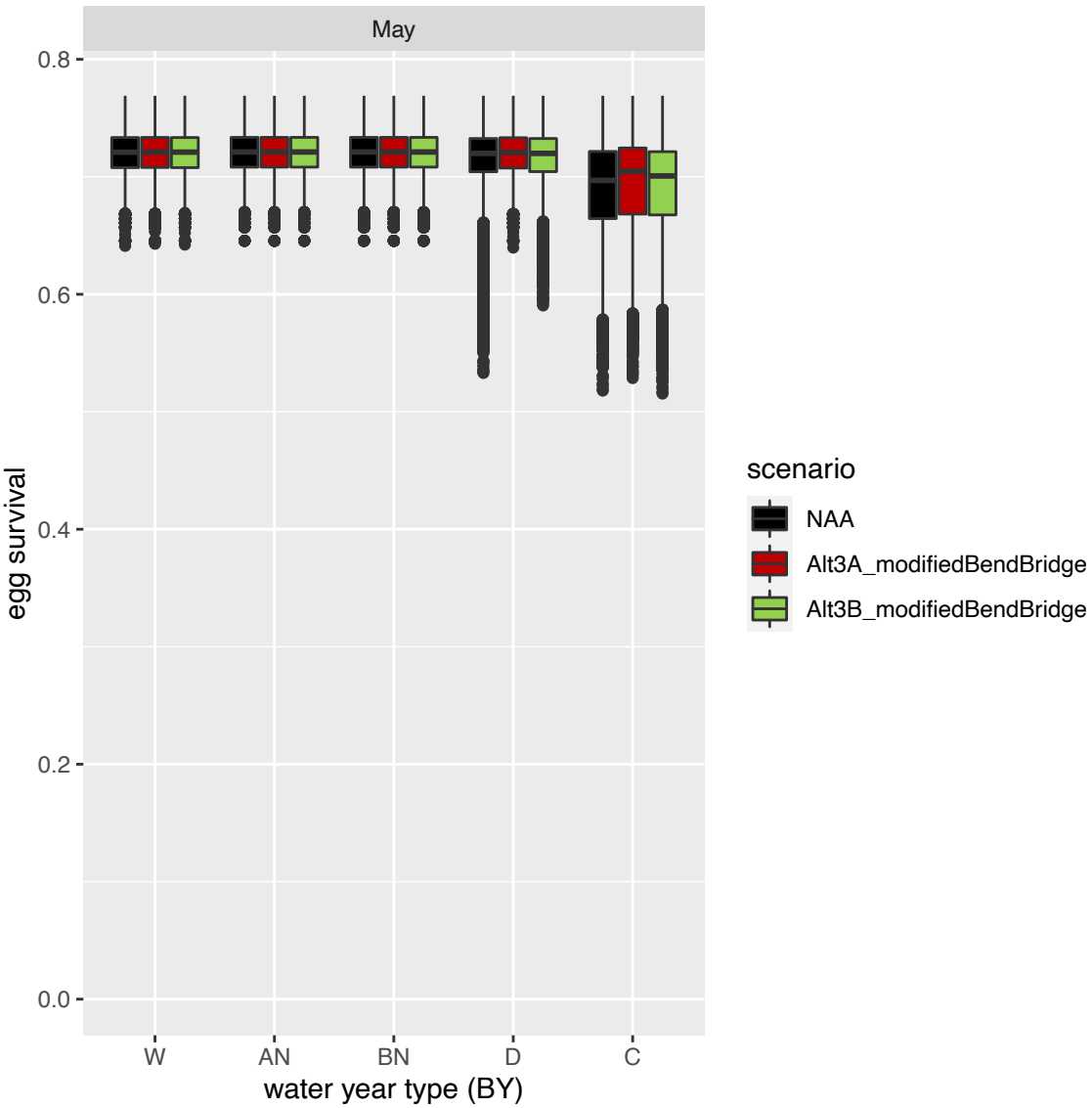

Figure 2: May egg survival by water year type.

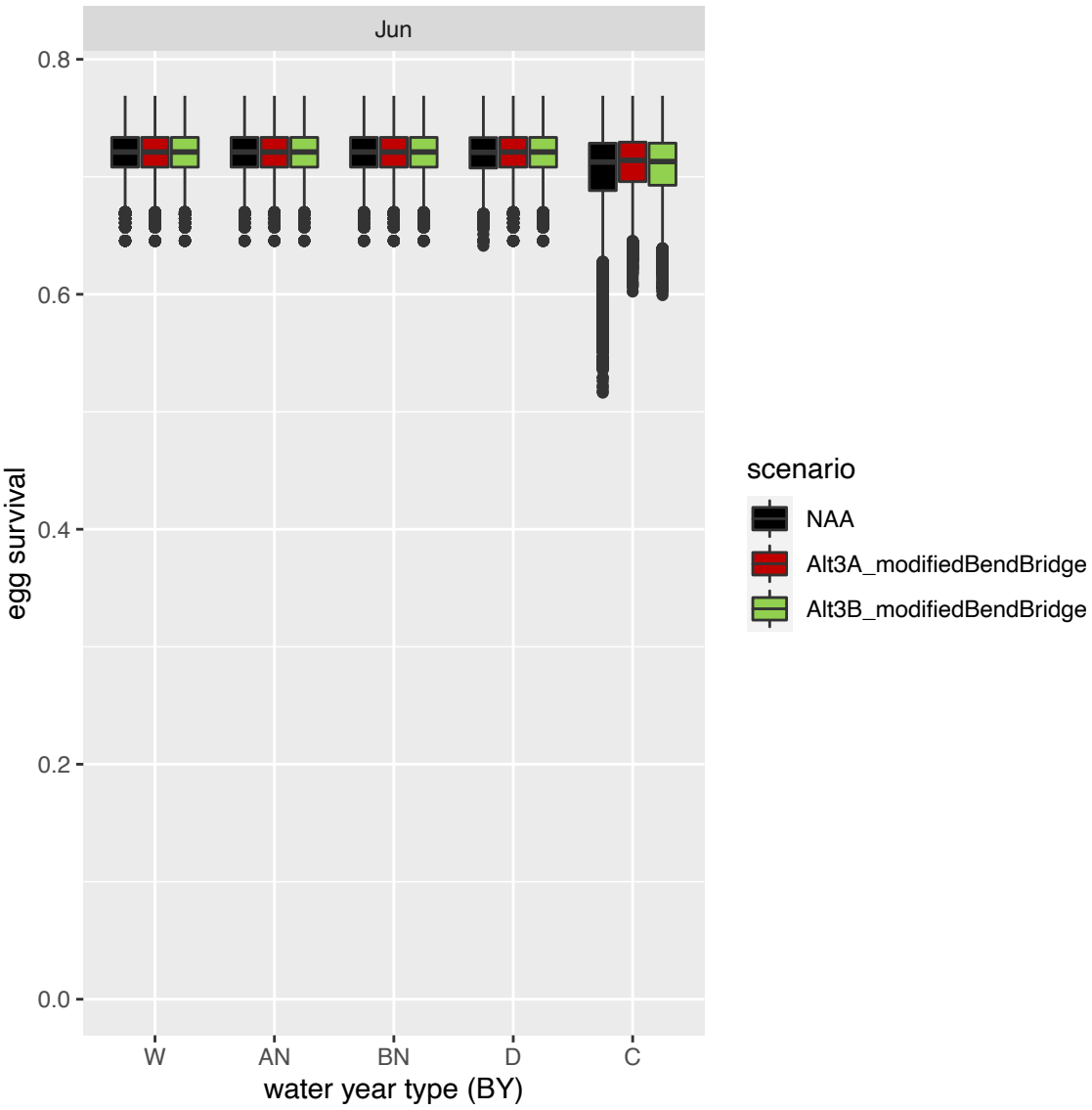

Figure 3: Jun egg survival by water year type.

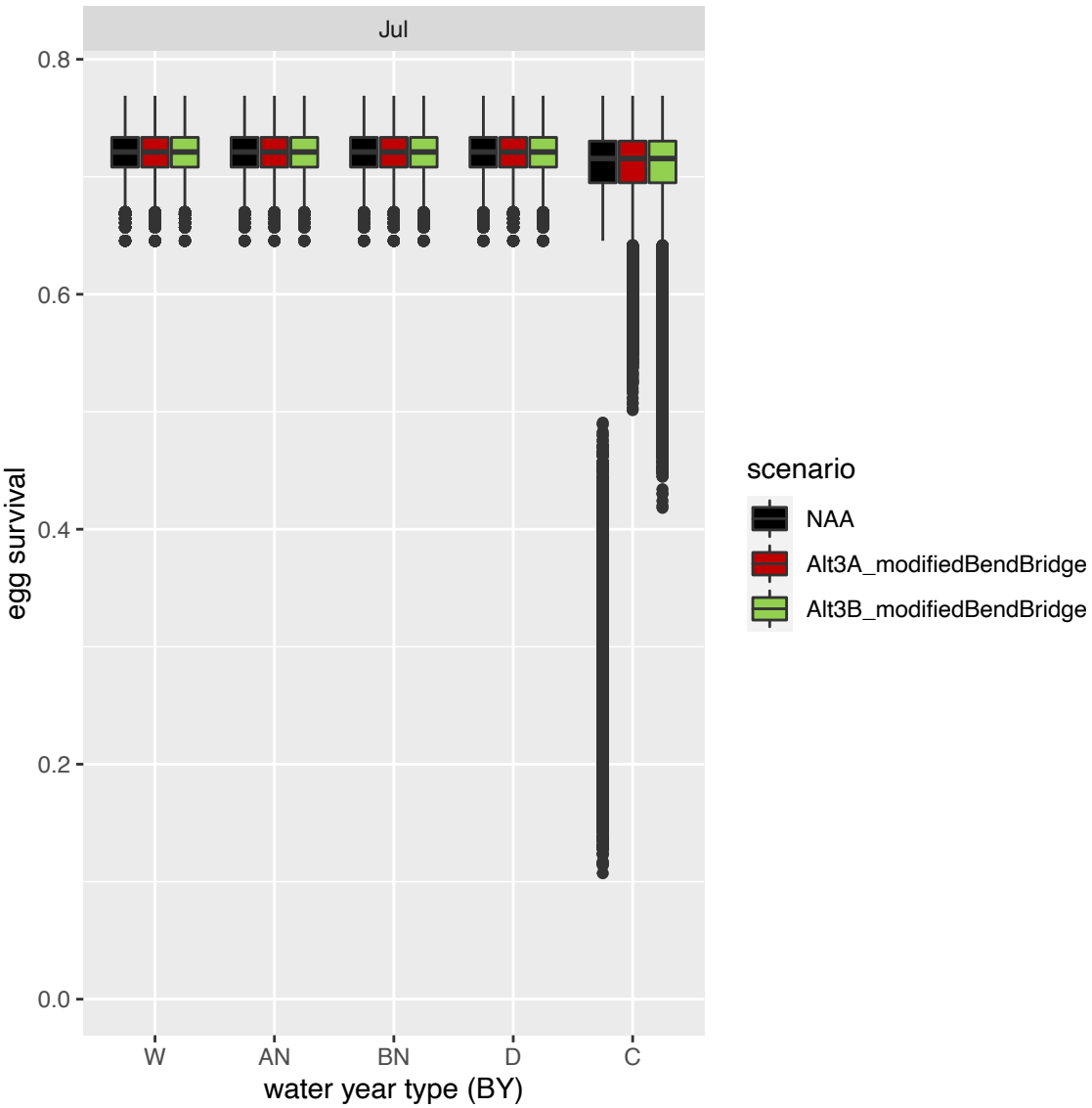

Figure 4: Jul egg survival by water year type.

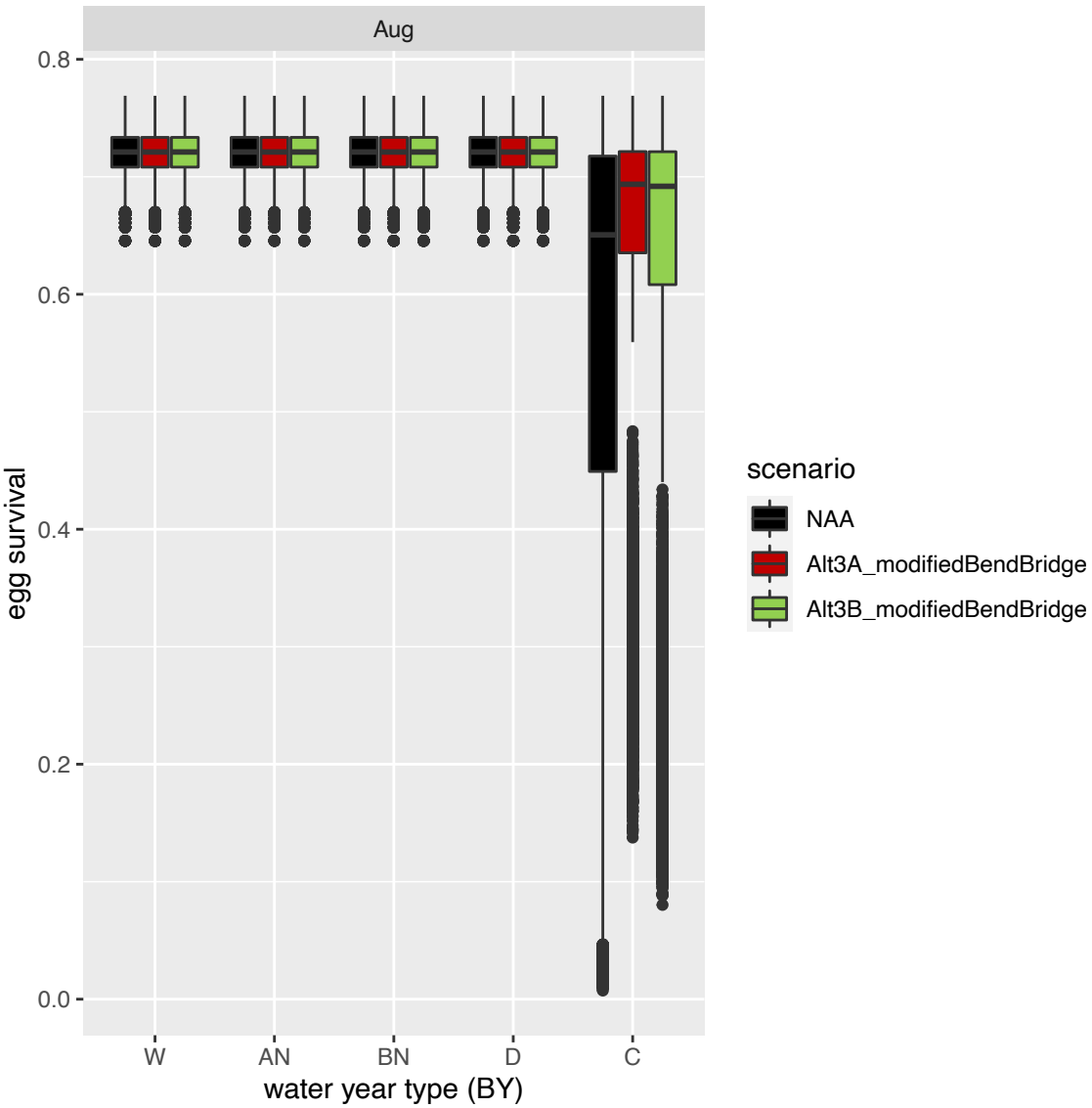

Figure 5: Aug egg survival by water year type.

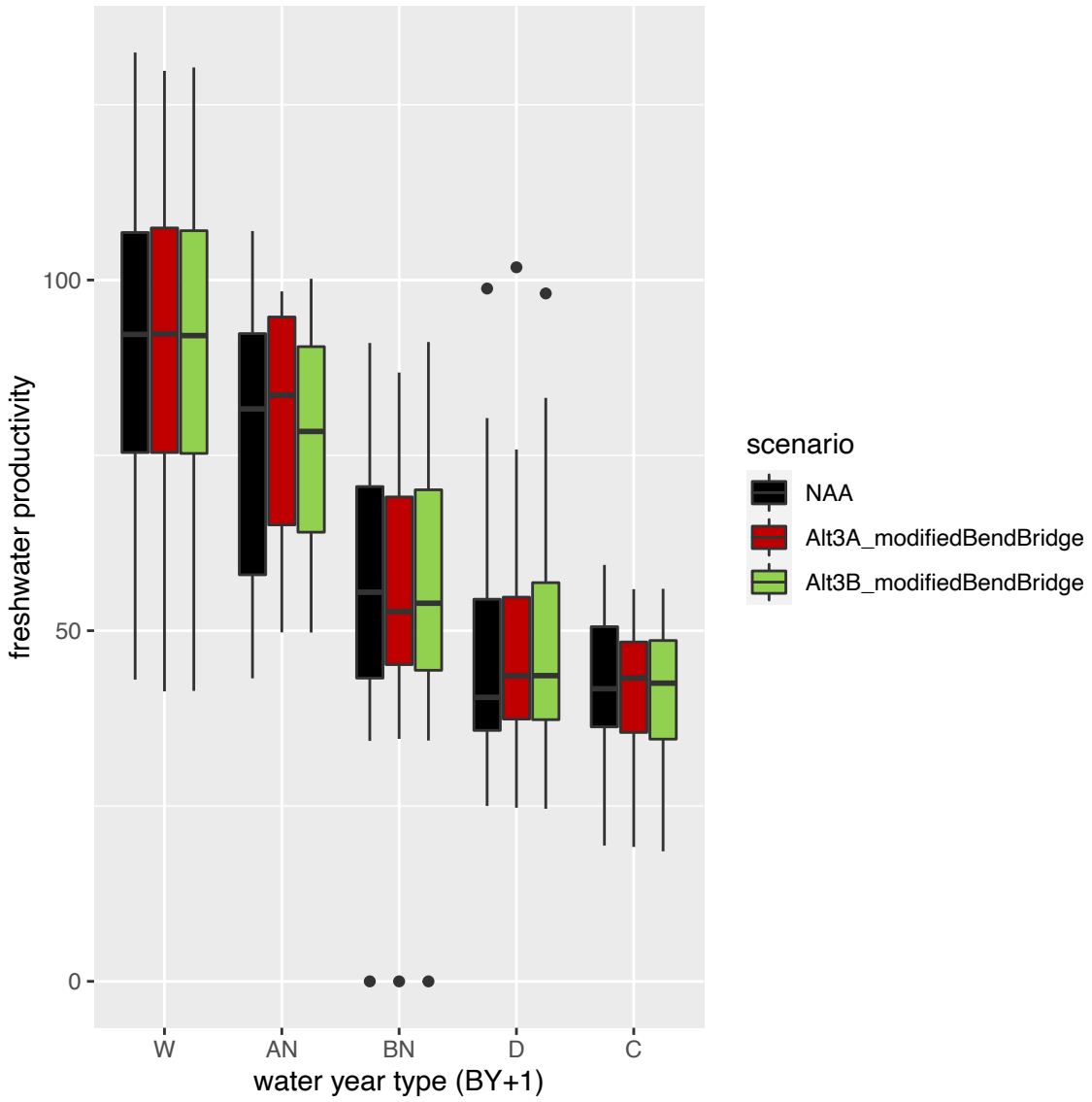

Figure 6: Boxplots of median freshwater productivity (gulf smolts per spawner) by water year type.

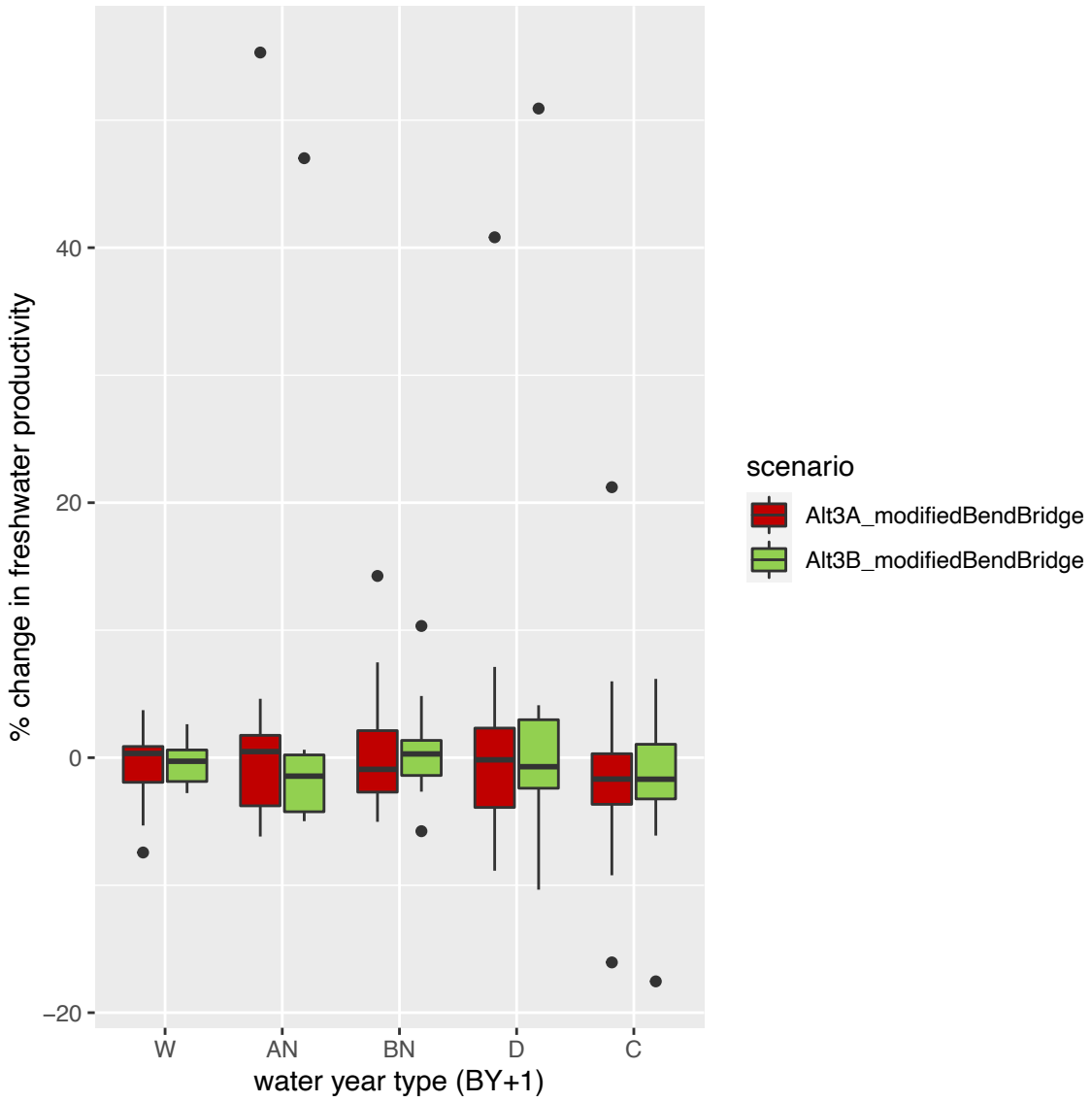

Figure 7: Boxplots of percent change in median freshwater productivity (gulf smolts per spawner) by water year type.

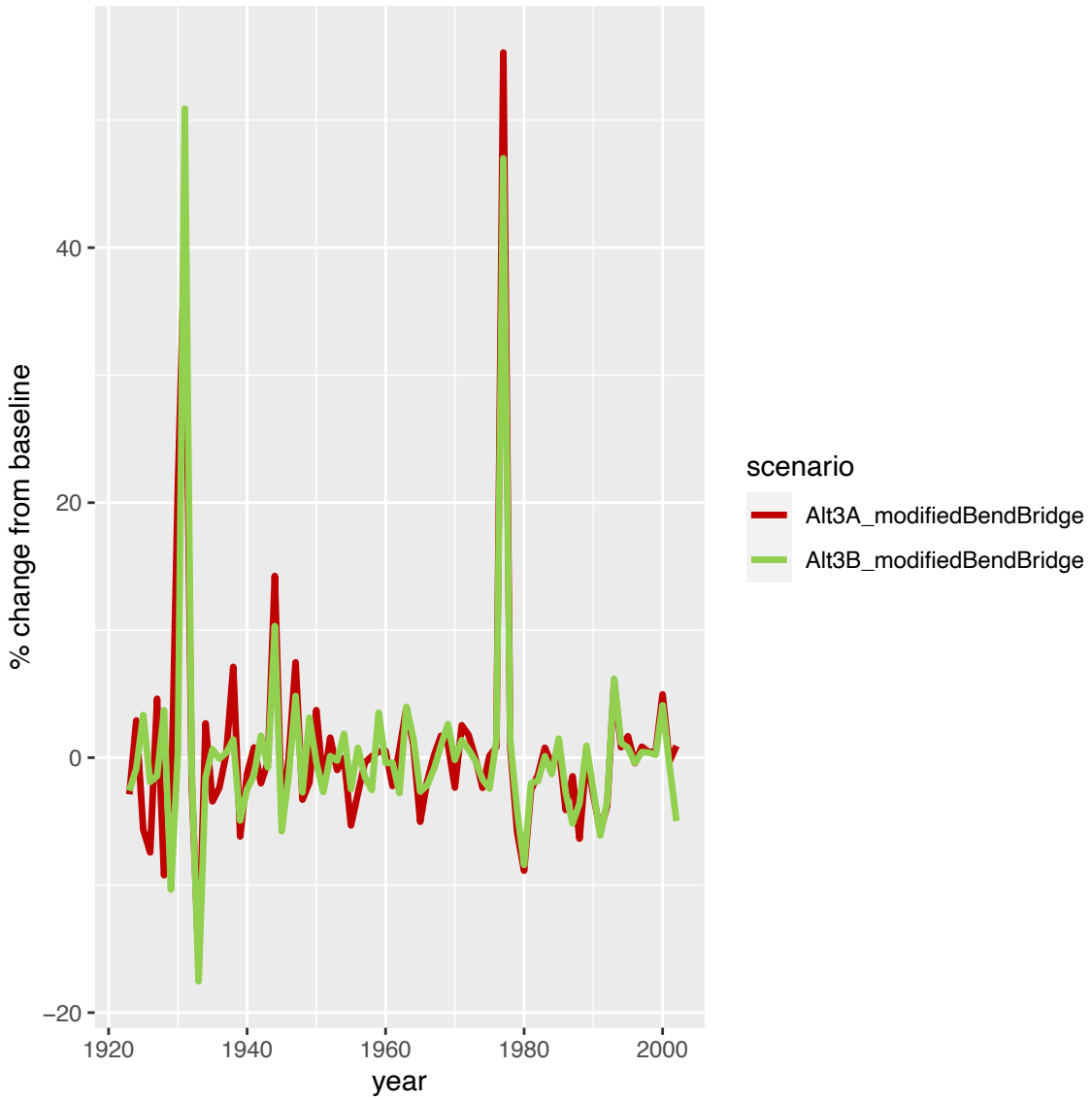

Figure 8: Percent change in freshwater productivity (gulf smolts per spawner).

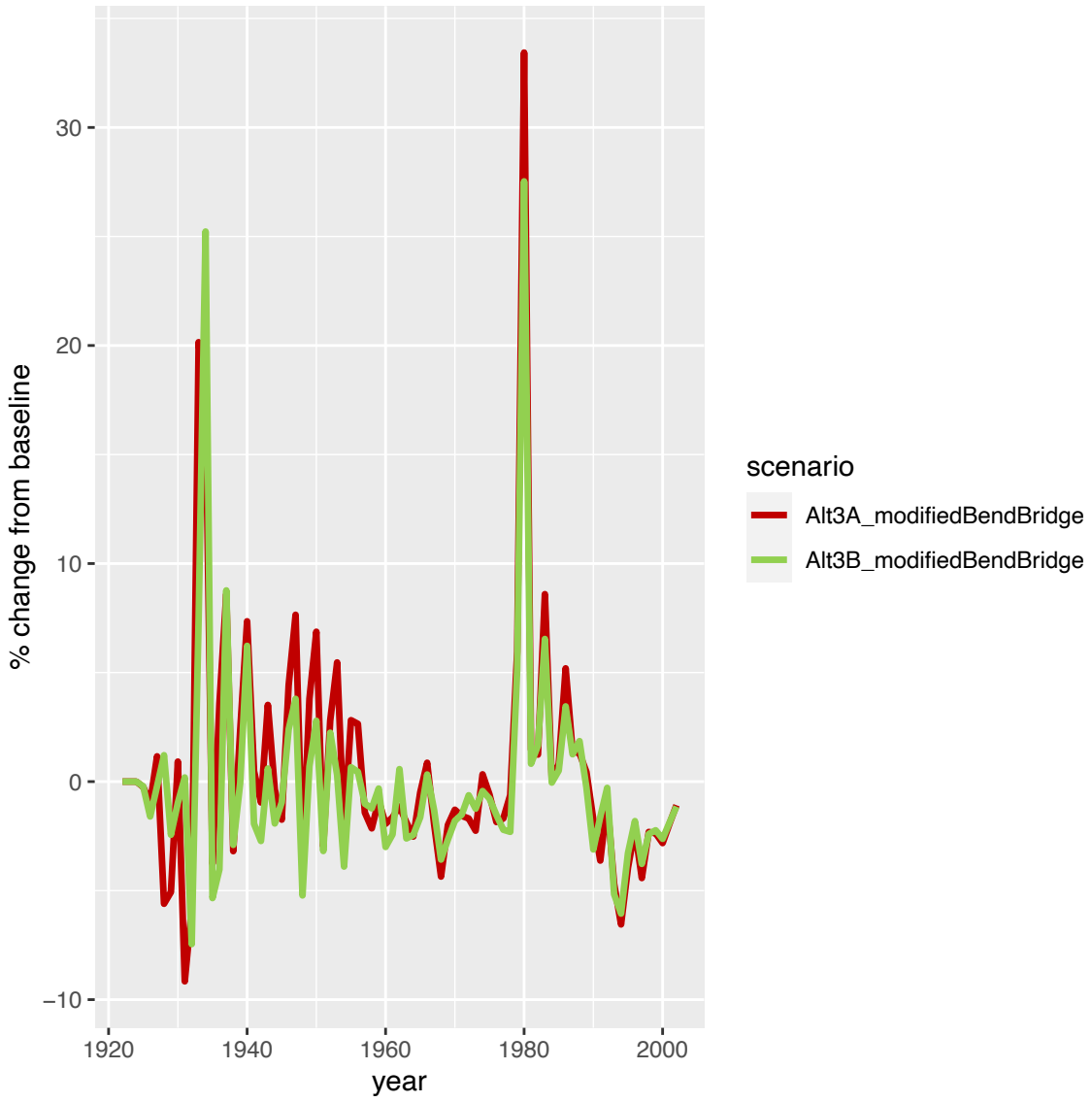

Figure 9: Percent change in annual escapement.

scenario	mean % change in abundance	95% CI	Pr(Alt>baseline)
Alt3A_modifiedBendBridge	1.08	[-5.93, 9.19]	0.65
Alt3B_modifiedBendBridge	0.34	[-9.12, 10.09]	0.55

Table 1: Mean of percent change in annual abundance (sum of in-river, natural, and hatchery-origin spawners) averaged across all years. Pr(Alt>baseline) is the probability that a realization of the alternative scenario will have a positive percent change averaged across all years.

scenario	mean % change in productivity
Alt3A_modifiedBendBridge	0.67
Alt3B_modifiedBendBridge	0.45

Table 2: Mean percent change in freshwater productivity (gulf smolt per spawner) relative to baseline

scenario	mean % change in CRR	95% CI	Pr(Alt>baseline)
Alt3A_modifiedBendBridge	1.37	[-1.02, 3.13]	0.76
Alt3B_modifiedBendBridge	1.31	[-1.71, 3.03]	0.67

Table 3: Mean of percent change in cohort replacement rate (CRR) averaged across all years. Pr(Alt>baseline) is the probability that a realization of the alternative scenario will have a positive percent change averaged across all years.

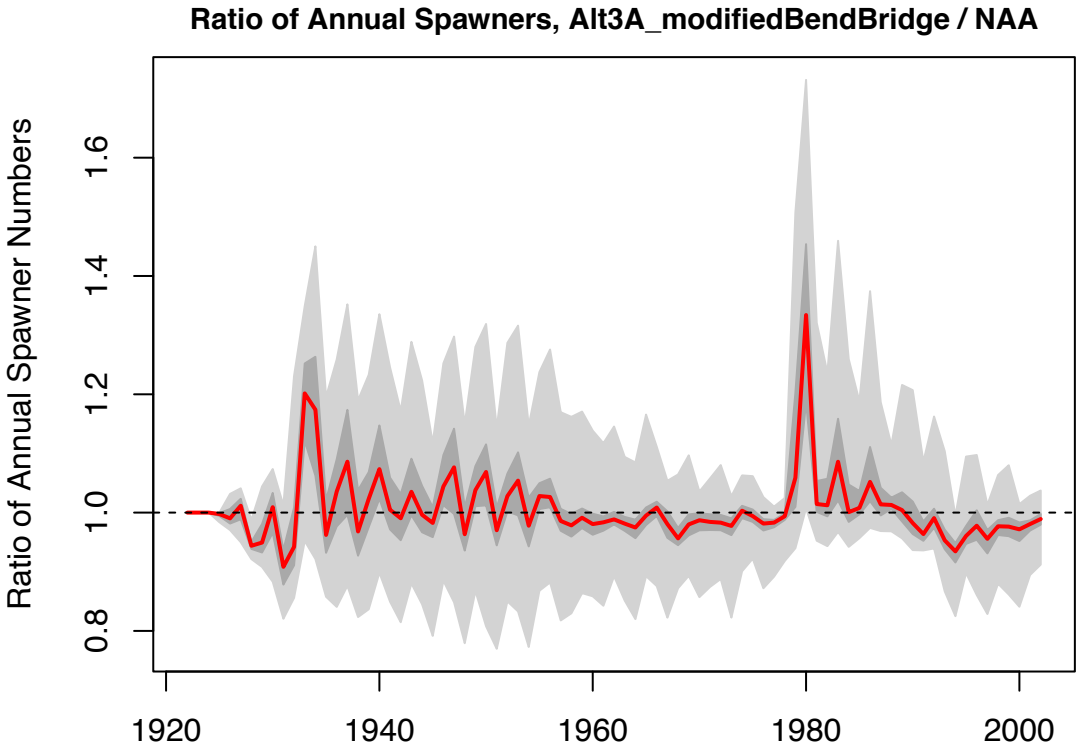

Figure 10: Ratio of number of annual spawners

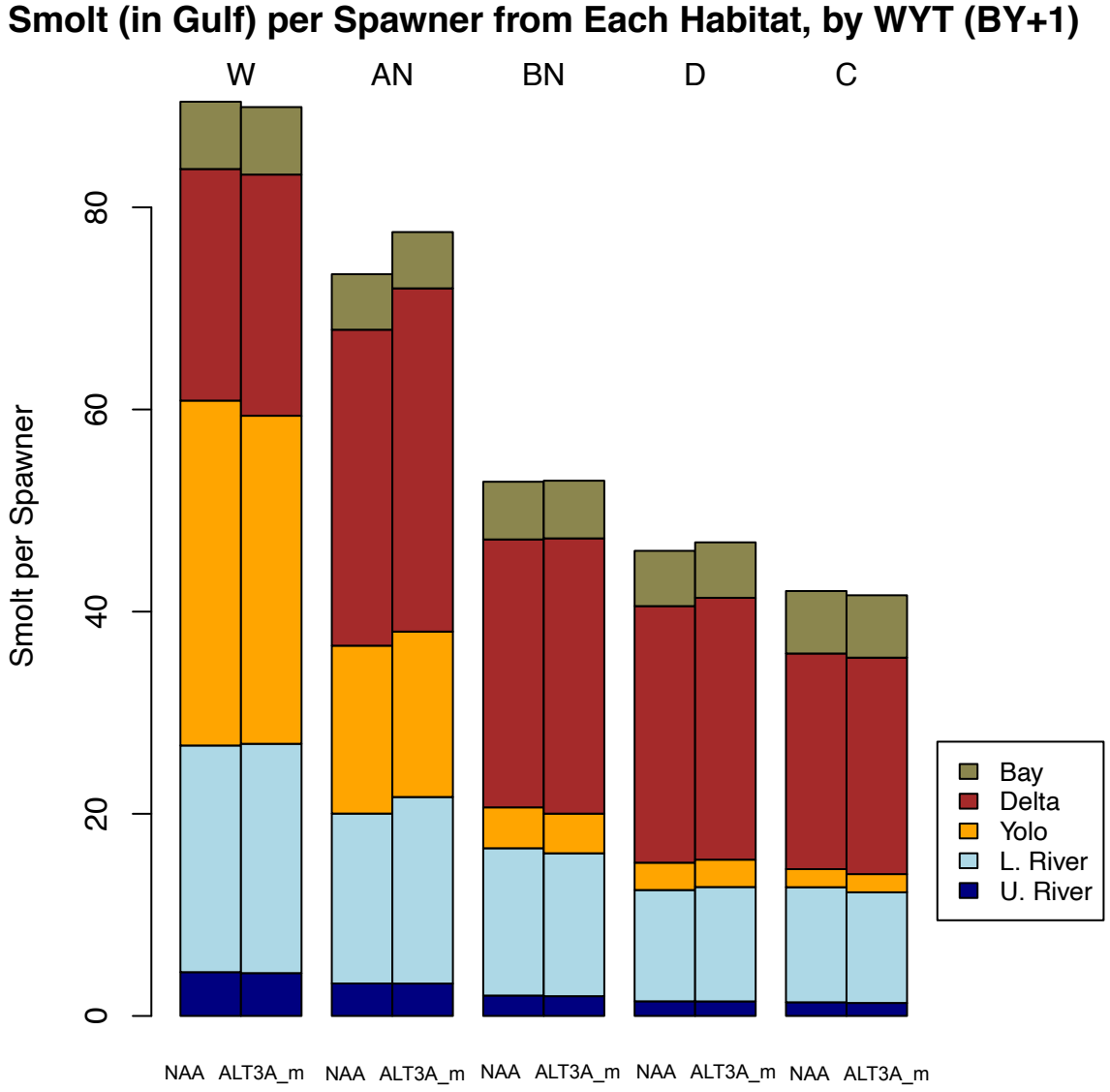

Figure 11: Median smolt per spawner by habitat and water year type

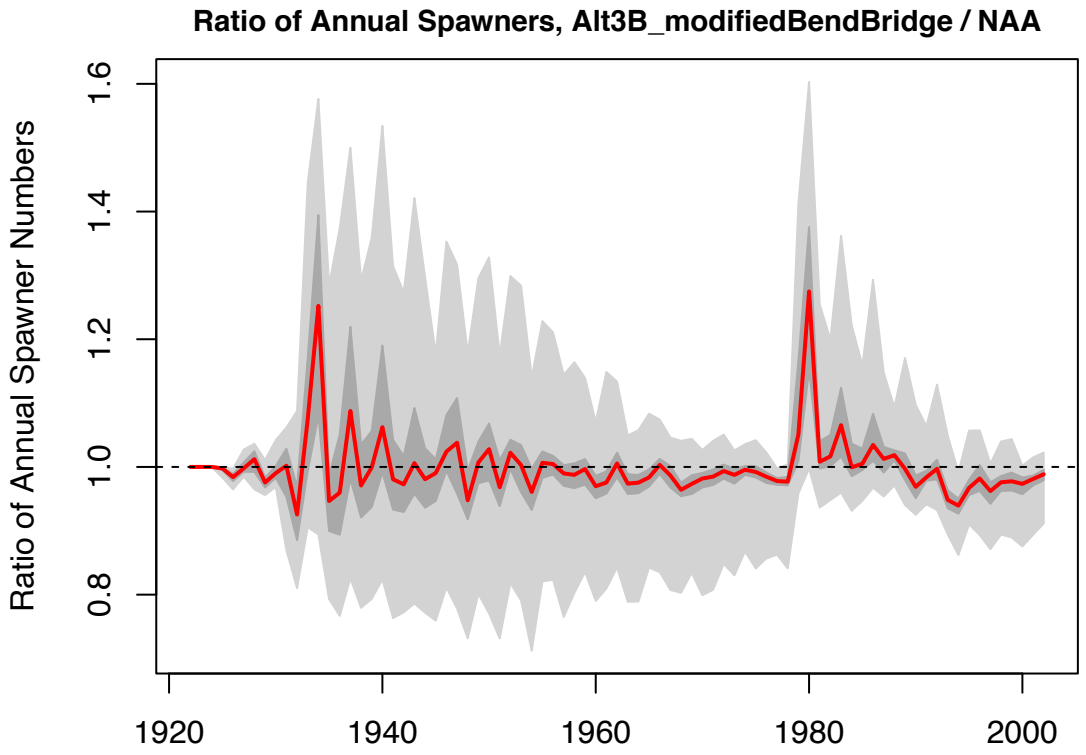

Figure 12: Ratio of number of annual spawners

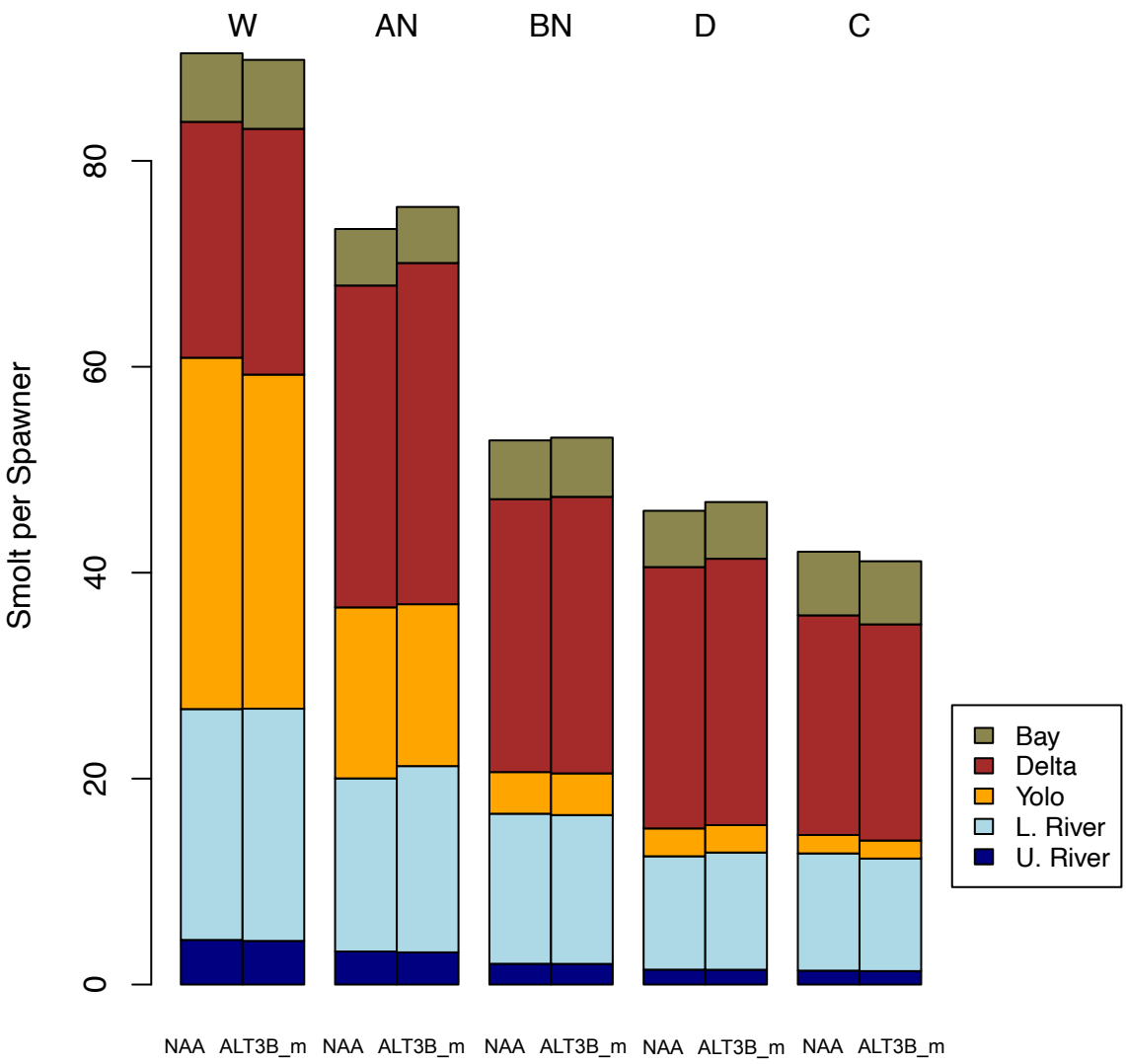

Figure 13: Median smolt per spawner by habitat and water year type